EXPERIMENTAL MEASUREMENTS OF THE MINOR LOSS DUE TO FIXED SCREENS AT SUCTION ENTRANCE FOR A CUTTERHEAD MODEL DREDGE

A Thesis

by

PAULO TADEU DE OLIVEIRA JÚNIOR

Submitted to the Office of Graduate and Professional Studies of
Texas A&M University
in partial fulfillment of the requirements for the degree of

MASTER OF SCIENCE

Chair of Committee,	Robert E. Randall
Committee Members,	Hamn-Ching Chen
	Achim Stössel
Head of Department,	Sharath Girimaji

May 2016

Major Subject: Ocean Engineering

ABSTRACT

The cutter suction dredge ranks among all types of dredges as one of the most widely used due to its capability to tackle almost any kind of soil for many different environments, depending on its size and power. Dredges of this type are often employed in locations where the seabed has debris and unexploded ordinances, which should be blocked from entering the suction line given their inherent system damage potential. Dredgers are required to install a screen over the suction inlet to keep not only these undesired particles, but also small animals and larger rocks from joining the produced slurry and reaching the pumps. However, with the installation of such fixtures the operator must account for minor losses, which must be taken into consideration in the overall calculations for the design of the system. The goal of this research was to evaluate the behavior of a designed fixed screen with 55% of its area cut out, and evaluate experimentally the minor loss coefficient across different values of flow rates, ladder arm swing speeds and cutterhead rotational speeds. Intending to cover all combinations of operating settings, a total of 72 tests for three different screen configurations with different opening areas were run and provided data that were further analyzed and compared to previous experimental research.

Preliminary results showed only a weak relationship between the specific gravity of the slurry and increasing values of the previously mentioned dredging parameters, which raised the hypothesis of the potential effect of the magnitude of the operating parameters on the overall results. This research also presented results that confirmed the

effect of the high cutterhead rotational speed over the conducted set of tests and its influence over the prediction of minor loss coefficient (k). The results from the proposed screen showed close correspondence with formerly developed prediction equations for the range of velocities employed and served as inputs for the computation of a new exponential model whose curve fit comprised all the data found in the literature for the phenomena under investigation. Moreover, the author found that the constants present in the prediction equation are actually functions of the cutter rotational speed and their study is recommended for future experiments across a wider range of fixed screen opening areas and operating parameters.

I dedicate this Thesis to my parents Maria Luiza Rohrer and Paulo Tadeu de Oliveira for all the support provided over the years of my Master degree studies and for always being a safe haven throughout my life. This Thesis is also dedicated to my brother João Alexandre de Oliveira who always stood by my side when I needed him the most.

ACKNOWLEDGEMENTS

First, I would like to thank my mother and my father for providing me a strong education and staying by my side in all hard moments of my life and whose support was essential for the accomplishment of this goal of mine. I also want to extend my gratitude to my brother, whose love and admiration were fuel to boost my dedication towards the completion of this thesis. Additionally, an affectionate thank you to Rebecca Fernandes, whose patience and support through these years were invaluable and had a major influence to this important achievement in my life.

Secondly, I am pleased to be one of the students advised by Dr. Randall, whose honor and reputation are vastly acknowledged within the Engineering community. His knowledge and passion towards Ocean Engineering spurred me to work harder and harder to successfully develop this research. I am also deeply grateful to Yuanzhe Zhi, Mr. John Reed, Mr. Kirk Martin and the undergraduate students, whose help and assistantship were essential during the conduction of the set of experiments at the Haynes Laboratory and throughout the development of this thesis.

I would also like to thank all my friends, old and new, and, in particular, my fellows from *"BD", "Pilastras", "Coisinhas"* and from *Texas A&M Judo*, whose cooperation and willingness to help in times of need were key to the achievement of this significant milestone in my life.

TABLE OF CONTENTS

Page

LIST OF FIGURES

Page

LIST OF TABLES

Page

CHAPTER I

INTRODUCTION AND LITERATURE REVIEW

Historical Background

Dredging operations can be traced back for thousand years, from the moment it was merely considered an art rather than science. Back then, the vessels employed in such operations were probably at the same size of rafts and the excavating tools as simple as a man with a bucket. The development of such method into the use of spoons and a bag dredger and their subsequent evolution to dredging machines is recounted repeatedly in the literature.

According to Gower (1968), the "art" of dredging began with the first communities that lived in the valleys of the Nile, the Euphrates, the Tigris and the Indus Rivers. It is also known that the Neolithic Man made use of tools, such as spades, hoe, pick, rake and baskets to carry out operations we nowadays would name Dredging.

Many references can be found in the literature confirming evidences that the Sumerians were responsible for the earliest dredged canals around 4,000 B.C., even though the Egyptians are acknowledged as being the first masters of the arts of dredging.

Even some modern techniques used by state-of-the-art vessels, such as the agitation dredging, can be traced back to ancient times. For instance, Gower (1968) reported that tree trunks weighted by stones were dragged downstream behind a boat to put the mud into suspension so that the current would be able to carry it away. Another

example of today's technology that dates back thousands of years ago, was the use of paddle wheels for propelling ships, which were rotated by oxen.

After a long period of stagnation, a grab dredging crane was built in the Netherlands in the 16th century, which is credited, by some people, to Leonardo Da Vinci. At that time, Netherlands had become the leading shipping and trading nation and more developed tools were needed to maintain its waterways open. It was also in this period that the Amsterdam mud mill was born.

Another hundred years went by when James Watt developed the first steam engine, which, initially, was used to drive ships (1786) and only in 1796 the innovation was first used in a dredging machine. Along this modernization other patents, like a machine for taking up ballast under water from a depth of 6 m (20 ft), were invented. Over the following years, many other equipment and accessories were better developed to meet the existing needs and many of the dredges we use today resemble the machinery employed by the people on their tasks.

During the late years of the 19th century, the U.S. Corps of Engineers conducted experiments on sea-going hopper dredger (Gower, 1968). A couple of years later, in 1867, the idea of the suction dredge was first introduced by Bazin at the Paris Exposition. The presented design was equipped with a rotating harrow under the bow of the ship and suction pipes under the stern (Herbich, 2000).

Dredging operations were gradually becoming more demanding and challenging, which yielded on development of the hydraulic dredges. This type of dredge was

interesting from the economic standpoint, once it reduced not only the capital expenditure, but also the danger during the operations. Modern dredges are designed to meet the needs of the modern society, whose growing demands range from operations in small canals and estuarine zones, to complex designs for offshore nuclear plants, airports, artificial islands and deep-water ports.

Dredging Technologies

Dredging operations can be summarized in three parts: Excavation, Transport and Final Disposal. These stages form a cycle that is repeated over time until a certain target quantity of dredged material is reached, as seen in Figure 1.

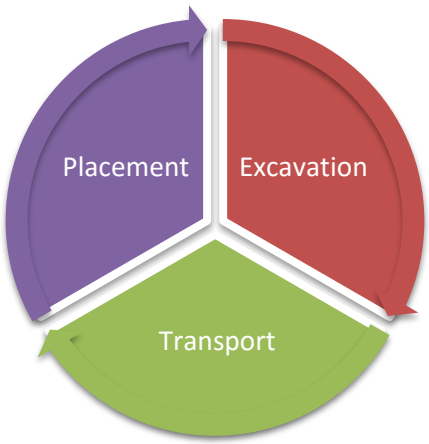

Figure 1: Phases of a regular dredging operation.

Throughout the years the industry has developed, methods have changed and technologies have improved. Nowadays, different applications require different types of processes. As mentioned before, dredging starts with the excavation of the site, which can

be carried out by a hydraulic or a mechanical dredge depending on the type of sediments and depths. The material is then transported by either ships, pipelines or barges to a suitable and approved placement area, where the last part is then executed, which is the material disposal. Dredges are normally classified as either Mechanical Dredges or Hydraulic Dredges, which are chosen depending on their suitability for the intended operation. Figure 2 shows the classification of all type of dredges and the most important are better detailed over the next sections.

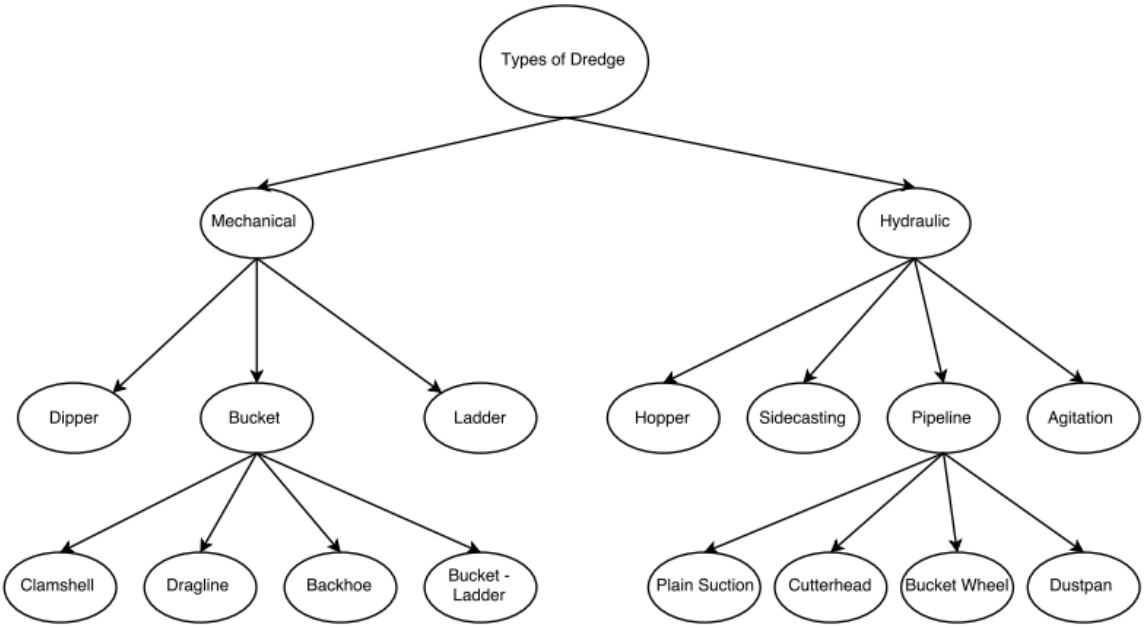

Figure 2: Classification of the existing type of dredges.

Mechanical Dredges

Mechanical dredges are simpler than the hydraulic ones and could be easily associated with excavating machines. Due to their lack of complexity, these types of equipment were the first to be developed and they are characterized by their inability to transport the excavated material over long distances (Herbich, 2000). On the other hand, they are ideal for operations in places where the access is not easy, such as docks and jetties

Bucket-Ladder Dredge

The Bucket Ladder Dredge, shown in Figure 3, is also called Buckets Chain Dredger and is equipped with an endless chain of buckets that are carried by the ladder arm situated in the well of a U-shaped pontoon. At the upper part of the ladder, an upper tumbler drives this chain, which is also connected to the lower tumbler at the bottom. This chain hangs freely at the bottom part of the ladder, while on its upper side, rollers are responsible for its guidance and support. By means of rotating over the upper tumbler, buckets that were filled during their rotation over the lower tumbler are then emptied. Shutes are responsible for guiding the soil from that location to an alongside layer barge. The size of buckets vary from 30 liters (1.06 ft^3) to 1200 liters (42.38 ft^3) and the rock bucket dredgers account with a set of buckets, which Vlasblom (2003) refers as “small rock bucket” and a “bigger soft soil bucket”.

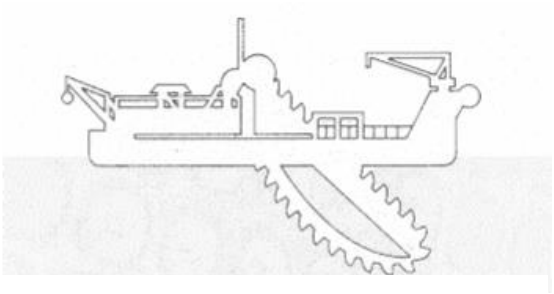

Figure 3: Schematic drawing of a Bucket-Ladder Dredge.
Source: Vlasblom (2003)

Clamshell Dredge

This is the most common dredger in the world, once it has a rather simple design and can be used with or without propulsion (Vlasblom, 2003). It is often referred as Grab Dredge, because the method used to remove sediments. The vessels are normally equipped with a hopper responsible for storing the dredged material and are moored by anchors or poles, which are called spuds. The capacity of a grab dredger is expressed in the volume of the grab, which vary between sizes less than 1 m^3 (35.32 ft^3) up to 200 m^3 (7,062.93 ft^3), and its opening is mainly controlled by the closing and hoisting wire or by hydraulic cylinders. (Vlasblom, 2003). In the United Stated, barges and scows are used alongside the crane instead of the aforementioned hopper.

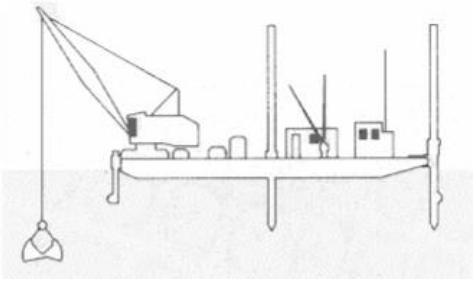

Figure 4: Schematic drawing of a Clamshell Dredge.
Source: Vlasblom (2003)

Dippers and Backhoe Dredge

Due to its great leverage and "crowding" action this type of dredge is mostly used when the presence of hard compact material or rock is noticed (Herbich, 2000) and it is commonly found in two versions, the backhoe and the front shovel (commonly referred as dippers). The difference between these two equipment is regarding their direction of action. In the first, the derrick pulls the bucket, while the dippers acts pushing it. Even though the backhoe dredge is the one used in most of the cases, front shovel dredges are needed in dredging operations of shallow areas.

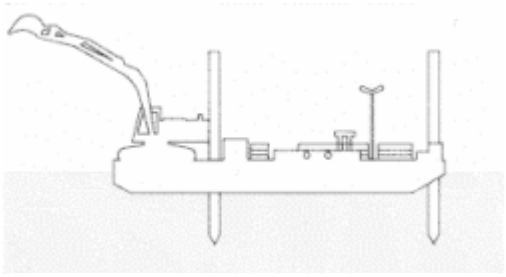

Figure 5: Schematic drawing of a Backhoe Dredge.
Source: Vlasblom (2003)

Hydraulic Dredges

Hydraulic Dredges are more efficient, versatile and economical to operate because of their continuous, self-contained digging and disposal logic of operation (Herbich, 2000). These dredges follow a standard path: the material to be dredged is firstly loosened from the seabed, secondly the mixture is sucked by a suction inlet and travels through a pipeline up to either a hopper barge to be soon after transported to a designated site or

pumped straight to the proposed placement area. All this process is powered by a centrifugal pump, which has to be well designed and depends on many different factors, and because of its importance it is better detailed on a dedicated chapter of this thesis.

Hopper Dredges (Trailing-Suction)

The Trailing Suction Hopper Dredger consists of a ship-like vessel with hoppers to store the dredged material. The development of this equipment changed the dredging industry by drastically reducing the overall inherent costs of the operation. The hopper dredges are suitable for almost all types of seabeds (not adequate for hard materials) and are the best for offshore environments (Herbich, 2000). The size of these dredges can vary in size ranging from a few hundred cubic meters (m^3) to approximately 33,000 m^3 (1,165,384 ft^3).

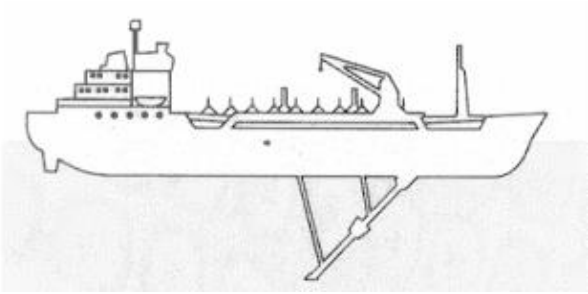

Figure 6: Schematic drawing of a Trailing Suction Hopper Dredger.
Source: Vlasblom (2003)

Two important scenarios should be carefully taken into consideration when dealing with this type of dredge. Dredging operations deal with, not only settling slurry, but also non-settling, which affects directly the way this equipment is to be operated.

In the presence of dredging-settling-slurry, the flow features an undesired turbulence that must be kept at a minimum to allow the material to settle quickly. Trailing Suction Hopper Dredgers use weirs that serve to control the overflow and are built on at the opposite end of the vessel, where the material is discharged into the hopper. This configuration enables the particles sufficient time to settle. Newer vessels have an updated distribution system, which decreases the turbulence level at the hoppers. Instead of discharging the slurry into the hopper from a certain height, what makes air molecules entrain the mixture, the discharge lines are placed at a lower height (generally below mid-depth) or even below the water level (Herbich, 2000). For non-settling slurries, the dredging operation is stopped soon after the mixture reaches the overflow.

Trailing Suction Hopper Dredgers face many different challenges that require engineers to keep developing and researching new operation mechanisms and methods. An important issue that hydraulic dredges must overcome is the cavitation, which is, not only related to undesired sounds and vibration issues, but also responsible for obstructing the slurry flow, which, in a drastic scenario could result in a failure of the pump, leading to problems in maintaining the previously designed head.

Because of all these matters, engineers came up with a draghead-mounted pump capable of reducing the chances of cavitation and enabling the dredge to operate at a deeper water level. As per Herbich (2000), this piece of equipment allows operation where the material to be dredged features sediments with a higher specific gravity.

Sidecasting Dredges

This type of dredge has an important advantage regarding the operation time limitation, since it can work continuously due to the distance from the disposal site and the place being dredged (commonly bar channels).

Figure 7: A Sidecasting Dredge in operation. Source: US Army Corps of Engineers.

The shape of the vessel is very similar to that of a hopper dredge, but, unlike the first, the "Sidecasters", which are often called Sidecasting Dredges, are not equipped with dedicated bins for dredged-slurry storage and the collected material is pumped overboard through an elevated discharge boom. The pipeline responsible for the discharge of the sediments is suspended outside the barge by a dedicated structure, which is supported by a crane or any kind of counterweight design. According to the U.S. Army Corps of Engineers (1983), this kind of dredge can perform work in remote locations and are normally assigned for projects for areas that are mostly non-stabilized, such as small inlets, which serve the fishing and small-boat industries.

Cutterhead Dredge

This type of hydraulic dredge is certainly the most well-known vessel in the dredging world, due to its efficiency and versatility. The cutterhead dredge is considered to be the America's favorite in terms of dredging operations, given its efficiency and versatility. It is also the most used type of dredge used in the United States due to its capability of dredging a wide variety of materials.

The cutterhead suction dredge is equipped with a rotating apparatus, called cutter, at the end of the intake section of the suction pipe, which enables it to efficiently dig and pump all types of alluvial material and compacted deposits such as clay and hardpan (Herbich, 2000). The vessel also uses two stern spuds that are responsible to hold the vessel in place, while the same is rotating around the spud-axis, and to advance the dredge into the next cut or excavating area, as shown in Figure 8.

Figure 8: Schematic drawing of a Cutterhead Suction Dredge. Source: US Army Corps of Engineers.

The swing arm is responsible for taking the cutterhead from side to side. Anchors attached to cables and anchored on each side of the dredge restrain the lateral movement of the dragarm. The cutterhead, directed by the swing arm, follows a pre-determined pattern. Figure 9 shows an example of the path followed by a cutterhead model dredge during laboratory experiments.

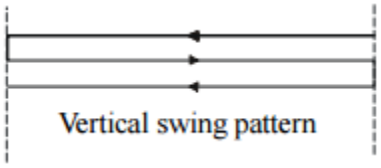

Figure 9: Usual vertical swing pattern followed by a cutterhead model dredge when in operation.

After the operation is completed, the dredged slurry may be disposed in approved placement areas, either in open water or in approved confined areas, located upland or in the water. When the upland option suits better, additional sections of shore pipeline may be required and a hopper barge is needed.

One of the major concerns when dealing with this kind of machinery is regarding the pumps. In this case, they were intensively developed and studied as the years went by. Researchers came up with a submerged pump, which is responsible, not only for increasing the concentration of slurry to be dredged, but also to secure its efficiency with deeper depths (Herbich, 2000). Another advantage of the submerged pump is concerning the fact that it avoids cavitation issues.

The production of this kind of dredge is given as the number of cubic yards of *in situ* material dredged within a certain period and expressed in $^{cy}/_{hr}$. Figure 10 below serves as a rough guide when designing the system.

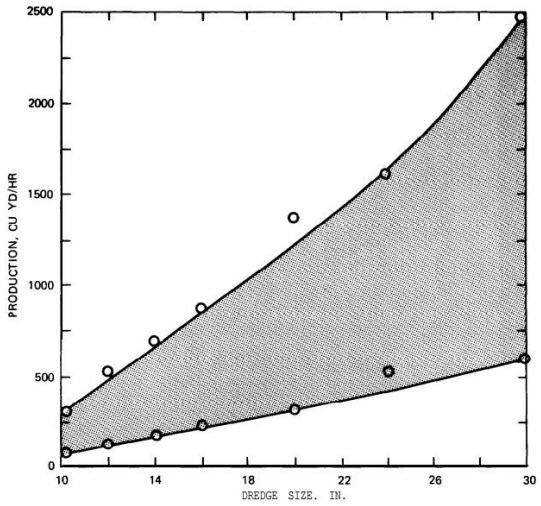

Figure 10: Chart displaying the production in $^{cy}/_{hr}$ for various sizes of dredges.
Source: US Army Corps of Engineers.

Applications for a cutterhead-type dredge varies according to the project needs and sometimes lead to some environmental impacts that should be taken into consideration. This type of dredge is best suitable for sites where the wave heights are not a threat, such as harbors, canals and outlet channels. If required, the cutterhead can be removed and the dredge can be operated as a Plain Suction Dredge.

Bucket Wheel Dredge

Pretty much like the cutter suction dredge, the bucket wheel dredge has a suction inlet, through which the sediment is transported until it reaches the disposal area. The difference between these two dredges is regarding the method used for loosening the material from the seabed. While the cutter suction dredge has a cutterhead built at the end of the swing arm, the bucket wheel dredge, on the other hand, uses a hydraulic rotating wheel that is responsible for excavating the seafloor, as see in Figure 11.

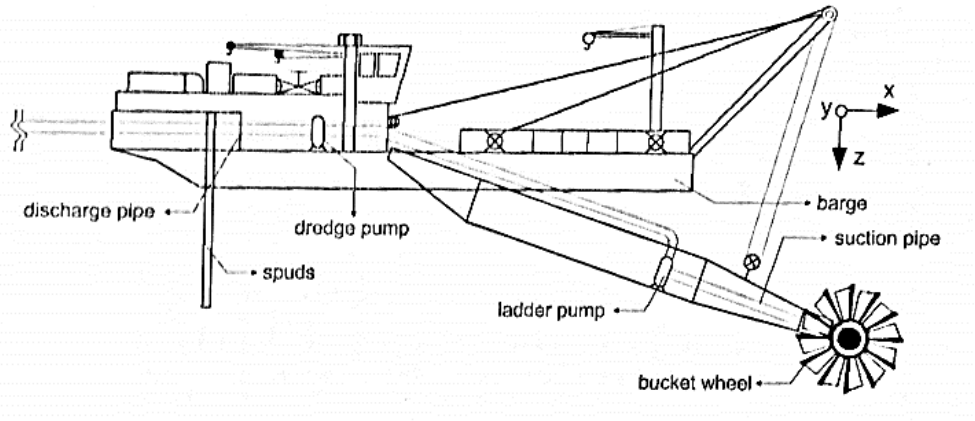

Figure 11: Schematic drawing of a Bucket Wheel Dredge. Source: Albar (2001).

The Dustpan Dredge

Named after its suction head resemblance with a large vacuum cleaner or dustpan this dredge is equipped with a pump responsible for drawing in the slurry from the deposit of sediments to be removed and pumping it through a floating pipeline to the disposal site, which can be either on shore or offshore.

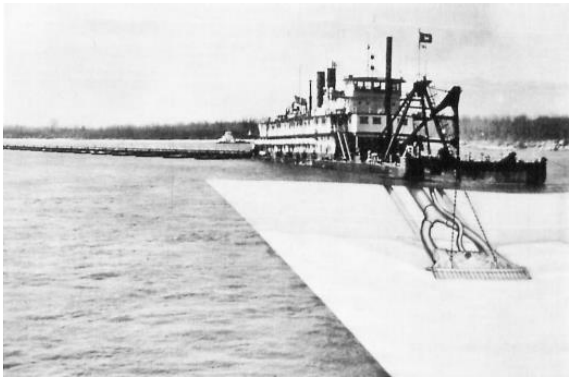

Figure 12: Schematic picture of a Dustpan Dredge in operation.
Source: US Army Corps of Engineers.

This type of dredge is mostly required for high volume operations and differently from the cutterhead dredge, it does not use a cutter at the suction inlet. For agitating and mixing the incoming material, the suction head is equipped with high-velocity water jets nozzles and has a shape of a rectangular box.

The Corps of Engineers was responsible for developing this equipment, which is intended to maintain navigation channels with uncontrolled rivers with bedload consisting primarily of sand and gravel (USACE, 1983). The first dredge of this kind was built to maintain navigation conditions on the Mississippi River during low river stages. These

types of dredgers are also used in borrow pits for reclamation areas as well as for the borrowing of sand for the concrete industry (Vlasblom, 2003).

CHAPTER II

RESEARCH OBJECTIVES AND METHODOLOGY OVERVIEW

Problem Definition and Research Objectives

Dredging operations are usually highly sensitive to the environmental conditions and therefore must be well designed and planned. These operations normally take place underwater, in shallow or deep waters, with fresh or saltwater. Being a process that encompasses many different variables is also something that makes the operation even more challenging and important. Additionally environmental legislations and constraints should be properly handled and must be taken into consideration throughout the process. During the operation, engineers and technicians involved will always be trying to operate under the perfect conditions to maximize the production. In other words, all type of losses are minimized while the environment is accordingly protected.

Dredges are classified into two general groups, mechanical dredges and hydraulic dredges. Considering the fact that the latter are the most employed when a site excavation is to be executed, the author sought to evaluate the losses associated with the installation of screens at the entrance of a cutterhead model dredge. The use of a screen on the suction inlet is of a significant importance, because it is responsible for avoiding undesired particles to go into the system and either damage the system or reduce its expected production. By undesired particles, the author means large debris, roots, wires, rocks, unexploded ordinances and whatever is too large or not expected to be dredged. On the

other hand, by placing a screen at the entrance of the suction line the operator should account for a minor loss in the system induced by the aforementioned apparatus, once the reduction of the opening area available for the inflow acts against the pump generated axial flow field. To overcome this issue more power is required to pump the mixture of water and sediment from the seabed up to the barge, which leads to a greater head loss of the system.

The objective of the present study was to investigate the influence of the screen on the suction inlet of a model dredge. Quantifying and determining the minor loss coefficient behavior, induced due to a fixed screen on the suction inlet, associated with different screen shapes and opening areas across different cutterhead rotational speeds, ladder arm swing speed and flow rates and its comparison to previous research. At the end, the author proposed a model that can be used to predict the minor loss coefficient (k) in real world dredging.

Methodology Overview

In this research, the author made use of a cutterhead model dredge available at the 25,000-square-foot Reta and Bill Haynes ‘46 Coastal Engineering Laboratory at Texas A&M University, which has been used over the years, not only for student research, but also for company experiments on the wide variety of topics involving dredging. The model dredge has a cutterhead at the entrance of the suction line, which is responsible for excavating the seabed (in our case constituted purely by sand). After being suspended,

most of the sediments go into the suction line, passing through the centrifugal pump, being finally directed to the storage vessel (hopper barge) through a discharge line. The mentioned cutterhead is connected to a ladder arm, which moves across the sediment pit following a set-by-the-operator path. Many parameters could be changed depending on what is being investigated by the researcher. Factors as, head losses (due to the change of pressure across the system), minor losses (due to several bends and the placement of a fixed screen at the suction entrance, etc.), frictional losses, valves, pump efficiency and power are example of characteristics that have a strong influence on the results.

Based on the results obtained the author compared the results found in Girani (2014) and Lewis (2014), whose experiments were similar to the research conducted by this author. Additionally, the author investigated the behavior of the minor loss coefficient (k-value) for 3 screen configurations under higher cutterhead rotational speeds and ladder arm swing speeds and greater flow rates.

CHAPTER III

THEORETICAL ANALYSIS

Fluid Mechanics Background

A proper characterization of fluid flows is of a great importance to dredging operations. Aspects such as mixture specific gravity, depth and pressure are common parameters to be assessed.

In dredging operations, calculations are made for real fluids, which means that viscosity is a parameter that plays a role and a more complex approach to the involved fluid mechanics is required. Nonetheless, some issues regarding, for instance, flow in pipes, head losses in elbows and valves and cavitation problems may benefit from more simplistic assumptions of fluid mechanics.

Even though the dynamics of flows in dredging are turbulent and resemble an unsteady flow pattern, the assumption made for this kind of operation is that the system is steady, in other words, the variables associated do not change with respect to time.

The velocity of the flow is a vector, which has magnitude and direction and when over a streamline is a function of both distance and time, as shown in Equation (1).

$$V = f(s,t) \tag{1}$$

Considering the velocity (V) is equal to the variation of the particle displacement (ds) over the increment of time(dt), one can write:

$$V = \frac{ds}{dt} \tag{2}$$

The same principle can be applied to the vector acceleration, given that it is the variation of the velocity over the increment of time, which yields:

$$a = \frac{dV}{dt} \tag{3}$$

Moreover, the acceleration in the streamline can be written as:

$$a_s = \frac{dV}{dt} = \left(\frac{d}{dt}\right)\left(\frac{ds}{dt}\right) = V\frac{dV}{ds} \tag{4}$$

This acceleration is composed of two components, the convective term and the local term as shown in Equation (5).

$$a_s = V\frac{\partial V}{\partial s} + \frac{\partial V}{\partial t} \tag{5}$$

Given the steady assumptions of the dredging operations, the local acceleration can be cancelled, since it is time dependent, which makes the acceleration over the streamline-direction only equal to the convective part $\left(V\frac{\partial V}{\partial s}\right)$.

Applying Newton's Second Law of motion to a component of the flow in a streamtube and considering the fact that we are dealing with a steady-state flow, we arrive at Equation (6).

$$\frac{dp}{\gamma} + dz + \frac{dV^2}{2g} = 0 \tag{6}$$

Equation (6) can be further integrated for incompressible and unidirectional flow into the most known form of the Bernoulli equation.

$$\frac{p}{\gamma} + z + \frac{V^2}{2g} = H \tag{7}$$

where p is the pressure, γ is the specific weight of the substance, which is defined by Equation (8).

$$\gamma_{mixture} = (SG_{mixture}) \cdot (\gamma_{water}) \tag{8}$$

where $SG_{mixture}$ is the specific gravity of the mixture. In the Bernoulli equation V refers to the velocity, g is the gravity, z is the elevation head and H is the total head.

Given the nature of the formula, a more versatile form of the Bernoulli equation can be written, which is often called the "Conservation of Energy" equation and correlates two different points on the system under analysis.

$$\frac{p_1}{\gamma_1} + z_1 + \frac{{V_1}^2}{2g} = \frac{p_2}{\gamma_2} + z_2 + \frac{{V_2}^2}{2g} + h_l - h_p \tag{9}$$

where h_l comprises all the losses across the system due to friction (h_f) and minor losses (h_m), such as: fittings, valves, elbows, contractions, swivel joints, pipe entrance and exit conditions. In Equation (9), h_p refers to the amount of energy per unit weight that has to be externally supplied (mainly in case of pumps) to overcome all losses.

Applying this equation of conservation of energy in a dredge system, we usually set the terms associated with the subscript 1 to a point right before the inlet of the suction pipe, since, at that point, the operator has all fluid information he needs. The point associated with the subscript 2 is taken depending on what the operator is looking for, or what part of the system is under evaluation, as can be seen in Figure 13 for an ordinary pipe.

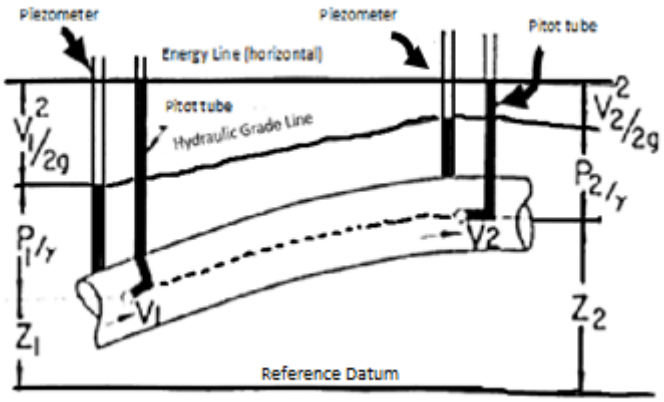

Figure 13: Visual representation of the acting heads in an ordinary pipe.

As mentioned before, the hydraulic losses associated with dredging operations are either due to friction (h_f) or due to minor losses (e.g. valves, swivels, joints, suction inlet, elbows, etc.) throughout the system (h_m).

To evaluate the losses due to friction in internal pipe flows or conduits, the Darcy-Weisbach equation is the standard method and is expressed as

$$h_f = f\left(\frac{L}{D}\right)\left(\frac{V^2}{2g}\right) \tag{10}$$

where f is the friction factor and can be determined either through the Moody diagram, where the parameter is determined as a function of the Reynolds number (*R)* and Relative Roughness $\left({}^{\epsilon}/_{D}\right)$, or through Equation (11) proposed by Swamee and Jain (1976).

$$f = \frac{0.25}{\left[log\left(\frac{\epsilon}{3.7D} + \frac{5.74}{R^{0.9}}\right)\right]^{2}} \tag{11}$$

where ϵ is the pipe internal roughness, which is dependent on the type of the material used, D is the pipeline diameter, R is the Reynolds number and L is the pipeline length. This equation is valid for $5x10^{-3} \leq R \leq 10^{8}$ and $10^{-6} \leq {}^{\epsilon}/_{D} \leq 10^{-2}$. The Reynolds number is calculated through Equation (12).

$$R = \frac{VD}{\upsilon} \tag{12}$$

where υ is the kinematic viscosity of the fluid and V is the velocity of the flow under investigation.

The losses due to singularities or minor losses (h_m) are calculated using the summation

$$h_m = \sum\left(k\frac{V^2}{2g}\right) \tag{13}$$

where k is the minor loss coefficient, which is different for each singularity across the hydraulic system.

The Transport of Slurry Flow in Pipelines

The transport of dredged material is an operation that takes many properties into account. Variables like, the distance required for the material to be transported, the geometric specifications of the system and the kinematic characteristics should be properly considered prior operations begin.

As discussed in Herbich (2000), the hydraulic transportation of mixtures is highly dependent on inertia and resistance forces and it is not possible to define the solid particle through a single intrinsic characteristic, given the fact that the solids have different shapes. According to Wiedenroth (1968), irregularly shaped particles should be approximated to spherical particles for the calculations.

Slurry Composition

The composition of these solid-water mixtures are determined as the ratio of the amount of solids to the total amount of the mixture expressed either by volume or by weight. The concentration of solids by volume (C_v) and by weight (C_w) are shown Equations (14) and (15).

$$C_v = \frac{SG_m - SG_f}{SG_s - SG_f} \tag{14}$$

$$C_w = \frac{SG_s(SG_m - SG_f)}{SG_m(SG_s - SG_f)} \tag{15}$$

where SG refers to specific gravity and the subscripts *f*, *s*, and *m*, refer to fluid, solids and mixture, respectively.

Mixture Flow Regimes

When the material goes into the suction inlet, that flow, for a given pipeline characteristics and mixture composition, is usually classified in four regimes (3 main classification and another hybrid one). It could be either a homogeneous flow, a heterogeneous flow, a flow with a moving bed, or a flow with fixed bed. It is also important to state, that there are no boundaries in the flow column; otherwise, they will most likely overlap.

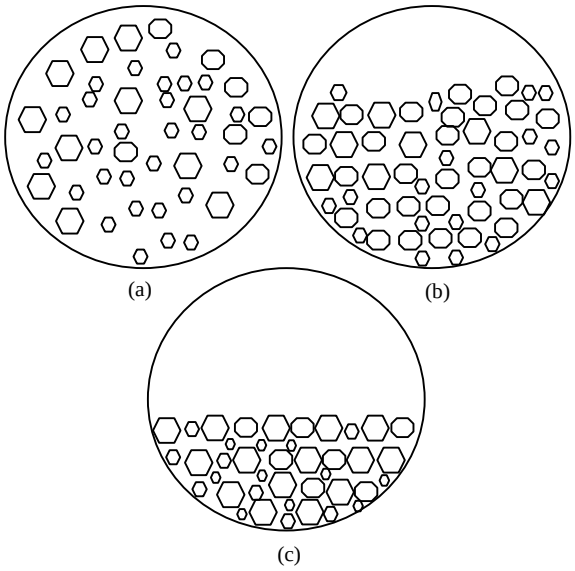

Figure 14: Representation of the three main general slurry flow classifications. (a) Homogeneous flow; (b) Heterogeneous flow; (c) Fixed Bed flow.

According to Herbich (2000), a flow regime with heterogeneous characteristics occurs when the vertical distribution of the particles are given in a such way that its concentration is greater at the bottom than near the top of the pipe, as shown in Figure 14b. It is with this configuration that the weight of material transported per unit of power required is maximized. This configuration makes this type of regime the most economical way to transport dredged material in pipes.

A flow regime in which the particles are highly concentrated at the bottom of the pipe and the mixture above is travelling with a considerably higher velocity is called a Moving Bed Regime. In this type of flow, it is easy to notice the formation of a bottom layer, which is responsible for frictional head losses, enhancing the pipe wear, which boils down to a rather uneconomical operation. The Stationary Bed Regime or Fixed Bed flow occurs when the transport of slurry will only take place above the so called stationary bed. This deposit bed constitutes a new boundary at the bottom of the pipe, which causes its partial blockage, thus reducing its efficiency, as displayed in Figure 14c

When the particles in the mixture are really small and prone to have small fall velocities, the vertical distribution is then almost uniform. In other words, the fall velocity is considered negligible compared to the velocity of the flow and it is called Homogenous flow, as seen in Figure 14a.

It is important to notice that not always the most flawless and without any kind of settlement flow is considered the optimal one. The focus consists on achieving the best

cost/effective relationship. This way, some projects are designed to account with some settlement or blockage of the cross-sectional pipe area.

Craven (1951), conducted series of experiments with three uniform sands having median diameters of 0.25 mm (0.0008 ft), 0.58 mm (0.0019 ft) and 1.62 mm (0.0053 ft). He found out that for high values of relative transport $\left({}^{Q_s}/_{Q}\right)$, the Darcy's hydraulic gradient (*i*) was given by the relationship displayed in Equation (Figure 1616).

$$i = \frac{dh}{dx} = C_3 \left(\frac{Q_s}{Q}\right)^{2/3} \tag{16}$$

where Q_s is the absolute rate of sediment transport and

$$C_3 = \begin{cases} \frac{1}{1.65}[(\gamma_s - \gamma_w)/\gamma_w], for\ sediments\ with\ 0.58\ and\ 1.62\ mm\ sands \\ \frac{0.6}{1.65}[(\gamma_s - \gamma_w)/\gamma_w], for\ sediments\ with\ 0.25\ mm\ sands \end{cases} \tag{17}$$

Another set of experiments was conducted by Vallentine (1955) in which he studied non-uniform sands of diameters equal to 0.53 mm (0.0017 ft) and 1.05 mm (0.0034 ft). The Darcy's hydraulic gradient may be written as in Equation (18).

$$i = \frac{fQ^2}{8gd^5}\psi(B) \tag{18}$$

where $\psi(B)$ is called the blockage function and it is approximated by Equation (19), whose function is plotted in Figure 15.

$$B = \emptyset\left[\frac{Q}{d^{2.5}}\sqrt{\frac{\rho}{\gamma_s - \gamma_w}}\left(\frac{Q_s}{Q}\right)^{-1/3}\right] \tag{19}$$

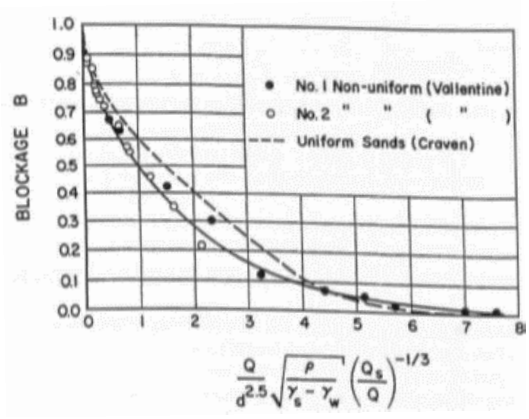

Figure 15: Representation of the Blockage function variation for non-uniform and uniform sands. (After Vallentine, 1955)

Head Losses

Calculating the head losses in a system is something that must be done carefully, since, from an economic standpoint; the power required by the system is proportional to the head loss and is a key factor for the system design. Figure 16 shows the relationship between the head loss and the mean velocity of mixture for different sediment concentrations.

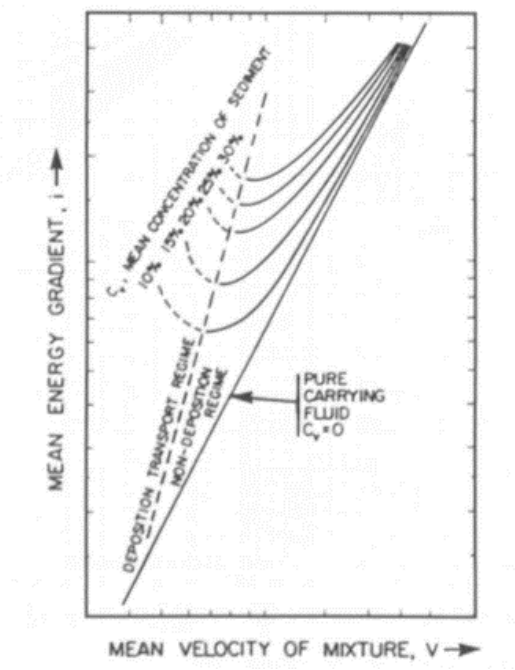

Figure 16: Representation of the head loss variation for increasing mean velocities of the mixture. (After Shen, et. al., 1970)

These curves correspond to the pattern followed for different mixtures, sediment characteristics and pipe configurations. On the left side of the dashed line are the points (concentrations of sediments) that are likely to settle, whereas on the right side of the line are the points that follow a non-deposition regime flow.

It is important to notice that there is a minimum head loss, occurring at a certain mean velocity, associated with each mixture concentration. This velocity is often called in the literature as deposit velocity, economical velocity, critical velocity, etc. In this research, the author decided to use the third name for practical reasons.

Head Loss due to Friction for Slurry Flows

According to Wilson, et. al. (2006), for a system that features a heterogeneous flow, the head loss per unit length of the pipe can be calculated as in Equation (20).

$$i_m = \frac{fV^2}{2gD} + 0.22(SG_s - 1){V_{50}}^{1.7} C_v V^{-1.7} \tag{20}$$

where f is the friction factor, V is the slurry mean velocity, D is the pipe inside diameter, C_v is the concentrations of solids by volume and V_{50} is a parameter that correlates the impact of the suspension mechanisms for the carrier fluid and the hydrodynamic lift acting on sediments larger than the sub-layer thickness in the near-wall region (Albar, 2000) and can be defined as Equation (21).

$$V_{50} = w\sqrt{\frac{8}{f}} cosh\left[\frac{60d}{D}\right] \tag{21}$$

where d is the median particle diameter and D is the inside pipe diameter. In the equation above w is a parameter associated with heterogeneous flows, which has dimensions of velocities and it is defined as:

$$w = 0.9 \cdot v_t + 2.7\left[\frac{(\rho_s - \rho_f)g\mu}{{\rho_f}^2}\right]^{1/3} \tag{22}$$

where v_t is the terminal velocity of the particle and ρ_s and ρ_f are the densities of the solids and fluid, respectively. For the total head loss due to friction to be computed, the head loss per unit length must be multiplied by the length of the pipe (L), as shown in Equation (23).

$$h_m = L \cdot i_m \tag{23}$$

Schiller (1992) developed the empirical equation below for the settling velocity (v_t) as function of d_{50}, which is the median grain diameter, based on sieve analysis and given in millimeters.

$$v_t = 134.14 \cdot \ (d_{50} - 0.039)^{0.972} \tag{24}$$

Production

According to Hayes, et. al. (2000), the production of the cutterhead dredge is highly dependent on physical and operational characteristics, such as: the total plant length, the ladder length, the pump horsepower, the cutter diameter, the cutter length, the swing width, the rotation speed of the cutter, the sediment removal thickness, the swing speed, the maximum dredging depth and the flow rate. Environmental aspects, such as the composition of the material to be dredged, also have a great impact on the operation performance.

The production of dredging operations is often measured by production meters that are composed of a velocity meter and a densitometer. A display installed on the control

panel is responsible for showing the output of both gages in units of mass rates (usually $yd^3/_{hr}$, $m^3/_{hr}$, $ft^3/_{hr}$ and $ton/_{hr}$).

According to Randall (2016), the calculation of the estimated production for each set of tests is given by Equation (25).

$$P\left(\frac{yd^3}{hr}\right) = 0.297 \cdot Q(GPM) \cdot C_v(\%) \tag{25}$$

where C_v is the concentration by volume and computed by Equation (14). Although the particle specific gravity for sand used in this research was 2.65, the specific gravity used to estimate production should correlate with the solids found in-situ, which is equal to 2.08.

Pump Requirements

A centrifugal pump works in such a way that it creates a low-pressure zone that is responsible for drawing the dredged material from the inlet section of the system into the suction flow.

When designing a centrifugal pump for a dredge, it is necessary to consider more factors than those customarily considered in the design of a regular centrifugal water pump (Herbich, 2000). A dredging system must account with many different variables that challenge the pump design process. For instance, centrifugal dredge pumps require that

sufficient clearances must be provided for a scenario where gravel, rocks, debris and other bodies go into the system without getting stuck and come to cause jamming.

The slurry composition is also an important parameter that has to be taken into consideration when choosing the centrifugal pump configuration, as the pump may have to overcome issues regarding mixtures with varying viscosities, such as mixtures of clay, silt and water.

When selecting the right pump for the systems it is important to consider three important quantities: the power input required (P); the efficiency of the pump (η); and the head produced (H). Each of these parameters is a function of the density (ρ), the angular velocity (ω), the discharge (Q), the impeller diameter (D) and the dynamic viscosity (μ). The head, H, also depends on the gravity, since it represents the shaft work per unit weight of the fluid, so it is convenient to write the product gH, given the fact this relationship is independent of the gravity.

$$gH = f_1\,(\rho, \omega, D, Q, \mu) \tag{26}$$

$$P = f_2(\rho, \omega, D, Q, \mu) \tag{27}$$

$$\eta = f_3(\rho, \omega, D, Q, \mu) \tag{28}$$

After a set of dimensional analyses performed by Herbich (2000), it was shown that the hydraulic power P_w could be written as:

$$P_w = SG_f \cdot Q \cdot H \tag{29}$$

where SG_f is the specific gravity of the fluid.

Pump Characteristics

The main parameters that are responsible for the characterization of the pump used in the dredging industry are the same as those used by the water pump industry, which are: the total head (H), the break horsepower (bhp), the efficiency (η) and the net positive suction head (NPSH).

The total head is calculated by the difference between the discharge head (H_d) and the suction head (H_d), as shown in Equation (30).

$$H = H_d - H_s \tag{30}$$

H_d and H_s have units of energy per pound of fluid (either $ft \cdot lb/lb$ or $m \cdot kg/kg$), which is the same as ft or m and can be calculated as in Equations (31) and (32).

$$H_d = \frac{p_d}{\gamma} + \frac{V_d^2}{2g} + z_d \tag{31}$$

$$H_s = \frac{p_s}{\gamma} + \frac{V_s^2}{2g} + z_s \tag{32}$$

where p refers to the pressure, V is the mean velocity, z is the elevation head with respect to the centerline of the pump and γ is the specific weight of the fluid. The subscripts d and s stand for discharge pipe and suction pipe, respectively. The efficiency of dredge pumps is one of the most important factors and should not be overlooked. It is usually defined as:

$$\eta = \frac{water\ horsepower}{brakehorsepower} = \frac{whp}{bhp} = \frac{\gamma HQ}{550bhp} \tag{33}$$

Other important parameter is the Net Positive Suction Head, which is usually defined as the difference between the total absolute head and the head due to the vapor pressure, as shown in Equation (34).

$$NPSH = \frac{P_a}{\gamma} + \frac{P_s}{\gamma} + \frac{V_s^2}{2g} - \frac{P_v}{\gamma} \tag{34}$$

where P_a is the local barometric pressure and P_v is the vapor pressure of the liquid. It is important to notice that the first three terms refer to the total absolute pressure and the last one is the term correspondent to the head due to the vapor pressure. The *NPSH* is also a head and is expressed accordingly in units of feet of pumped fluid.

Influence of Solid-Water Mixtures on the Performance of the Pump

According to Stepanoff (1964), the head in meters of a mixture at the best efficiency point should be the same as that for clear water, differing only by the additional hydraulic losses due to the presence of solids in pump passages. The efficiency of the system is given by Equation (35).

$$\frac{H_m}{H} = \frac{\eta_m}{\eta} \tag{35}$$

where H_m refers to the head of the mixture expressed in meters, H is the head of clear water, η_m is the efficiency when pumping a solid-water mixture and η is the efficiency when pumping clear water.

Considering a homogenous mixture the power of the pump ($bhp_{mixture}$) increases with an increasing specific gravity (*SG*).

$$bhp_{mixture} = (bhp) \cdot SG_{mixture} \tag{36}$$

Based on Equation (35) and on Equation (36) the relationship for the brake horsepower, head of clear water and mixture and the respective efficiencies is defined as:

$$\frac{bhp_{mixture}}{(bhp)SG_{mixture}} = \frac{H_{mixture}}{H_{water}} \cdot \frac{\eta_{water}}{\eta_{mixture}} \tag{37}$$

Cavitation Problems of Dredge Pumps

Problems due to cavitation are very common in hydraulic systems and have been challenging engineers since the beginning of the 20th century. Cavitation is defined as the process of formation and collapse of low-pressure vapor "cavities" in a flowing liquid. This phenomenon is responsible for causing serious damages to pumps, propellers, etc. and has a negative effect on the system's performance that may lead to economic problems. As discussed in Herbich (2000), the cavitation phenomenon can be broken down into four parts: the formation of the cavity; its travel through the system; its final implosion; and the consequence of the collapse.

The formation of cavities is more likely to occur in low-pressure regions. When adjusting the inflow speed the operator has to be concerned about the velocity field created, once, according to the Bernoulli equation, a high-velocity profile is responsible for decreasing the pressure that, in case it is reduced to the same pressure of the vapor pressure at the same temperature, will likely give origin to cavities. Not only a high-speed/low-pressure profile induces the cavitation process, but also an abrupt change in directions, vortices, eddies, flow curvatures and separation of flow lead to the aforementioned problem.

When travelling downstream into a higher-pressure zone, the bubbles tend to collapse, which leads to tremendously high-localized pressures. These cavities have usually an irregular shape and contain droplets of fluid mixed with the bubbles. Upon the collapsing of these cavities, the liquid rushes with an enormous velocity into the voids causing the droplets to be shot at the wall's surface, which results, not only in a deformation of the material, but also produces a localized high-pressure that is transmitted radially outward with a velocity proportional to the speed of sound. These cavitation consequences are responsible for setting up forced vibration on the structure and the repeated stress reversals are a cause that leads the structure to fail by fatigue.

Cavitation in dredge pumps cannot be quantitatively determined, since it is difficult to determine the exact spots inside the system that are going to be affected by issues of this kind. Cavitation reportedly causes undesired noises, vibration, reduction of performance and even damage to metal passageways. Experimental analysis turns out to

be highly suggested in order to set the upper threshold, below which the cavitation process does not take place. According to Herbich (2000), many factors, such as vapor pressure, head and Net Positive Suction Head are responsible for giving origin to this problem and should be carefully studied.

The *NPSH* is considered one of the most important parameters when dealing with cavitation problems. As explained before, the Net Positive Suction Head (*NPSH*) is the absolute head available to the pump above the vapor pressure and is computed as shown in Equation (34).

As discussed in Herbich (2000), incipient cavitation is formed if the centrifugal pump operates below the critical *NPSH*, which is the value of the minimum Net Positive Suction Head below which cavitation will occur and the total head will be reduced by a certain value ΔH, what will lead to a decrease in the performance.

$$NPSH_p = NPSH_c + \Delta NPSH \tag{38}$$

where $NPSH_p$ is the plant *NPSH*, $NPSH_c$ is the critical Net Positive Suction Head and $\Delta NPSH$ is the associated variation of the *NPSH* because of the head loss due to cavitation. In other words, this equation states that the available *NPSH* should not be less than the *NPSH* required by the pump; otherwise, the pump will likely suffer from cavitation problems.

Basco (1971) presented a method for determining the available *NPSH* for dredging operations, in which the pump was located below the water surface and the suction pipeline was equipped with either a cutterhead or a draghead.

For that study, Basco (1971) chose two different points, at the entrance of the suction line and right before the main pump, and wrote the energy equation, which is expressed in feet or meter of mixture, accordingly.

$$\frac{P_1}{\gamma_m} + \frac{V_1^2}{2g} + \frac{z_1}{S.G._m} = \frac{P_2}{\gamma_m} + \frac{V_2^2}{2g} + \frac{z_2}{S.G._m} + h_l \qquad (39)$$

where P/γ_m is the pressure head in foot-pounds per pound of mixture,

$V^2/2g =$ velocity head in foot-pounds per pound of liquid.

$Z/S.G._m =$ the elevation head in foot-pounds per pound of mixture.

$h_l =$ the head loss between both points in foot-pounds of water per pound of mixture.

$S.G._m = \frac{\gamma_m}{\gamma_w} =$ is the specific gravity of the mixture (specific weight of the mixture divided by the specific weight of the water).

The subscripts 1 and 2 refer to spots where the flow was evaluated. In this research, they were taken at the entrance of the suction inlet and right before the centrifugal pump, respectively.

Basco found out that the available *NPSH* could be calculated as:

$$Available\ NPSH = \frac{P_a}{\gamma_m} - \frac{P_v}{\gamma_m} + \frac{d}{S.G._m} + z_2 - h_l \quad (40)$$

where *d* is the cutting depth set by the user during dredging operations and the subscripts *a* and *v* refer to atmospheric conditions and to vapor, respectively.

The *NPSH* at the suction side of the pump is defined as:

$$NPSH = H_a + \frac{P_s}{\gamma} + \frac{V_s^2}{2g} - h_v \quad (41)$$

where H_a is the atmospheric pressure in feet of liquid $\left(= {}^{P_a}/_{\gamma_m}\right)$, P_s refers to the suction pressure, ${}^{V_s^2}/_{2g}$ refers to the velocity head at the entrance of the suction line (in feet or meter of liquid) and h_v is the vapor pressure in feet of liquid $\left(= {}^{P_v}/_{\gamma_m}\right)$.

Influence of the Operating Parameters on Dredging Operations

It is known that many factors play an important role in dredging operations, which must be well understood and wisely handled. According to Hayes et. al. (2000) and as previously indicated here, the most influencing parameters in general dredging operations for cutterhead suction dredges are: the rotational speed of the cutter head and its power; the swing speed of the ladder arm; the size of the slurry constituent particles; the depth of the dredging operation and its cutting thickness; the properties of the soil; the flow rate at which the operation is being performed; and, mainly in deep-water dredging, the environmental conditions.

Influence of the Flow Rate on Dredging Operations

A proper selection of the operating flow rates in dredging operations is one of the most important stages of the conceptual planning phase, since it affects dramatically the overall production and consequently the overall cost estimation.

According to Henriksen (2009), an increase in the production is expected with an increase in the flow velocities, which could be verified with a decrease in the turbidity levels seen around the cutterhead. This phenomenon can be explained by the fact that with higher values of flow rates the near-field, i.e. the flow field around the cutterhead, accounts with relatively greater suction forces in comparison to the centrifugal forces induced by the cutterhead rotational speed onto the sediments around. Nevertheless, Henriksen (2009) reported that for extremely high flow rates an increase in the spillage was observed due to the high level of turbulence, which was also responsible for enhancing the rate of turbulent diffusion. As discussed in Henriksen (2009), there would be an optimum ratio between the cutterhead rotation speed and the flow rate, for both undercutting and overcutting, beyond which the axial forces caused by the centrifugal pump suction pressure would be outweighed by the existing centrifugal forces and spillage would likely occur.

$$\frac{\omega R_c}{V_i} = 0.42 \tag{42}$$

where ω is the rotational speed, R_c is the cutterhead radius and V_i is the suction intake velocity.

In order to achieve the highest production it should be desired to increase the flow rate up to a limit, which there would be no solid resuspension and consequently no losses, which means a higher specific gravity in the ‘produced’ dredged material. Nonetheless, with an increase in the flow rates it is also expected that an increase in minor losses through the system would occur, which should be taken into consideration during the project planning and equipment design phases.

The influence of the flow velocities on the minor losses of the system was investigated at some extent on experiments done by Girani (2014) in which he identified the positive relationship between the inflow velocities and the minor losses because of the placement of a screen at the cutter head suction inlet. According to Girani (2014), higher values of specific gravity were responsible for higher losses due to the fixed screen. These losses were seen to be less pronounced for higher specific gravities, as can be seen in Figure 17.

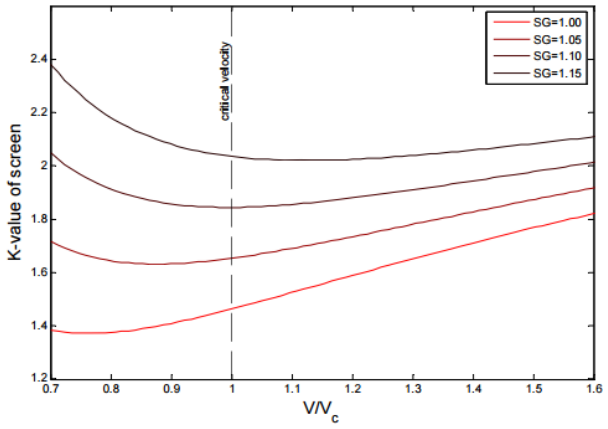

Figure 17: Representation of the Minor Loss Coefficient as function of non-dimensional velocities for specific gravities ranging from 1.00 to 1.15 (After Girani, 2014).

The k-values for the various Specific Gravities tend to converge to a common point at a velocity approximately 1.6 times higher than the critical velocity, which is an important parameter when selecting the operational flow rate. For greater specific gravities, the k-value is higher for velocities below the critical velocity, which can be explained by the fact that at that flow rate the particles would tend to settle around the suction inlet, which would result in greater k-values, due to friction.

Effect of Flow Rates on the Production and Specific Gravity

The effects of a change in the values for the nominal flow rates were compared to the specific gravity of the slurry produced and the estimated production. Across the literature, this author found an intense correlation between the flow rate and the production. Conventionally, in dredging operations, for an increase in the operational flow

rate a higher production is normally expected. However, according to Ogorodnikov, et al. (1987), a threshold exists.

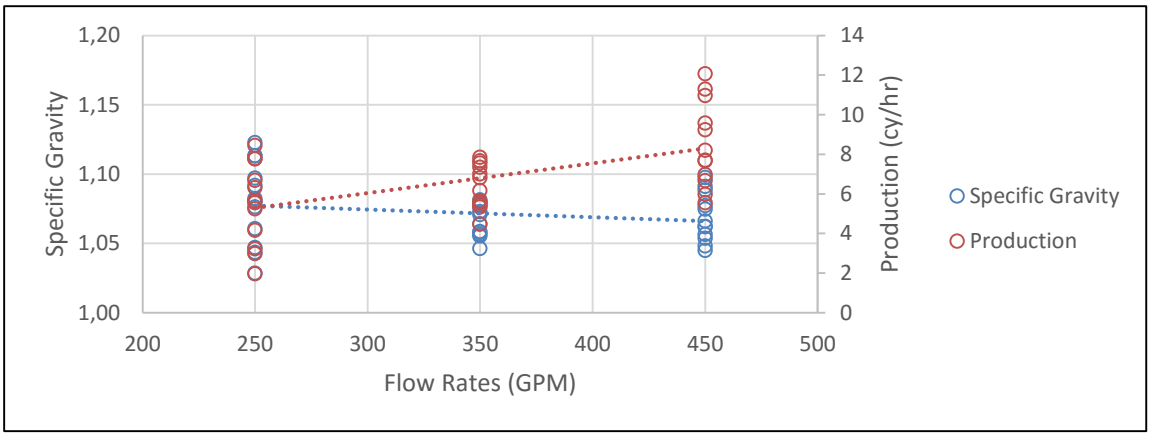

Figure 18: Variation of the specific gravity and production across the investigated nominal flow rates.

The plot displayed in Figure 18 shows the behavior of the average specific gravity of the dredged material (SG_m) and the respective production (cy/hour) across increasing values of the nominal flow rate used in the set of experiments. The author observed that a greater flow rate would indeed result in a higher production, given the associated higher pumping capabilities, but it would also lead to a decrease in the produced material specific gravity. Although the slightly negative relationship with the specific gravity, this observation is of great importance regarding the determination of the optimum flow rate, i.e the flow rate that would maximize the production and the produced specific gravity.

The decreasing trend presented by the specific gravity suggests that the highest values for this parameter would be found at lower nominal flow rates. This fact is indeed true. The highest values of specific gravities were observed for a nominal flow rate of 250

GPM. Not only greater flow rates contributed for a decrease in the produced specific gravity, but they also masked the changes in the other operational parameters and the minor losses due to placement of the screen. This author suggests that one of the reasons that might have led to this event was the induced turbulence given the operating high velocities. The author will better explain these phenomena over the following chapters.

Influence of the Cutter Head on Dredging Operations

As previously mentioned, two of the most important parameters for cutterhead dredge operations are the power of the cutter head and the rotational speed of the cutter. Not many information on how variations of the cutter head rotational speed would affect the nearby flow field were found in the literature, which turns this topic into a potential theme for future studies. As investigated in Lewis (2014) and also witnessed in this research, higher cutter head rotational speeds are responsible for spillage, which would cause losses to the overall production and must be avoided in real world operations at all costs.

The Cutting Power

The minimal power used to cut a determined type of soil is essentially a function of the soil and can be translated as the Specific Cutting Energy (*SPE*), which is basically the work needed to cut a m^3 of soil or, in other words, the Power (*P*) required to maintain a desired production Q_{cutter} (Vlasblom, 2005).

$$SPE = \frac{P_{cutter}}{Q_{cutter}} \left[\frac{N}{m^2}\right] \quad (43)$$

Given the fact that, because of the intrinsic variability of the soil, to maintain a constant cutting power across the whole dredging operation is unrealistic, the terms "average cutting force" and "peak force" are more often used. According to Vlasblom (2005), the peak forces for rocks may be twice higher than the average forces.

Table 1 presents the factor by which the *SPE* must be multiplied in order to secure operations.

Table 1: Factor ranges for the respective dredged material.

$\frac{F_{peak}}{F_{avg}} = 1.5 \sim 2$	Mostly used for rocks
$\frac{F_{peak}}{F_{avg}} = 1.25 \sim 1.5$	Mostly used for sand
$\frac{F_{peak}}{F_{avg}} = 1.1 \sim 1.5$	Mostly used for clay-type sediments

Cutterhead Rotational Cutting Speed

Henriksen (2009) conducted a study to investigate the influence of variations of the cutter head speed in the near-field and concluded that the rotational speed of the cutterhead and the turbidity are positively related, which means that higher rotational

speeds are generally responsible for more sediment spillage. Such phenomenon was observed in this research for the range of rotational speeds investigated.

den Burger (1999) concluded through experimental researches that there is indeed a point where the production is maximized, which can also be considered a threshold. Figure 19 indicates that greater values for the cutter head speed lead to a higher production for a single mixture velocity up to a point where the production is then maximized. den Burger (1999) fitted a curve through the experiment data points for five different velocities investigated in his tests.

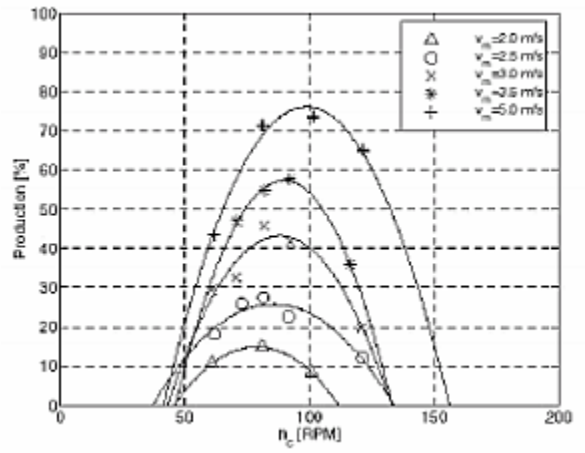

Figure 19: Evolution of the production (%) as function of cutterhead RPMs for various velocities (After den Burger, 2003).

The first half of the chart shows a positive relationship between the cutter head rotational speed and the production, which is only kicked off around the 50 RPM mark. This is due to the fact that at lower rotational speeds the gravitational forces acting on the sediment particles are greater than the centrifugal forces induced by the cutterhead

rotation. This characteristic contributes for the settlement of particles at the lowest point of the cutterhead, which makes them not to be properly mixed and in consequence not to flow into the system. The relationship between the rotational speed and the production are because of the better mixture of the sediments caused by their collisions with the blades of the cutter head (den Burger, 1999). A positive trend for higher mixture velocities is also presented in the graphic and better clarified in Figure 20.

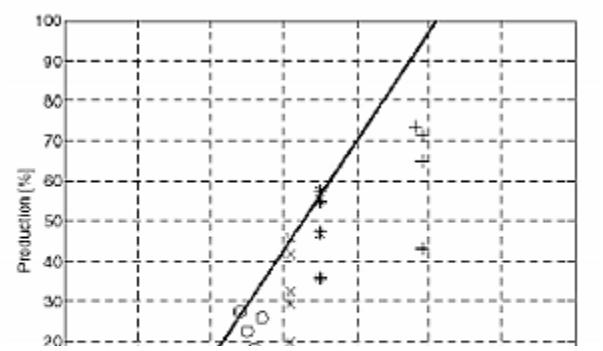

Figure 20: Variation in the production (%) as function of the mixture velocities (After den Burger, 2003).

According to den Burger (1999), the increase of maximum production with increasing values of mixture velocities follows a linear pattern across the lower velocities range, whereas for higher velocity values this pattern is not representative anymore.

The second half of Figure 19 can be explained by the fact that the extremely high rotational speeds caused the centrifugal force to outweigh both the gravitational and the drag forces. This phenomenon is responsible for causing the particles to segregate and be thrown out of the cutterhead near-field. Moreover, this induced flow field is also responsible for creating an effect that den Burger (1999) describes as a '*pump effect'*,

which causes the enhancement of this outgoing flow, while the suction flow rate remains constant. This configuration is propitious for leading the particles away from the suction region, which in turns results in a lower specific gravity of the dredged material.

An important consideration when analyzing the data from den Burger's set of experiments is that they were performed for a certain type of sediments with a specific grain size. The results presented above are intended to serve as a trend analysis, since the sediments at the Haynes Laboratory used for this research are significantly smaller than those used by den Burger (1999), which were mainly cemented gravels. This grain size difference has a direct effect on the near-field forces, i.e. the gravitational forces and centrifugal forces induced by the cutter head over the particles are difference. Another issue with these experiments, which also leads to some level of disagreement, is related to the angle of the ladder arm, which was set to 45º and described as an *"unfavorable situation in practice".* In the present research, the ladder arm was adjusted for an angle of 30º, which were concluded to be a much better configuration in terms of productivity.

In an attempt to quantify the level of disagreement between the sediment type and the ladder arm angle used by den Burger (1999), these parameters were plotted along the results for sand particles against the dimensionless flow number $\frac{Q}{wR^3}$ and presented in Figure 21.

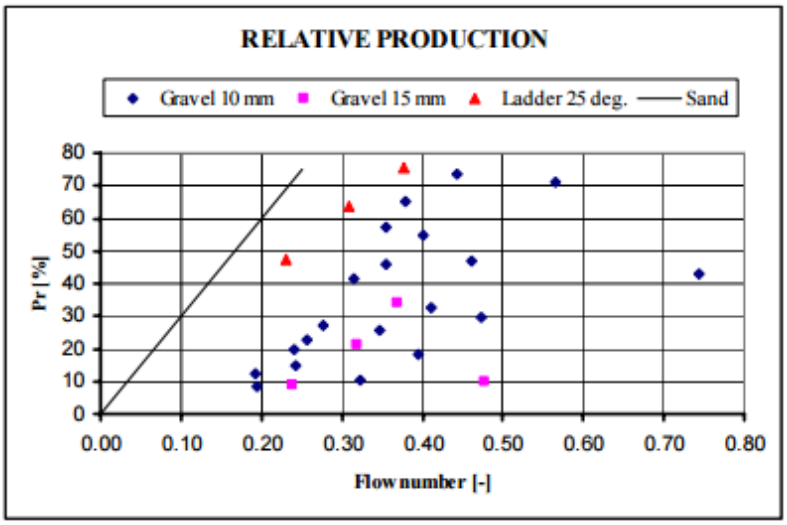

Figure 21: Relative production for different types of materials as function of the non-dimensional flow number $\left(\frac{Q}{wR^3}\right)$ *(After Vlasblom, 2005).*

The results presented by Vlasblom (2005) show the tremendous difference between the two types of sediments such as the existing disagreement for different ladder angle configurations.

More information is needed in this field for a better understanding of the disturbances created by greater cutter head rotational speeds at the flow field around the suction inlet, since all the information available suggest that the higher the rotational speeds the greater is the sediment spillage.

Effect of Cutterhead Rotational Speeds on the Production and Specific Gravity

The analysis of the effect of the rotational speed on the production is also important in order to achieve the conceptual project that would maximize the operation the most.

The plot in Figure 22 shows that variations of the cutterhead rotational speed had almost no influence neither on the production rate, nor on the specific gravity of the slurry. The author believes that this weak correlation was due to the turbulent environment induced by the high velocities flow field. More studies are required to further investigate this hypothesis and to better understand of the behavior of specific gravity and production with changes of this operational parameter within high velocities flow fields.

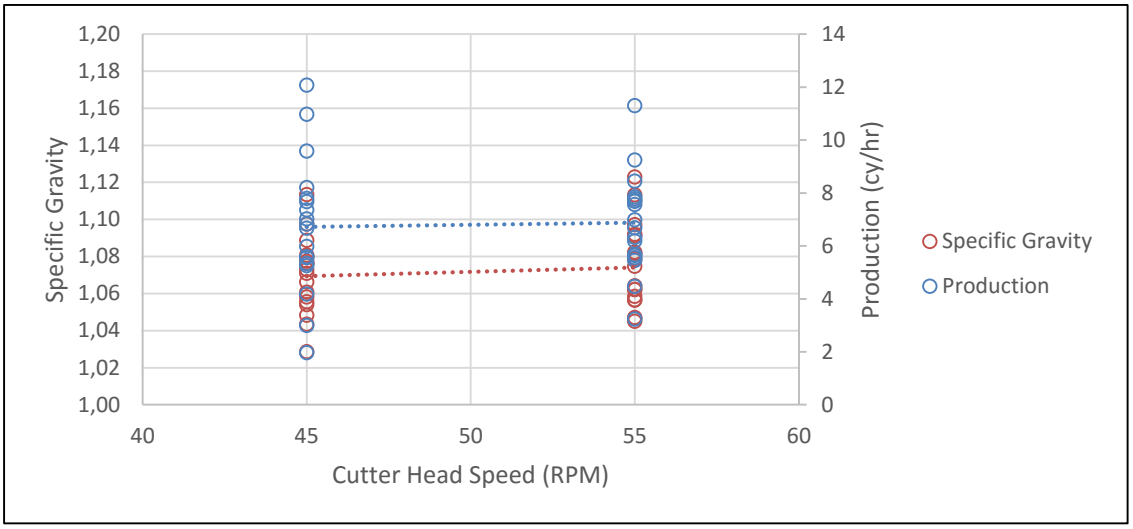

Figure 22: Variation of the specific gravity and production for an averaged flow rate across the nominal cutterhead rotational speeds.

Intending to investigate the influence of the cutterhead RPMs with the employed operating flow rates, the author plotted in Figure 23 a chart for the same parameter, but, this time, for only the 250 GPM flow rate.

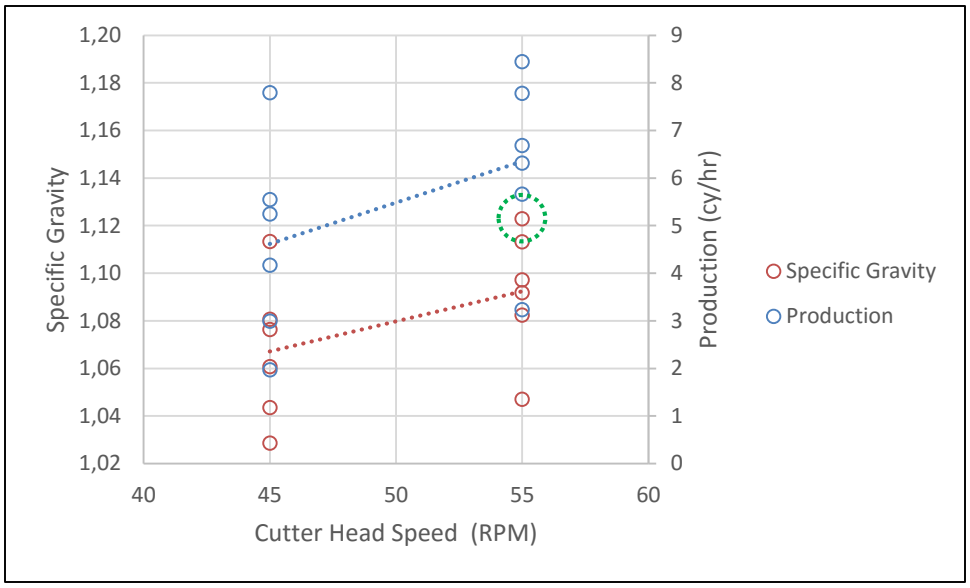

Figure 23: Variation of the specific gravity and production for the 250 GPM flow rate across the nominal cutterhead rotational speeds.

The results from the observations showed a much steeper trend for the specific gravity and production for both studied RPMs. The author concluded, then, that for lower flow rates a change in the cutterhead rotational speed had a much greater influence over production and specific gravity than when under higher flow rates. The data point circled with a green dashed line represents actually the point with the greatest specific gravity found throughout the experiments, which is the result from a test with the ladder arm swing speed set to 3 in/s, which also presented a close relationship with the production and will be discussed on the next section.

Even though the results presented in this section are positively correlated to the ones observed in Lewis (2014), it becomes clear the low specific gravity values found in this research. The specific gravity of the slurry on his set of experiments ranged from 1.08

to 1.20, whereas on this research the highest specific gravity found was equal to 1.13. This fact can be particularly explained by the turbulent environment caused by the high velocities that were responsible for dispersing the sediments rather than removing them from the seabed. This author is sure that if more experiments across a wider range of velocities were conducted at the Haynes Laboratory, this trend would be more clearly observed.

Influence of the Ladder Arm Swing Speeds on Dredging Operations

Upon the initiation of dredging operations, there are two working methods of the dredge that depends on the direction of the cut, which are called undercutting and overcutting.

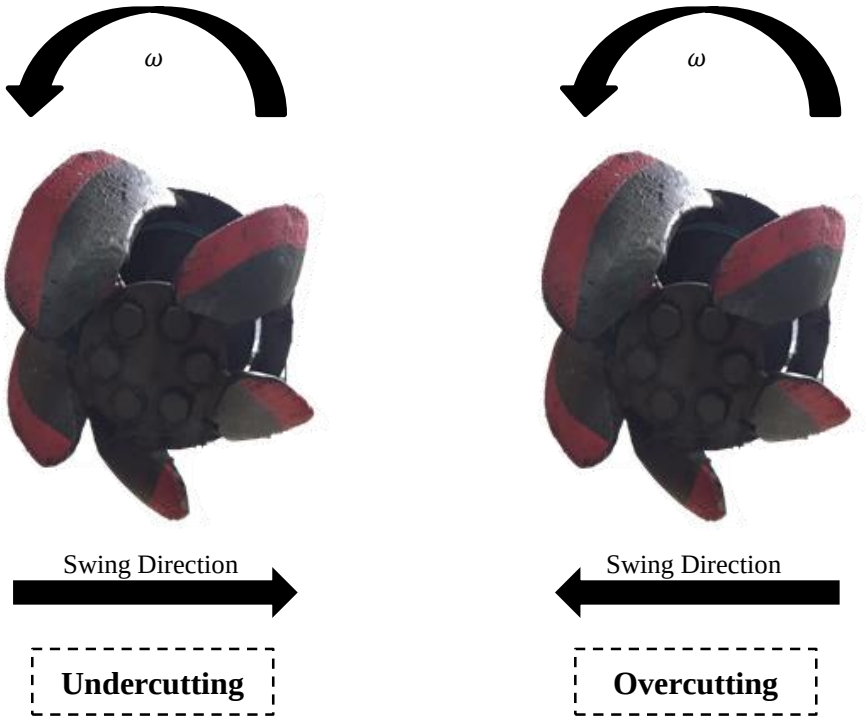

Figure 24: Schematic drawing of the Undercutting and Overcutting dredging methods.

Reports in the literature suggest that the undercutting mode is responsible for achieving greater net production than overcutting, i.e. increasing the specific gravity of the slurry. Selecting the better method of cut to be employed on the operation is a task that demands knowledge of the environment under consideration. According to Bray (1979), when the operation is being executed in an environment with the presence of hard material, the best method to be implemented is the 'undercutting', while both methods are suitable for soft material. It is also important to consider, when selecting the swing speeds, the forces exerted by the soil onto the ladder arm in order not to cause damage to the equipment.

Very few data could be found relating the swing speed of the dredge's ladder arm with productivity and spillage. Most of the results found in the literature, when relating the production rate with the swinging movement of the dragarm, also analyzed the influence of the cutting direction, i.e. undercutting *vs.* overcutting, which seems to influence more the operation's productivity than the swing rate itself.

According to Glover (2002), the higher the speed for the ladder arm, the greater the spillage would be and, as per definition, the greater the losses. Conversely, Slotta, et. al. (1977) found that there was an almost linear and positive relationship between the ladder arm swing speed and the production for any cutting direction. This evidence had been formerly shown by Yagi, et. al. (1975), which is displayed in Figure 25, where he compared the production on the y-axis, by means of a measurement of the solids concentrations, against a wide range of ladder arm swing speeds on the x-axis.

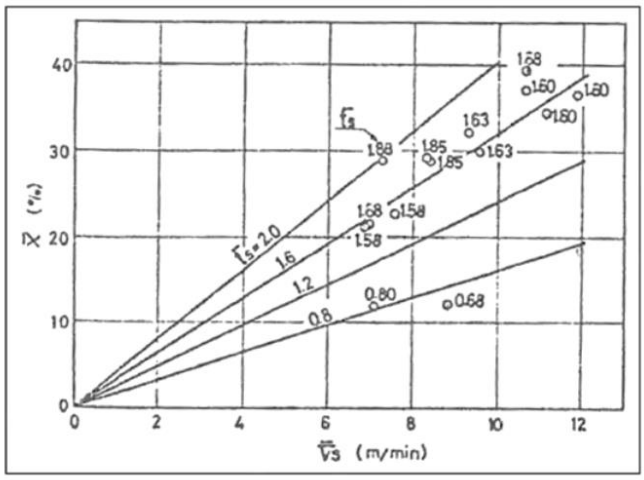

Figure 25: Variation of the production (%) for different cutting thicknesses as a function of the ladder arm swing speeds. (After Yagi, et. al., 1975).

Each of the lines plotted in the chart represents the results for four different cutting thicknesses: 0.8; 1.2; 1.6; and 2.0. The linear trend aforementioned can be easily identified along an also positive relation between the cutting width and the rate of production. Figure 25 should also serve the reader only as a comparison tool, once the sediments used in these experiments were classified as silt a clay, which have different behavior than the sand.

Experiments conducted by Mol (1977c), investigated the influence of undercutting and overcutting for sands, with $d_{50} = 120\ \mu m$, on the production rate. The results found for the swing speeds showed almost no correlation between the production rates and an increase in the ladder arm swing rates for overcutting, whereas when analyzing the same parameter for undercutting the positive relationship was confirmed and was attributed to the better mixing inherent of undercutting processes rather than for overcutting.

Regarding the sediment resuspension, a study done in Lavaca Bay concluded that there was an increase in the suspended solids due to an increase in the summation of the cutter head rotational speed and the ladder arm swing speeds. Upon analyses during overcutting-only processes it was evidenced that the sediments were relatively more resuspended, which strengthens the hypothesis that the production is smaller for this type of cutting method.

According to Slotta, et. al. (1977), the efficiency of the operation, i.e. the amount that goes into the suction inlet *vs*. the amount cut, is not related to the swing speed for overcutting processes and actually has a negative relationship with an increase in swing speed for undercutting.

More studies in the area are needed to better understand the effects of the variation of the ladder arm swing speeds during undercutting and overcutting processes not only on the production, but also on the sediment resuspension and other losses.

Effect of Ladder Arm Swing Speeds on the Production and Specific Gravity

The ladder arm swing speed was the last parameter investigated. The plot in Figure 26 shows that for the set of experiments conducted at the Haynes Laboratory, no major relationship was found between variations of the swing speed and changes on production and specific gravity. Given the extensive literature confirming the positive relationship between the specific gravity and the production with increasing values of the ladder arm swing speed, the author suggests that its effects on production and specific gravity were

hindered by both high cutterhead rotational speeds and high suction velocities induced by the operating flow rates.

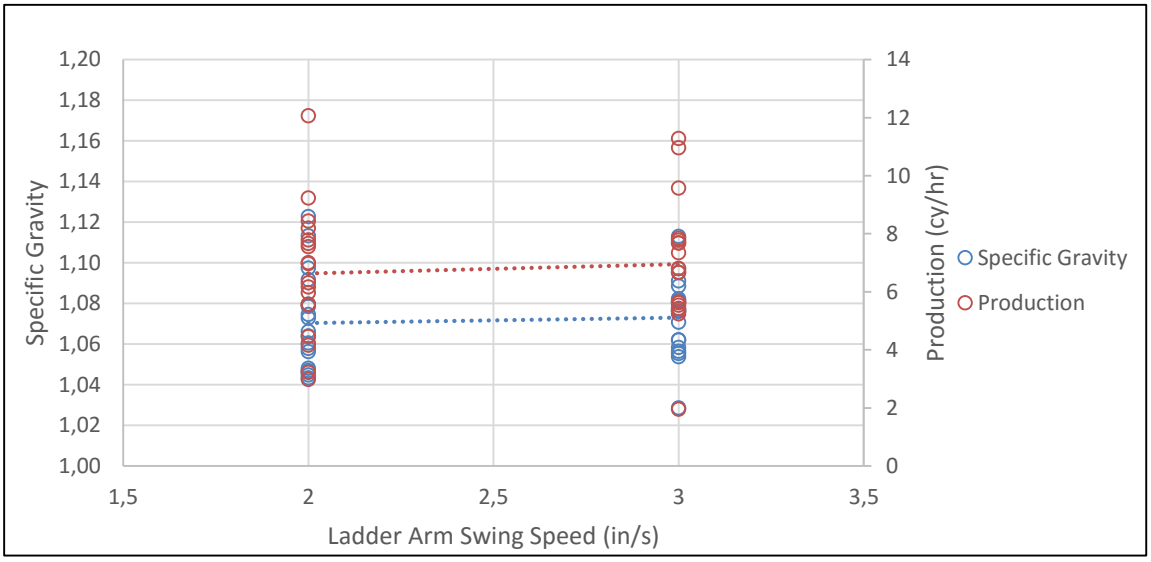

Figure 26: Variation of the specific gravity and the production for an averaged flow rate as function of the ladder arm swing speed.

To verify the aforementioned statement, this author plotted the same chart but this time, only for the 250 GPM as can be seen in Figure 27.

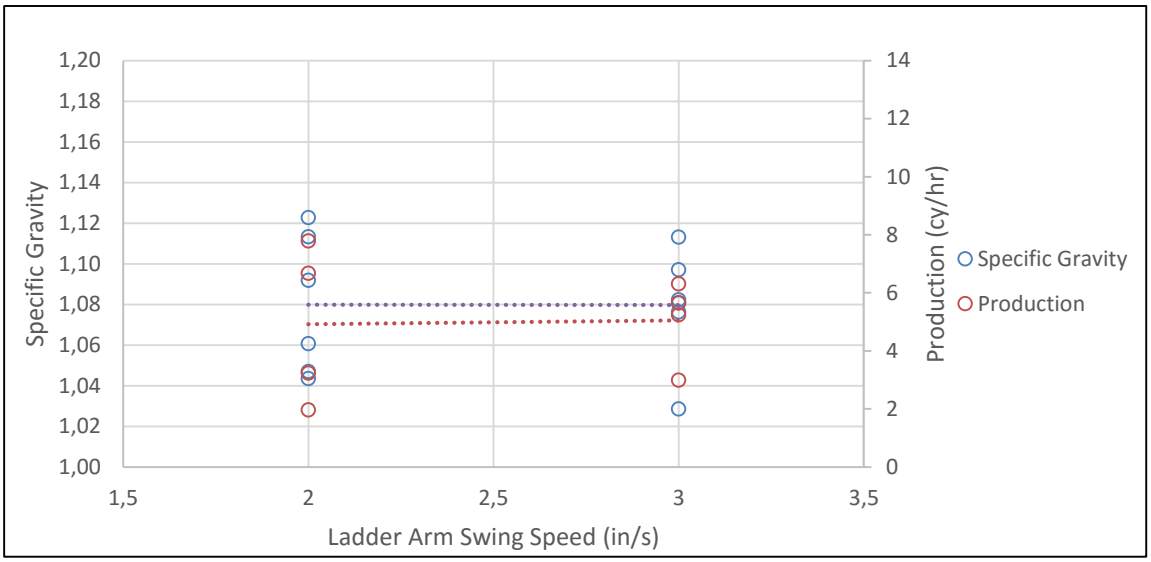

Figure 27: Variation of the specific gravity and the production for the 250 GPM flow rate as a function of the ladder arm swing speed.

It is observed that also for the minimum flow rate, there was no connection between the ladder arm swing speed and both production and specific gravity. A hypothesis for this phenomenon is regarding the magnitude of the velocities on the y-direction. According to Henriksen (2009), the study at Lavaca Bay concluded that the summation of the cutter head rotational speeds and the ladder arm swing speeds induced the sediment resuspension. Hence, an increase of the ladder arm swing speeds in a high velocity environment would not necessarily result in a greater production. In fact, an increase in the velocities in an already turbulent flow field would actually contribute positively for the observed spillage.

CHAPTER IV

EXPERIMENTAL SETUP

Model Dredge Scaling

In any set of experimental tests, the scaling of the involved parameters is of great importance if the applicability in the real world of the observed results is something desired. For dredging operations, some key parameters must be investigated and properly scaled if the use of a model dredge is intended. For experimental studies on a cutter suction dredge the variables to be considered are: the diameter of the cutterhead; the rotational speed of the cutter; the swing speed of the ladder arm; the grain size; and the induced suction velocity. Glover (2002) designed the cutterhead suction dredge available at the Haynes Laboratory in which he made use of the scaling equations to compute the system's dimensions. Coming up with an ideal scaling ratio has been always a challenge in research conducted with model dredges, since some inherent characteristics of the model are not easily scaled, such as: the water depth; the suction line length; the pump elevation above the water level; and the sediment grain size. As the time went by many researches proposed scaling laws, which were results from both dimensional calculations and their further comparison with experimental data. These scaling laws are characterized by similarity with respect either to Reynold or to Froude relationship (Randall, 2016).

According to various dredge model studies conducted by Slotta (1968), Joanknecht (1976), Brahme and Herbich (1986) and den Burger (1997), the scaling laws can be

classified into three mains groups: based on similarity with the sediment pick-up behavior, based on similarity with a non-dimensional number (Froude or Reynolds) and based on similarity to cavitation during the cutting process.

Given the fact the flows taking place at this research are mostly confined, the scaling equations used to model the selection of the flow rates, cutterhead rotational speeds and ladder arm swing speeds follow the kinematic scaling (related to the Froude number) and are given by Equations (49), (45) and (46).

$$Q_{model} = Q_{prototype}\left[\frac{(D_{cutter})_{model}}{(D_{cutter})_{prototype}}\right]^{5/2}, for\ flow\ rates \tag{44}$$

$$\omega_{model} = \omega_{prototype}\left[\frac{(D_{cutter})_{prototype}}{(D_{cutter})_{model}}\right]^{1/2}, for\ cutterhead\ rotational\ speeds \tag{45}$$

$$(V_L)_{model} = (V_L)_{prototype}\left[\frac{(D_{cutter})_{model}}{(D_{cutter})_{prototype}}\right]^{1/2}, for\ ladder\ arm\ swing\ speeds \tag{46}$$

Choice of the Flow Rates

For choosing the flow rates to be employed the author had to take into consideration the settling velocity of the particles present in the sediment pit, which would be subject to the dredging operations. The critical velocity was determined to be equal to 1.88 m/s (6.17 ft/s), determined visually through the nomograph proposed by Wilson, et. al. (2006). The flow rate associated with the aforementioned velocity for the 4 in suction line diameter is 241 GPM (0.91 m^3/min). With that in mind, the author chose the 250 GPM (0.95 m^3/min) flow rate as the minimum limit. The two other flow rates tested were the 350 GPM (1.33 m^3/min) and 450 GPM (1.70 m^3/min). These values fit well the kinematic scaling model used by Glover (2002) on the design of the cutterhead dredge.

Choice of the Cutterhead Rotational Speeds

The selection of cutterhead RPMs to be employed on the set of experiments was the most challenging parameter to be determined. Lewis (2014) and Girani (2014) investigated rotational speed ranging from 15 RPM, which was considered too low, up to 45 RPM, which was concluded to be a rotational speed at which spillage was observed. Given the fact that one of the objectives of the present research was to validate previous results across new operating parameters values, this author chose to test cutterhead rotational speeds equal to 45 and 55 RPMs.

Choice of Ladder Arm Swing Speed

The choice of the Ladder Arm Swing Speed was also based on the kinematic scaling method used by Glover (2002) and the 2 in/s and 3 in/s swing speeds were employed throughout the set of experiments. It is recommended to maintain these velocities at relatively lower values in order to avoid major issues with the existing y-forces, which may cause some interference on the data measurements.

Cutterhead Scaling, Sediment Scaling and Water Depth Scaling

The cutterhead, sediments and the water depth could not be properly scaled due to the facility limitations. The cutterhead was donated to the University and was the only one available at the Laboratory. It accounts for a scale ration equal to 1:4, which would not meet the desired geometric ratio of 1:10 proposed by Glover (2002). The sediment choice was also limited to the laboratory availability. The tank of water was also a parameter that could not be changed and did not meet the desired 1:10 geometric scale, since its depth is something that cannot be changed and resulted in a scale equal to 1:8.

The model dredge located at the Texas A&M University's Reta and Bill Haynes Laboratory '46 Coastal Engineering Laboratory is suitable for researches using a 1:10 scale and was designed by Glover (2002), in which he used of a 76.2 cm (30 in) cutter suction dredge as reference. A summary of the parameters used in the experimental measurements is shown in Table 2 next to a potential real world prototype.

Table 2: Summary of the investigated operational parameters for a prototype and the model dredge.

Operational Parameters	**Prototype**	**Model**	**Scale**
Cutter Diameter	163 cm (64 in)	40.6 cm (16 in)	1:4
Water Depth	12.2 m (40 ft.)	1.83 m (6 ft.)	1:8
Cutting Thickness	91.4 cm (36 in)	25.4 cm (10 in)	1:3.6
Grain Size	0.0005 m (0.00164 ft.)	0.0003 m (0.0009 ft)	1:2
Settling Velocity	0.06 m/s (0.207 ft/s)	0.03 m/s (0.108 ft/s)	1:2
Suction Diameter	101.6 cm (40 in)	10.2 cm (4 in)	1:10
Max Suction Flow Rate	54.51 m^3/min (14,400 GPM)	1.70 m^3/min (450 GPM)	0.031
Cutter Speed	22.5 to 27.5 RPMs	45 to 55 RPMs	2:1
Arm Swing Speed	10.2 to 15.2 cm/s (4 to 6 in/s)	5.1 to 7.6 cm/s (2 to 3)in/s	1:2

Haynes Laboratory Cutter Suction Model Dredge

The Haynes Coastal Engineering Laboratory has a model dredge situated in a tank with dimensions of 149.5 ft. in length (x-direction), 12 ft. in width (y-direction) and a depth of 10 ft. (z-direction). Within this tank is found a sediment pit, which is normally covered by metal plates for safety reasons. This pit is a 24.5 ft. long opening with a 5 ft. depth and is filled with sediment and water for dredging related researches.

Figure 28: Photo of the carriage connected to the barge in the tow tank.

As seen in Figure 28, on the top of the tank there is a rail, which guides the carriage through the x-direction. There, the operator, who is also responsible for setting the excavation patterns and the data output format, runs tools for monitoring and controlling

the unit. Also on the topside of the hydraulic system an important step for the data acquisition takes place; the homogenization of the flow. Many sensors such as, a nuclear density gauge and an electromagnetic flow meter are also installed on a vertical pipe located there.

The cutterhead model dredge is equipped with a ladder and an articulating arm, whose angle must be adjusted in accordance to the research requirements, so it matches the appropriate cutting thicknesses described on the project. At the end of the ladder arm the 12 in cutterhead and the 4 in suction line, which ends at the entrance of the centrifugal pump, are to be found. It is in this section where the screen is placed as can be seen in Figure 29b. Holding the suction line there is an articulated arm, whose angle can be adjusted by the operator and where a $GoPro^{®}$ camera was installed, so visual recordings of the operations could be done. The whole assembly can be seen in Figure 29a.

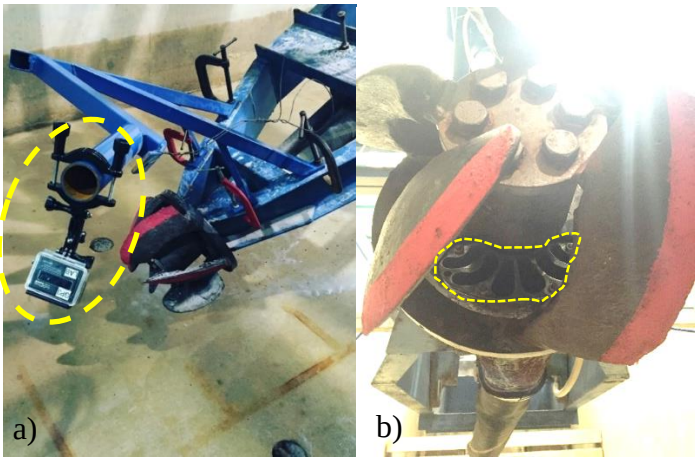

Figure 29: (a) GoPro® camera mounted over the cutterhead (yellow-dashed lines); (b) Bottom view of the cutterhead with screen 2 in place (yellow-dashed lines).

An electrical system powers the centrifugal pump that requires a priming pump to fill and keep the system with water before the main pump is properly started as shown in Figure 30a. An operator has to fill it with water from the top of the carriage to provide enough head to start the main pump.

Figure 30: (a) Operator starting the main pump through the utilization of a priming pump; (b) Location of the centrifugal pump (yellow-dashed lines).

This priming pump was installed there, since the main pump could not have been better placed, due to existing physical limitations. According to Randall, et. al. (2016), the lower the pump is placed in the water column, the more efficient it will be in terms of productivity. The centrifugal pump on the dredge has 14.9 kW (20 hp) and a 31 cm (12.2 in) vane diameter made by GIW Industries with connections to a 4 inches suction line and

3 inches discharge line. According to the maker, this pump is capable of working with a flow rate of 37.9 L/sec (600 GPM) when dredging only water. When pumping a mixture of sediments and water, the pump is supposed to work with an efficiency of 80% with a flow rate equal to 25.2 L/sec (400 GPM). Moreover, the dredge is attached to a hopper barge, as displayed in Figure 31, which is equipped with a 6 x 24 inches overflow weir that is responsible for keeping the level of the barge constant and for letting the excess of water (with no sediments) to be drained back to the tank.

On the bottom of the hopper barge, there are two manually operated doors, which can be opened by the operation of 33 kN winches installed with wire rope and chain, as displayed in Figure 31.

Figure 31: 3 in discharge line into the barge, which is equipped with two winches (yellow) and a weir (red).

The cutter head is located at the end of the suction line and consists of a 5-blade-device that is responsible for scooping up the sediment on the seabed and bringing it into suspension. The suction intake has a kidney-bean shaped inlet that vacuums in the suspended material into the 4 in (10.16 cm) suction line. It is on the top of this inlet entrance that fixed screens are installed. The dredged material travels through the line into the centrifugal pump and thereafter into the hopper barge or sand separator through the 7.62 cm (3 in) discharge line for further processing. Figure 32 shows two views side-by-side of the cutterhead, one from the top and from the front with its respective dimensions.

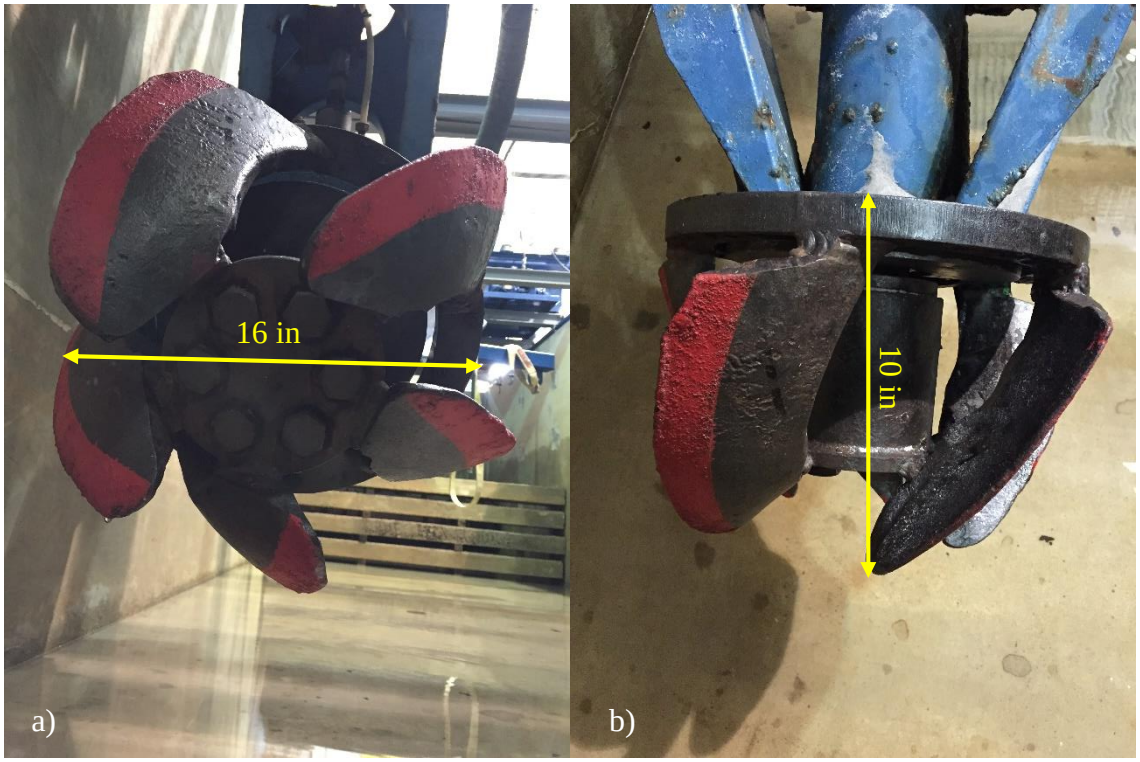

Figure 32: (a) Front view and diameter of the cutterhead; (b) Top view and length of the cutterhead.

Screen Configurations

As mentioned previously, the screen goes on top of the suction inlet entrance and is responsible for avoiding undesired material to be pumped into the system and, consequently , to cause major damages in the equipment. When installing a screen on the suction intake the reader may expect the system to experience head losses due to the reduction of the suction mouth opening.

In this research, the author sought to add additional results for a different screen opening percentage in comparison to the one investigated in Lewis (2014), and to propose a new screen configuration for the studied conditions. In this sense, the author chose one out of the three screens proposed by Lewis (2014) and came up with a new one. Both screens are displayed in Figure 33a and Figure 33b, respectively.

a) b)

Figure 33: (a) Screen 1 proposed by Lewis (2014) with a $\beta = 61.7\%$; (b) Screen 2 proposed by de Oliveira (2016) with a $\beta = 55\%$.

The screens were cut out of metal sheet by a CNC machine. It is important to say that the screen chosen has an opening area of 61.7% (or $\beta = 0.617$) (Figure 33a) and the

one with the new configuration has an opening area of 55% (or $\beta = 0.55$) of the total opening area (Figure 33b).

In the experiments Screen 0 was determined to be the no-screen situation, in which just a frame was plugged in the suction inlet and 100% of the suction mouth area was left open, whose area is equal to 90.32 cm² (14.00 in²).

Screen 1 was chosen to be the one from the former research carried out by Lewis, with an opening coefficient (β) equal to 0.617. Screen 2 was the one that the author came up with a correspondent β-value equal to 0.55.

Determination of the Opening Area Coefficient (β)

To determine the total area of the screen and to come up with a new configuration for a new screen the author scanned the metal screen, traced it and scaled it using SolidWorks 2015®, as shown in Figure 34. After this procedure has been undertaken, the area of openings and the total area of the screen could be measured and the β-coefficient, then, calculated using the equation below.

$$\beta = \frac{Total\ Area\ of\ Openings\ for\ a\ given\ Screen}{Total\ Area\ of\ Suction\ Entrance\ Area} \quad (47)$$

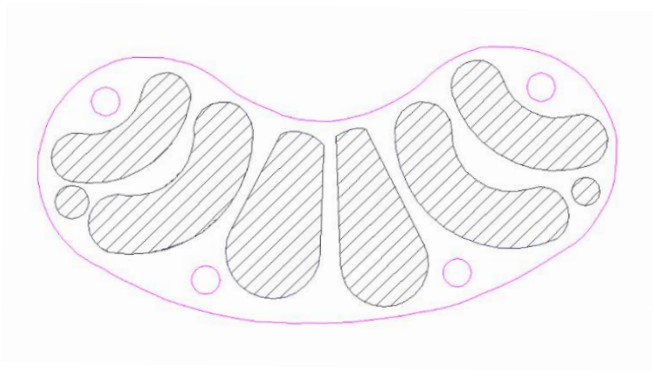

Figure 34: SolidWorks® model of the screen proposed by de Oliveira (2016).

Experiment Setup, Instrumentation and Data Acquisition

Sensors

Flow Meter

The flow meter (or velocity meter) is an important apparatus in dredging operations, since the calculation of the amount of dredged material is always a parameter to be considered.

The electromagnetic flow meter mounted on top of the dredge carriage operates under the induction law of Faraday, in other words, the voltage induced in a conductor moving at right angles through a magnetic field would be proportional to the same conductor's velocity through the field, as shown in Equation (53).

$$E(V) = K(H)V \tag{48}$$

where V is the velocity of the flow that causes the voltage E to appear. H is the strength of the magnetic field and K is the proportionality factor.

For a dredge, the fluid that passes through the pipelines is the conductor and as it flows across the magnetic lines created by the flowmeter, a voltage proportionally to its velocity is induced in the liquid, which is then transmitted to the built-in flowmeter receiver instruments. Upon the determination of the velocity, the flow rate is simply calculated by means of multiplying by the cross-sectional area of the pipeline.

The model cutter head dredge at the Haynes Laboratory is equipped with a flow controller that is responsible for regulating each of the studied flow rates and for keeping them relatively constant as the experiments went through. In the past, a person was required to stand on the top of the carriage to, manually, adjust the flow settings. A change, proposed by Lewis (2014), was made and the flow meter is now connected to the ground control system, which automatically controls the flow rate to keep it around the nominal flow rate without great deviations. This change awarded the system a better accuracy and ease of use. This flow controller is of a great importance to the system, since it attempts to keep the velocity near a constant set value. The flow controllers have also a positive effect on the overall cost of the operation given its increased efficiency (Randall, 2016).

The electromagnetic flow meter attached to the dredge, is factory wet calibrated by way of direct comparison of volumes and is capable of maintaining a high accuracy for any flow profile (Girani, 2014). According to the maker of the sensor (Khrone, Inc),

measurements as high as 60.32 Liters/sec (956 GPM), with an accuracy of over 99.7% of the measured values and a repeatability of 0.1% of the maximum value, could be achieved.

Given the pump limitations, the highest flow the dredge is designed to reach is up to 37.9 Liters/sec (600 GPM), which results in an accuracy approximately equal to 0.1134 L/sec (1.8 GPM). For the proposed tests in this research, the errors in the measurements would be of 0.75, 1.05 and 1.35 GPM, for the 250, 350 and 450 GPM flow rates, respectively.

Nuclear Density Gauge

Nuclear density gauges are used to determine the density of the material passing through the pipes, which provides an important parameter for calculations, not only of the total material dredged, but also the mass flow rate of the operations.

The nuclear density gauge is the only radioactive device installed on the carriage. The sensor is an Ohmart GEN 2000® that sends a gamma ray energy stream (Cesium 137), which is read by an ionization chamber (receiver), on the other side of the flowline transporting the slurry that is responsible, not only for measuring the amount of isotope reaching it, but also for converting it into electrical signal. The calibration of this kind of equipment is done by means of comparison against a known density, in our scenario the water was used for this purpose.

The Ohmart GEN2000® is mounted on a vertical section of the discharge pipe that goes into the hopper barge and includes a 1 mCi (37 MBq) radiation source of the Cesium-

137 isotopes and a receiver with an output range of 4-20 mA (Ohmart Vega Corp., 2006a). The device came calibrated from the factory for specific gravity measurements ranging from 1.0 to 2.0. According to the maker of the density gauge, the accuracy of the apparatus is around 0.71% of full scale, which corresponds to an absolute specific gravity of about ± 0.00761. Such a minimal error did not induce much error in the analysis and could only be noticed in form of noise in the specific gravity data. The gauge was incorporated in the hydraulic system, connected to the ground control computer and is set to record data at a rate of 1 Hz.

In order to have more realistic results, the author averaged the data relative to the specific gravity for water-only test for each particular screen configuration and compared against what is the known for water specific gravity (1.0). Based on that, Equation (49) was applied to determine the adjustments needed to be done for the specific gravity for all other tests for that day.

$$\overline{S.G.}_{calibration} = \overline{S.G.}_{acquired} - S.G._{water} \tag{49}$$

Table 3 summarizes the calibration applied onto specific gravities across the experiments with the different screen configurations.

Table 3: Specific gravity calibration based on the water-only tests for each screen configurations.

Experiment	Screen 0	Screen 1	Screen 2	Average
$SG_{calibration\ avg}$	0.1650	0.1736	0.1648	0.1677

Pressure Gauge

The cutterhead suction dredge at the Haynes Laboratory has two pressure transmitters, which are located essentially before the centrifugal pump and before the discharge line (after the pump). For practical reason, the author chose to work only with the data from the gauge before the pump that provided information about the vacuum pressure induced by the rotation of the pump's impellers. Thus, the details presented in this section refer only to that sensor. The examined pressure gauge is a Rosemount 1151 with a reference accuracy of $\pm 0.25\%$ and a rangeability of 50:1. This level of accuracy range corresponds to a nominal value of ± 0.015 psig for the suction pressure values. The pressure transmitter used in the research is set to provide readings ranging from 0 psig to -14.7 psig. The variation of the suction pressure readings across the set of experiments along with changes of the other parameters is displayed in the Appendix section of this thesis.

Given the fact that the sensor was actually not right next to the centrifugal pump, but about 48.26 cm (19 in) above it, the author had to adjust the results to account for that head loss. Moreover, before dealing with the vacuum pressure readings from the pressure gauge the author took into consideration the water column height and cutting thickness associated with the operation and added the corresponding pressure contributions to the pressure sensor output data.

Acoustic Doppler Velocimetry

Acoustic Dopper Velocimeters, or simply ADVs, are high resolution devices used to measure the water velocity in three dimensions. This type of sensor computes the velocity of the investigated direction by sending out an acoustic signal to a parcel of water in that direction and calculating the called Doppler Shift of that signal, which is basically the change in frequency of an emitted wave signal for an observer/object moving relative to its source. This signal is sent back to the device and the three probes "listen" to the frequency variation. The velocity is, then, calculated for the x, y and z directions, according to Equation (50).

$$v = c\frac{\Delta\lambda}{\lambda_o} \tag{50}$$

where v is the calculated velocity at a given direction; c is the sound velocity; $\Delta\lambda$ is the wavelength shift; and λ_o is the wavelength of the source not moving. With the velocity calculated, the author was able to find out the correspondent distance from the receiver. Figure 35 shows a sketch of the used ADV in the set of experimental measurements.

The ADV was run after the regular tests for a 25.4 cm (10 in) cutting thickness for both screens 1 and 2, so a comparison of the effect of each screen on the seabed profile could be determined. The main use of this Acoustic Doppler Velocimeter relays on its also built-in capability to measure the distance to the receiver, which in our case is the seafloor. This indirect measurement was used to calculate the bathymetry associated with that particular point under investigation.

This recently purchased profiler is a Nortek Vectrino Profiler with a high vertical resolution of 1 mm over a range of 30 mm, as seen in Figure 35.

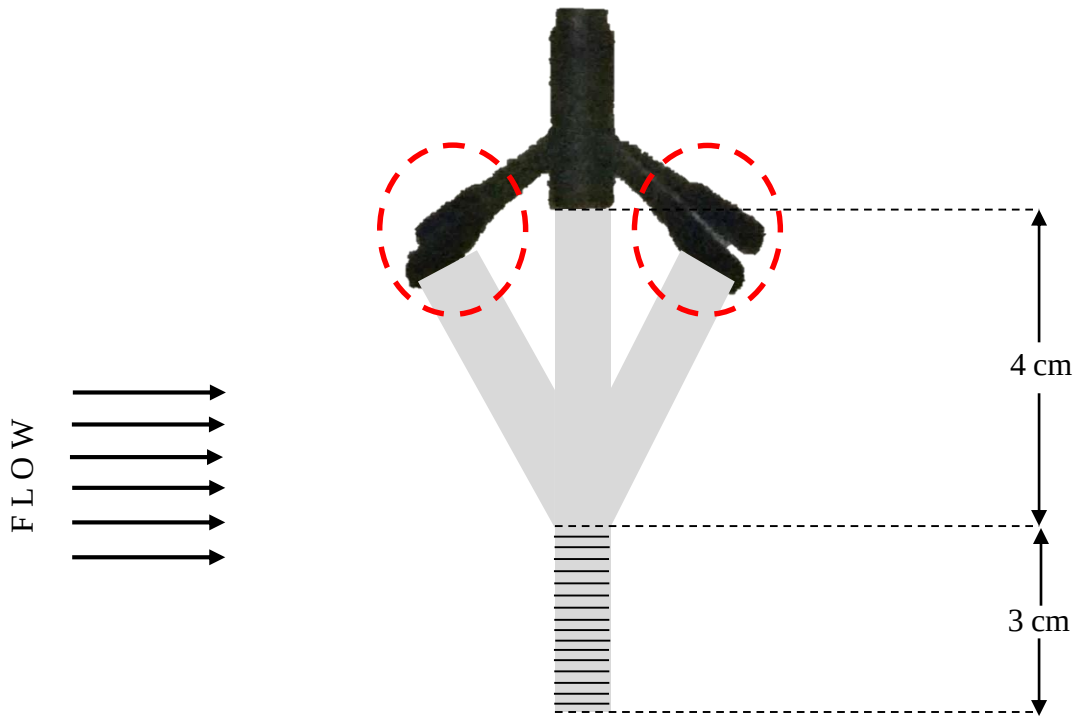

Figure 35: Sketch of the ADV screening resolution. Beams responsible for the seabed scanning circled with red-dashed lines

According to the maker, the output rate capability of the ADV is equal to 100 Hz for velocity measurements and equal to 10 Hz for distance measurements. Moreover, its pc interface is designed to provide instantaneous plots of the measurements. Its data collection and processing system also allows the user easily to export files (*.mat*), which can be manipulated in MATLAB®. According to the Nortek's user manual, the accuracy

of the ADV is equal to ± 0.5% of the measured values for the velocity profiling and 0.5 mm at 1 mm cell size.

The intrinsic capability of the Vectrino Profiler goes beyond the scope of this research and turns out to be a great investment for the Haynes Laboratory. Considering the fact that the use of this device was more an attempt to verify its usability in controlled experimental measurements, rather than to establish correlations between the studied parameters. Many aspects that might have had some effect on results, like the amount of time between the last test run and the ADV screening and the best seabed scanning path for bathymetry measurements, were overlooked. Moreover, the lack of repeatability, given the limited time at the Haynes Laboratory, made the results to be analyzed as "potential trends", or "potential indicators".

Data Acquisition

Cutter Suction Dredge Measurements

Before the results were analyzed and further processed a built-in system was properly set to control and manage the data acquisition. The dredge system is equipped with a software, operated by a technician, which is responsible for the dredge's advancement through the desired path. A code included in the, also, built-in software is responsible for running the chosen path across the tank. An example of a standard dredging path that was used for the proposed study is shown in Figure 36.

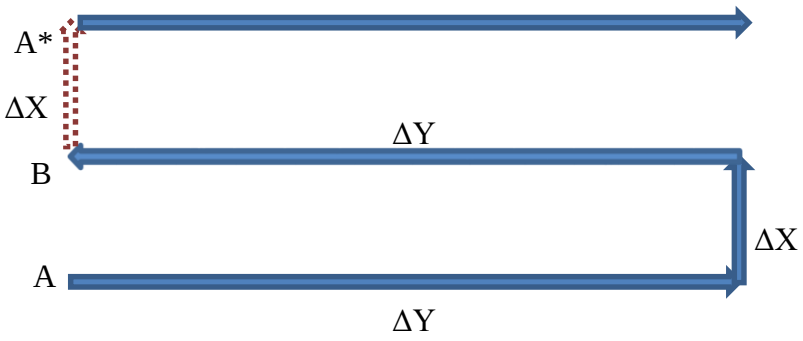

Figure 36: Path followed by the cutterhead model dredge when excavating the sediment pit.

The path starts at the point A and ends at the point B being repeated over and over throughout all the experiments. From the point A to the point B the carriage advance in the positive direction of the Y-axis and after it coursed a predetermined distance set by the user the dredge then advance in a perpendicular direction through the X-axis up to a point the carriage is set to travel back in the negative direction of the Y-axis, where it comes to reach the position identified as B in the scheme above. After the described path is made, the operator then places the dredge in the new point A, shown in Figure 36 as A*. Following this procedure the dredge is provided "virgin sand" for the subsequent cut. As consequence of the dimensions of the pit in the tank, the dredge was set to run the described path ten times before it was brought back to the original XY coordinate for the following set of tests.

The dredge's user control interface is equipped with a software that controls the set of movements executed by the dredge and pre-determined by the operator. Figure 37 shows a screenshot of the aforementioned user's interface.

Figure 37: Graphic interface of the software Apollo used to control the cutterhead model dredge.

Figure 37 presents the values of the parameters set for a fictional path described previously. The ΔY and the ΔX in Figure 36 are, respectively, the “Ly” and “Δx" on the software screenshot, which were the inputs on the software for commanding the ladder arm to swing from and to either the port or starboard side of the carriage and for making it advance in the tank longitudinal direction for the next cut to be performed. The advance in the x-direction, i.e. the distance between cuts, was set by the operator to be equal to 40 cm (15.75 in) in order to account for the length of the cutterhead and to make sure a virgin and undisturbed layer of sand was reached. The arm swing, which takes place across the tank width, was theoretically set to be equal 230 cm (90.55 in), but given the dredge overshooting the real value actually fluctuated around this value.

To determine the depth of cut (cutting thickness of the operation), the author took into consideration past researches where it was found that the optimum cutting depth that would maximize the production and not lead to excessive forces in the cutter head was at 25.4 cm (10 in). However, once the pit was completely ran for the 10 in cut operations, and refurbishing the pit for just 2 experiments for each Screen configuration (Screen 0, 1 and 2) would be quite time-consuming and practically unfeasible, the author decided to run those 6 tests with a greater cutting depth of 50.8 cm (20 in), two for Screen 0 configuration, two for Screen 1 and two for Screen 2. This way, the pit just needed to be releveled three times overall.

The appropriate cutting thickness was reached with help of the force sensors which showed whether there was a resistance in the cutter head. Therefore, the ladder arm was lowered in the negative direction of the Z-axis until one of the five blades of the cutter head touched the sand. At that point, the force sensor displayed an increase in the measurements, which indicated that the sand had been touched and the 0 in cutting thickness had been reached.

Bathymetry Measurements

The measurements of the bathymetry were performed after the last slurry tests for both screen 1 and screen 2, i.e. only for fixed screen condition testing, and given a software problem only the second screening (for screen 2) was properly recorded. Ideally, the more the experimenter ran a test, the better it would be. However, the availability of time and capital for a longer set of experiments did not prove to be feasible. Nevertheless, the ADV was run several times for each time a seabed screening was to be performed, which provided a reliable set of results for that particular run.

Running the ADV sensors over the sediment pit for a proper measurement of the bottom characteristic required that brackets on the carriage's port and starboard sides were properly installed to avoid undesired contact to the tank boundaries. Figure 38 shows the ADV mounted on the cutterhead dredge prior to the seafloor screening.

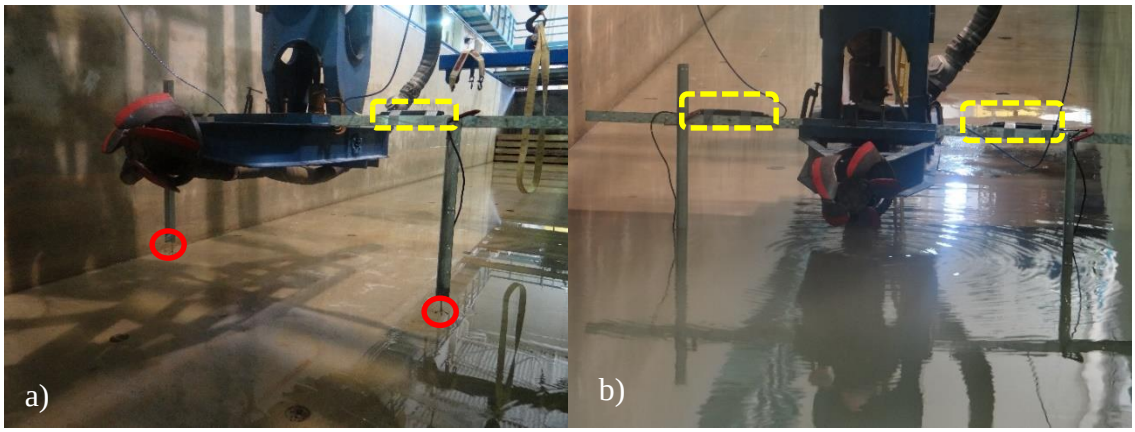

Figure 38: (a) ADV mounted atop the steel brackets (yellow) and its beams in a lower position (red) ready for screening; (b) Bathymetry-scanning assembly in operation (beams are underwater).

After the probes were installed the operator had to lower the ladder arm to 26.67 cm height (10.5 in), measured from the bottom of the pit (Figure 38b), which was the depth that would maximize the readings from the 4 beam (circled in red) while maintaining a good degree of safety for a whole run, given the fact that the water layer covering the bottom was thick enough to impair visual contact with the seabed and its uneven configuration created due to dredging.

The beams responsible for the seafloor screening were placed on the lower part of the brackets. The one on the starboard side of the carriage was placed at about 7.62 cm (3 in) away from the wall and 113.67 cm (44.75 in) below the metal arm of the support bracket. The probe on the port side of the cradle was fixed at 12.7 cm (5 in) from the respective wall and 113.67 cm (44.75 in) below the metal arm.

Upon the completion of the ADV setup, the carriage was set to run the sediment pit one more time in a straight line, slow enough so the probe could do the measurements as accurately as possible.

Test Plan

As discussed in the objectives of this thesis, the goal of this research is to compare how the new proposed screen behaves with changes on the parameters that have a major influence on the dredge production and, this way, to compare the obtained results with the ones found by Lewis (2014). Moreover, this author sought to fill the gap in between the opening percentages used by Lewis in his set of experiments.

The experiment test plan accounts with change in parameters such, the screen configuration (screen 0, 1 or 2), the depth of cut (water only – 0 in and slurry – 10 in), the angular speed of the cutter head (45 RPM and 55 RPM), the flow rate (250 GPM, 350 GPM and 450 GPM) and the swing speed of the ladder arm (2 in/s and 3 in/s).

Firstly, the cutter head speed was set constant at 45 RPM, while the swing speed of the dredge ladder arm varied across the two investigated values: 5.08 cm/s (2 in/s) and 7.62 cm/s (3 in/s). Each screen was tested for two cutting thicknesses: 0 and 25.4 cm (10 in) that refer to water-only and slurry, respectively. Secondly, the swing speed (V_L) was held constant at 7.62 cm/s (3 in/s), while the cutter head varied across two different values: 45 RPM and 55 RPM. Each of the aforementioned scenarios was tested for three different flow rates: 15.77 L/s (250 GPM), 22.08 L/s (350 GPM) and 28.39 L/s (450 GPM).

A flow chart summarizing all 72 tests conducted for the three different screen configurations is shown in Figure 39 and the spreadsheets with all experiments are found in the Appendix chapter of this thesis.

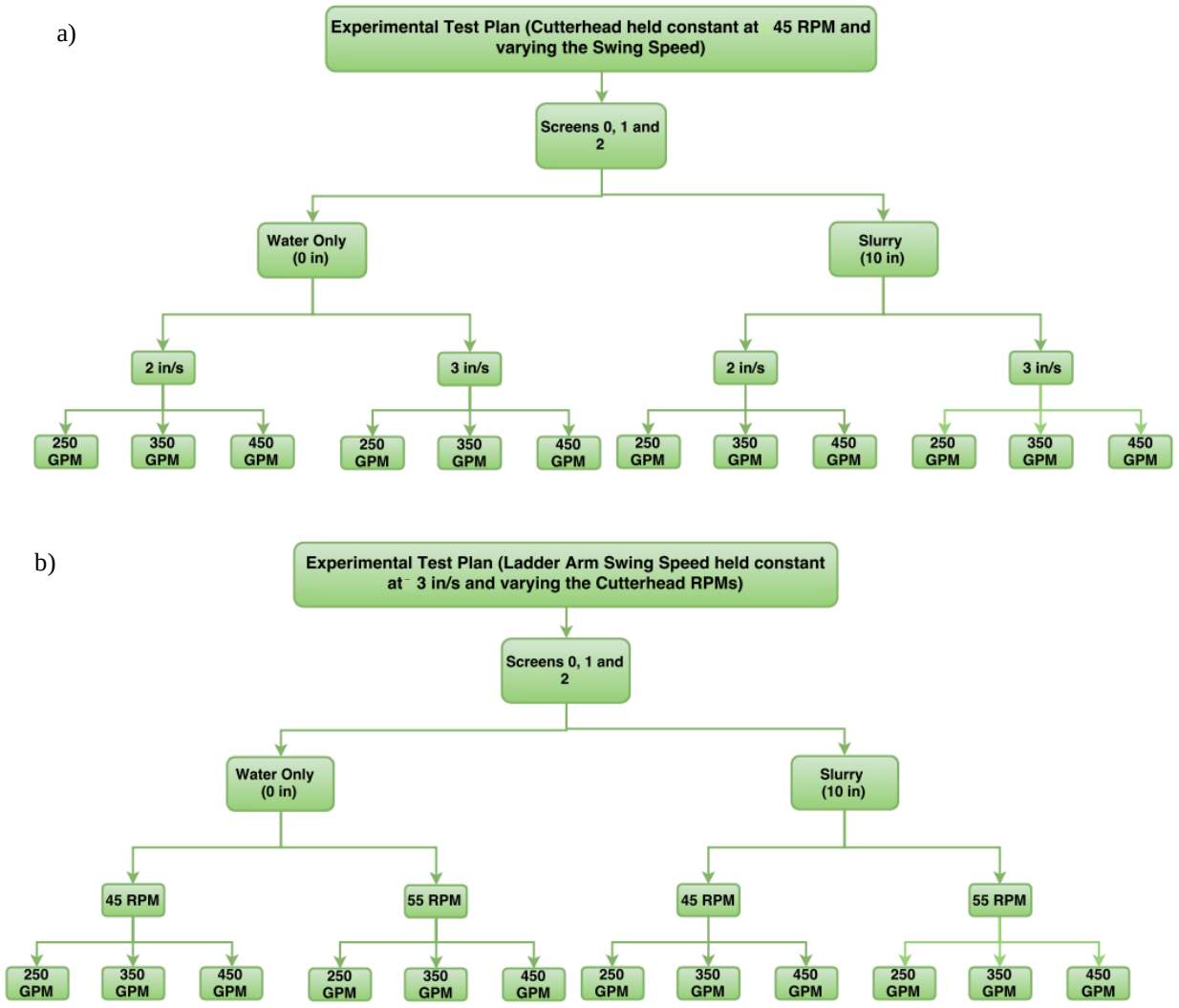

Figure 39: Flow chart of the performed experimental test plans. (a) Cutterhead held constant; (b) Ladder arm swing speed held constant.

In previous researches, an operator controlled the flow rates manually. This, surely, had some negative effects on the results. Lewis (2014) recommended a flow regulator to be installed, so the system could be more accurately controlled. Nowadays, the dredge has an automatic flow controller, which had never been used before this research took place.

CHAPTER V

METHODOLOGY FOR DATA PROCESSING

Data Filtering

The output data from the model dredge were spreadsheets separated with information for various parameters, such as the vacuum pressure from the centrifugal pump; the instantaneous flow rate; the density of the homogenized slurry being pumped; the x, y and z coordinates of the cutterhead; the speed of the carriage; and the speed of the ladder arm. The number of data points for each test varied and was an important parameter for the data treatment. Given the offset of the nuclear density gauge, its calibration had to be done in accordance to the water-only tests carried for the particular screen configuration under investigation, as already explained in Chapter IV.

As any experimental measurements, errors and instantaneous disturbances creep into the recorded data points and this is the reason why the data were filtered before any calculation was attempted. Given the limited time available at the Haynes Laboratory, the author could not carry out many different tests for the same conditions, which would grant repeatability to the research and result into a more reliable data. Because of this limitation, the author treated the data in two different ways. Considering the fact the set of data was relatively small compared to what is usually found in the literature for experimental research, a visually based identification of the outlier was found to be an extremely satisfactory method for removing the undesired data. These visual identifications were

done at two distinct moments of the processing. In the first moment, the author looked at the raw data and eliminated the points that clearly did not follow the same pattern shown by the other data points. The second visual inspection was done right after the application of a selected model for eliminating outliers numerically, which is explained later in this chapter. This second verification was executed to ensure the data removed would not negatively affect any given trend, nor would it actually be part of a physical process backed by the nature of the experiments and can be physically explained. In a scenario like that, the author would have to properly consider these observations and include them in the results appraisal.

Chauvenet Criterion

Sometimes there are some data points that are not easily spotted, but must be delete from the investigated set given its non-representability. Careful analyses of the results were done and the detected “wild point”, responsible for biasing the studied phenomena, were properly removed.

The Chauvenet Criterion, detailed in Holman (2012), is a technique in which the investigator defines an acceptable range of scatter points, in a statistical sense, around the mean value of the scrutinized test. The method employs a condition which all retained data points should fall within the band around the mean that corresponds to a probability expressed by Equation (51).

$$Prob = 1 - \frac{1}{2n} \tag{51}$$

where n is the number of tests or 'readings' of that particular dataset (Holman, 2012). Figure 40 displays the visual representation of the employed criterion.

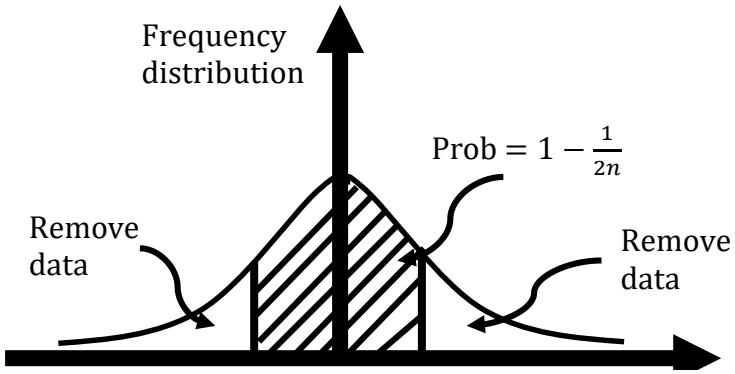

Figure 40: Probability distribution function for the Chauvenet Criterion.

The probability of a particular data to be retained can be related to the standard deviation of the respective dataset and is given by the ratio represented by Equation (52).

$$\tau_{max} = \frac{d_{max}}{\sigma_{sample}} \tag{52}$$

where τ_{max} is the threshold of a given sample, above which the reading should be rejected; d_{max} is the maximum allowed deviation a reading could have to be included in the computations; and σ_{sample} is the inherent standard deviation of the sample under investigation.

In other words, if a certain data point has a larger deviation from the mean than the particular threshold for that dataset, that point is considered then to be an outlier. Figure 41 shows a plot of the Ration of Maximum Acceptable Deviation to the Standard Deviation (τ_{max}) on the y-axis with the number of readings (n) on the x-axis.

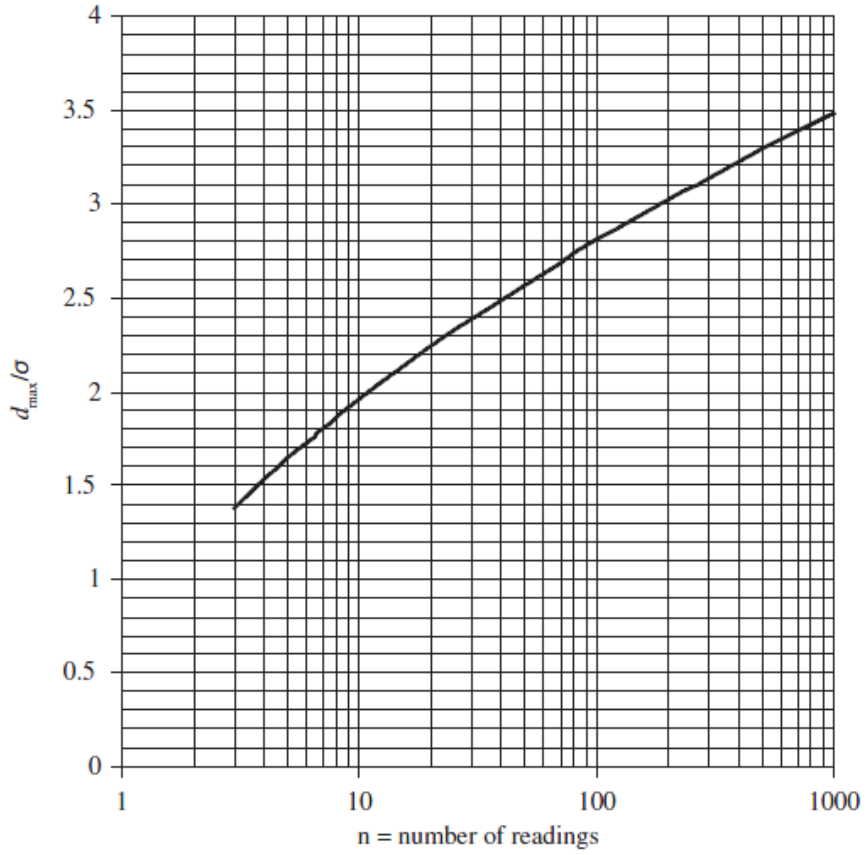

Figure 41: Plot of the Ration of Maximum Acceptable Deviation as function of the number of readings. Source: Holman (2012).

CHAPTER VI

QUALITATIVE OBSERVATIONS

Screen Clogging

When dredging is being studied, the author must have knowledge of potential issues inherent of the ongoing operations. For this research, an important contributor for clogging formation was the reduced suction entrance area due the fixed screen, that when associated with the induced flow field may have given origin to clogging.

Previous researches done at the Haynes Laboratory Model Dredge reported the formation of clogs when screens with opening area equal to 50%, or less, were installed on the suction inlet. It is also expected clogging to be more likely to occur with cutterhead model dredges, given the fact that sediment scaling has proven to be a constant challenge, once the resources for experimental measurements of this kind are usually limited. Ideally, the sediments used on operations of this nature would also be geometrically scaled and should match the scaling laws associated with the physical model under investigation. The area of the openings “carved” on the fixed screen is also a relevant indicator of the likelihood of the apparatus to experience clogging.

Because of sediment downscaling limitations, the researcher should expect that the formation of clogging for a particular set of experiments, or for a specific operational setting, would most likely not resemble what would happen in a real world prototype version of the investigated configurations. Considering these assumptions, this author

identified all points that were explained by this undesired phenomenon and removed them from the calculations. Unfortunately there was no possibility to record the phenomenon on video, which would be useful for the data analysis. As the formation of clogging had already been experienced by other researchers, it was decided that after each set of tests, the flow rate would be reduced to a value that would result in the suction velocity to be smaller than the critical velocity of 1.88 m/s (6.17 ft/s). This would allow the sediments to settle onto the bottom of the pit and prevent the next set of tests to be affected by a potential screen clogging.

The identification of the points featuring clog formation was done by visual inspection of the respective average suction pressure for the set of tests and compared with the usual value found for similar tests. After careful analysis of the results it was seen that not many tests suffered from clogging, which led this author to come up with three potential hypothesis that might explain the reason. The first would be explained by the shape of openings on the proposed screen, which may have influenced the near-flow field at some extent, and might have created a favorable condition for the slurry to be properly dredged. At the conceptual phase of the screen design, the author thought to propose a screen with its openings cut in a way to match the rotational motion of the cutter head, which yielded in the new screen (Screen 2) investigated in this research.

The second hypothesis would be given the operational conditions under which the experiments were done. Considering the facts that the high centrifugal forces caused by the rotational speeds were not only responsible for the spillage seen on the experiments,

but also for outweighing the axial forces, the author hypothesizes that the aforementioned phenomenon was probably responsible for hindering the formation of clog.

Lastly, the pump speed was reduced to a value that lowered the flow rate to a point below its critical value and induced the sediments to settle, which may have avoided the particles to build up on the screen and induce clogging.

Turbidity

Turbidity and spillage are phenomena closely related and often seen when dredging operations are being investigated. A cutterhead dredge works in such a way that its draghead is responsible for scooping up the seabed material and bringing it close to the suction entrance, where the theoretically predominant axial forces induced by the suction pressure are responsible for bringing the sediment into the system. When the centrifugal forces are relatively higher than the axial forces sediment particles are launched out of the flow field boundary layers. This spilled sediment can either settle back to the bottom, or become a resuspended sediment (Bridges, et. al. 2008). den Burger (2003) defines spillage as being the amount of material scooped by the cutter from the seafloor, but not removed from the system by the suction line. For the experimental tests performed in this research, the generated turbidity did not cause major problems on the tank, besides the video recording and visual remarks. On real world dredging operations, the induced turbidity is sometimes dangerous to the environment that hinders light penetration and negatively affects local species. This effect coupled with the enhanced diffusive rate, caused by the

high centrifugal forces and/or existing currents, worsens the, already dangerous, scenario. It is intuitive to think of spillage as a loss of the system to the environment, which is, then, intended to be minimized so that the maximum possible production could be achieved.

In this research, the author investigated two cutterhead speeds that, in former research, were believed to potentially generate spillage. However, given the fact that the objective of this research was to investigate the behavior of the minor loss coefficient due to the fixed screen at the suction inlet and not to find the optimum parameters for a maximum production, this phenomenon was not treated as an issue, but rather as a "qualitative observation". Unlike the screen clogging, both the spillage and turbidity caused by the high velocity flow field were recorded by the GoPro® camera mounted atop the cutterhead ladder arm. The series of pictures in Figure 42 show the level of spillage associated with the rotational speeds of the cutter for when the ladder arm advanced in the overcutting direction, i.e. from the port side to the starboard side.

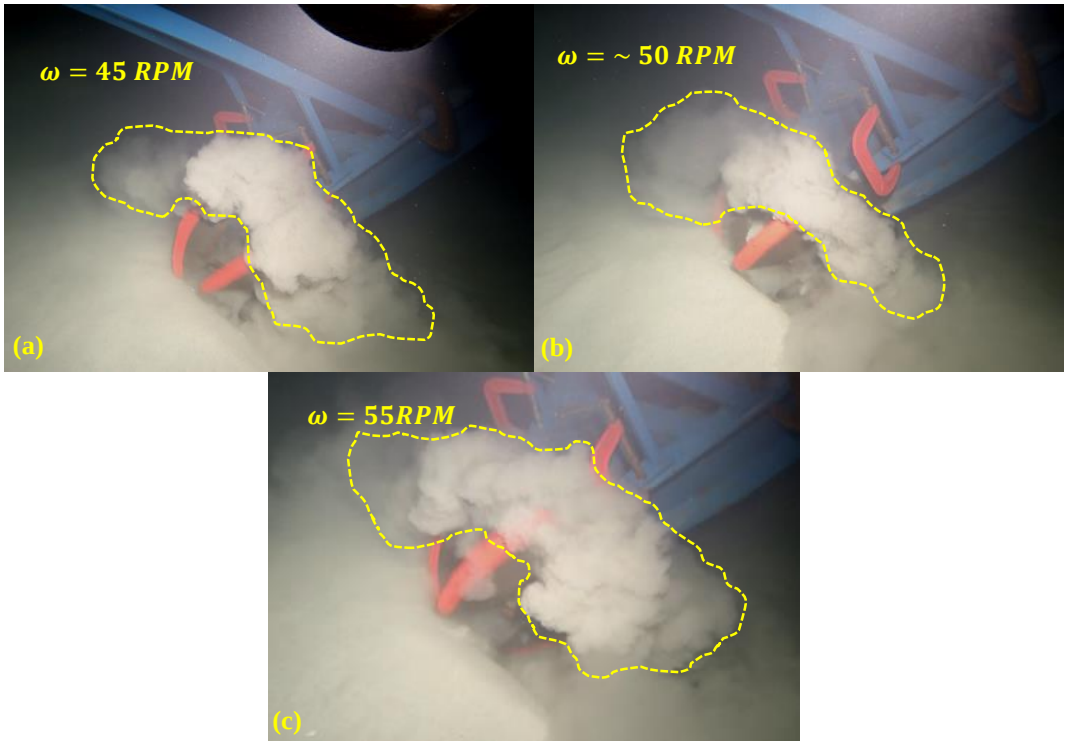

Figure 42: Spillage induced by the high cutterhead rotational speeds employed. (a) Cutterhead speed at 45 RPM; (b) Cutterhead speed around 50 RPM; (c) Cutterhead speed at 55 RPM.

Figure 42 shows a positively relationship between the cutterhead rotational speed and the spillage, phenomenon that was also reported by Hayes, et. al. (2000).

CHAPTER VII

DATA ANALYSIS

Minor Loss Equation Formulation

As already explained in this thesis, the basic equation used as starting point for the calculations of the head losses due to the fixed screen is a modified Bernoulli equation, also refereed as the Energy Equation. This formulation represented by Equation (13) can be referenced at any point of the studied system and becomes more useful upon the comparison of two different locations. In this research, the author chose two different points in the tank given their convenience for calculations. Figure 43 depicts a sketch of the cutterhead model dredge located at the Haynes Laboratory with those points represented.

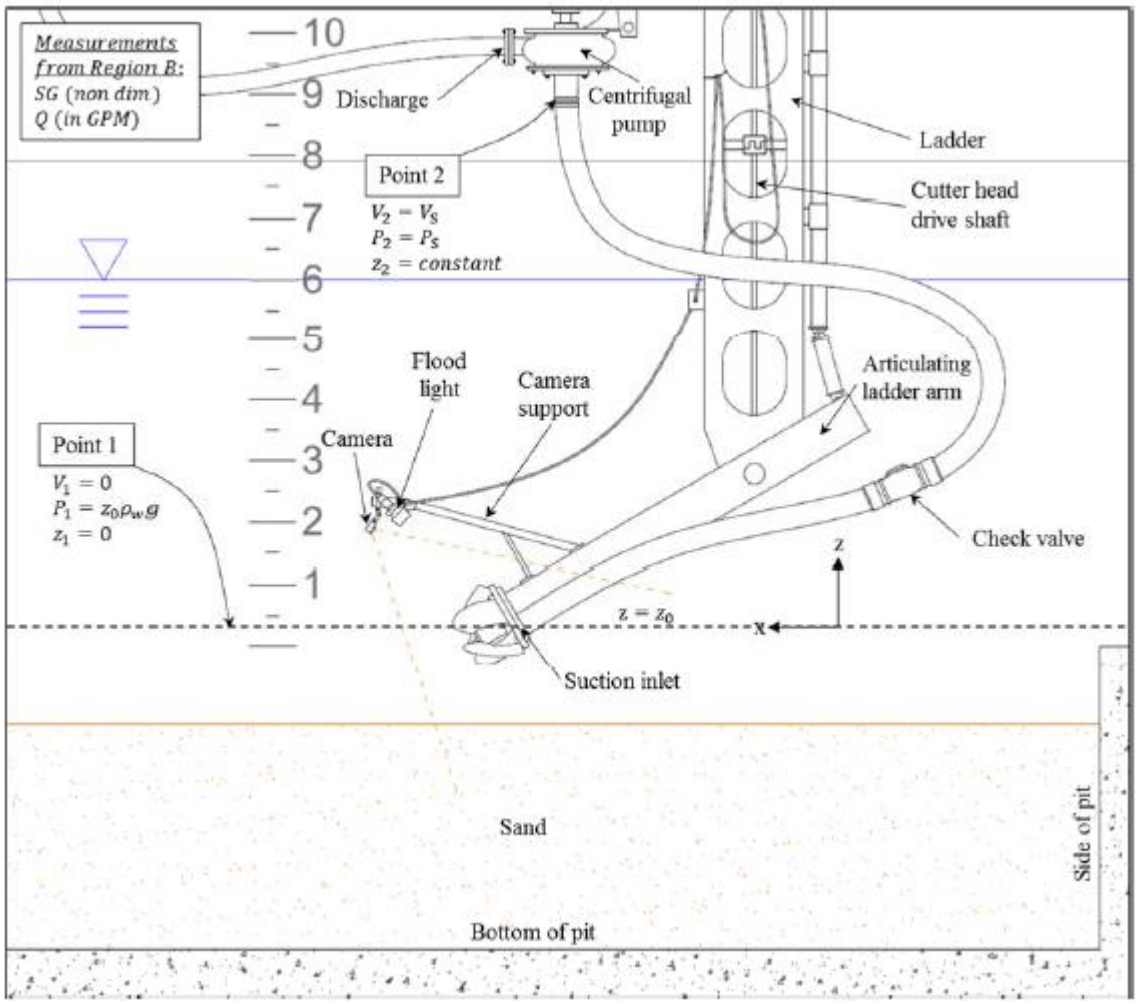

Figure 43: Schematic drawing of the cutterhead model dredge with the investigated points and their corresponding variables. Source: Lewis (2014).

Point 1 was picked in quiescent water given its known characteristics. The only variable the author had to take into consideration for the calculations was related to the hydrostatic head of the water column, which changed depending on the cutting thickness being done. Point 2 was chosen right at the entrance of the centrifugal pump, since sensors responsible for the flow rate and suction pressure readings are located there.

Nevertheless, the final objective was to calculate the minor loss due to fixed screens at the suction inlet. The computation of this parameter required the manipulation of the modified Bernoulli equation until the term correspondent to the minor loss (k_n) was isolated and function of known variables.

To identify the effects of the installation of the aforementioned screens, the author basically compared the head losses for each point before and after its placement on the suction mouth, whose difference would result in a head loss variation due to the mentioned screen, which was here called Δh_{Ln}. Equations (58) and (54) were formulated based on Equation (7) for both points 1 and 2 shown in Figure 43.

$$h_{L0} = \frac{p_{10}}{\gamma_{mixture\ 0}} - \frac{p_{20}}{\gamma_{mixture\ 0}} - \frac{{V_{20}}^2}{2g} - z_2 \tag{53}$$

$$h_{Ln} = \frac{p_{1n}}{\gamma_{mixture\ n}} - \frac{p_{2n}}{\gamma_{mixture\ n}} - \frac{{V_{2n}}^2}{2g} - z_2 \tag{54}$$

where the subscripts $'n'$ and $'0'$ refer to the condition "with screen" and "no screen", respectively. The terms $\frac{p_{1n}}{\gamma_{mixture\ n}}$, $\frac{p_{2n}}{\gamma_{mixture\ n}}$ and $\frac{{V_{20}}^2}{2g}$ refer to the heads related to the hydrostatic pressure, suction pressure and suction velocity. The specific gravities for each condition ("with screen" / "no screen") are different and the average for each set of experiment was used.

After arriving at those formulations, the author subtracted Equation (54) from Equation (53), so that a general equation for the minor losses due to the investigated fixture, represented by Equation (55), could be reached.

$$\Delta h_{Ln} = h_{L0} - h_{Ln} = \left(\frac{p_{2n} - p_{1n}}{SG_{mixture\ n} \cdot \gamma_{water}}\right) - \left(\frac{p_{20} - p_{10}}{SG_{mixture\ 0} \cdot \gamma_{water}}\right) + \left(\frac{{V_{2n}}^2 - {V_{20}}^2}{2g}\right) \quad (55)$$

Equation (55) was used across all the datasets to calculate the inherent minor head loss due to the screen at the suction entrance and served as an input for computing the minor loss coefficient associated to each screen condition. Across the calculations and comparisons of Equations (58) and (54) the friction-related terms and minor losses across the pipe canceled out due to the fact they were essentially equal to each other for every screen configuration.

The calculated head loss due to the screens was, then, plugged into Equation (13) and after its rearrangement originated Equation (56), which was used for calculations of minor loss coefficients across all datasets.

$$k_{screen\ "n"} = \Delta h_{Ln} \cdot \left(\frac{2g}{{V_{2n}}^2}\right) \quad (56)$$

Analysis of the K-values for Water Tests with Different Cutterhead Speeds

Evolution of the K-values Varying only the Cutterhead Speed for an Averaged Flow Rate

In this part of the study, the author evaluated the evolution of the k-values with the cutter head speed. It was not possible to identify a clear trend based on a data for only two different speeds, once the time available at the Haynes Laboratory was limited and only a single run of each test was possible. However, a comparison of the results presented here with the ones found by Lewis (2014) is certainly of great relevance.

Figure 44 shows how the k-values behave with varying speeds of the cutter head for an averaged flow rate.

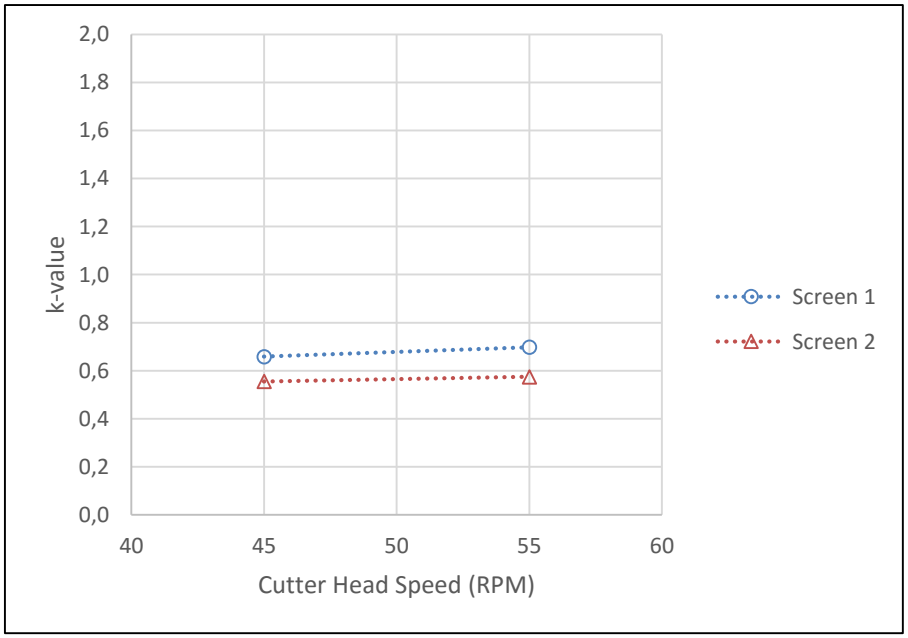

Figure 44: Variation of the Minor Loss Coefficient (k-value) as function of the cutterhead rotational speed for an averaged flow rate.

No major trends could be concluded from this first chart, once the data showed that for cutter head speeds ranging from 45 to 55 RPMs the k-values tend to keep constant around 0.6 and screen 1 presented greater k-values than screen 2. This is theoretically inconsistent, since the k-values are expected to increase with a smaller opening area.

The similar trend observed for both screens may be a proof that variations of the cutter head speeds do not play a major role on variations of the k-values. The same trend was observed by Lewis (2014), which strengthens the theory that the variation of both parameters are not correlated.

More investigations need to be done for high rotational speeds of the model dredge's cutterhead at the Haynes Laboratory not only to better understand how the parameters are related, but also to confirm the findings in this research.

Evolution of the K-values Varying the Cutterhead Speed for each Different Flow Rate

A more detailed analysis of the measurements could be attempted when the values for the minor loss coefficient for each of the three different Flow Rates were compared to the varying cutterhead speeds.

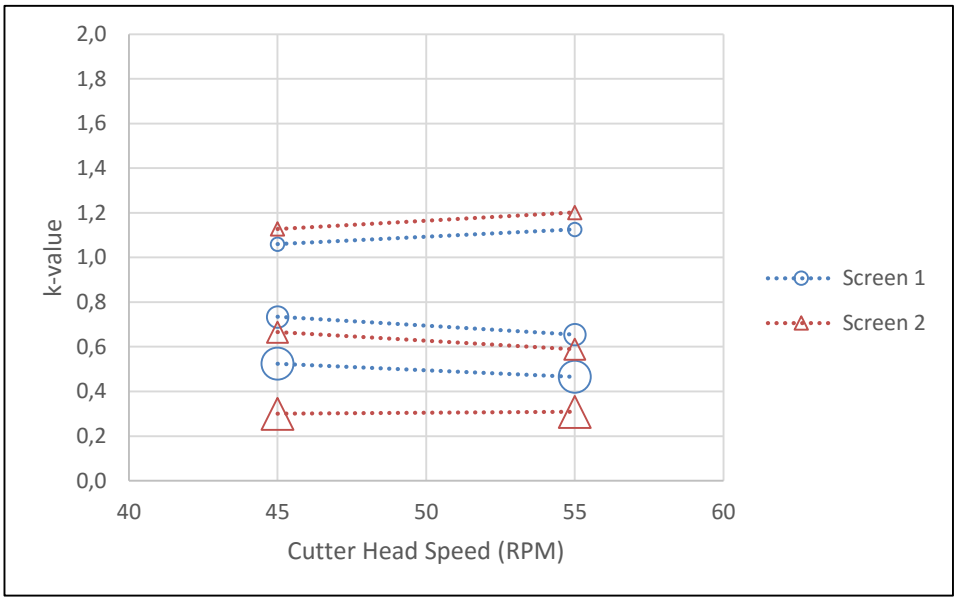

Figure 45: Variation of the Minor Loss Coefficient (k-value) as function of the cutterhead rotational speed for each nominal flow rate. Small, medium and large symbols refer to the 250, 350 and 450 GPM flow rates, respectively.

Figure 45 shows the variation of the k-values for each of the different flow rates across the two rotational speeds and confirmed the constant trend in all set of test for these parameters. Both screens 1 and 2 at a flow rate equal to 250 GPM presented higher k-values than for higher suction intake velocities. The data plotted in Figure 45 displays a large spread of k-values and led the author to infer that high flow rates would contribute to eclipsing the real behavior of the minor loss coefficient due to fixed screens.

Evolution of the K-values Varying the Cutterhead Speeds across the Different Flow Rates

In this section, the author studied the variation of the minor loss coefficient across the three Flow Rates for different cutter head speeds, which, as expected showed a strong relationship.

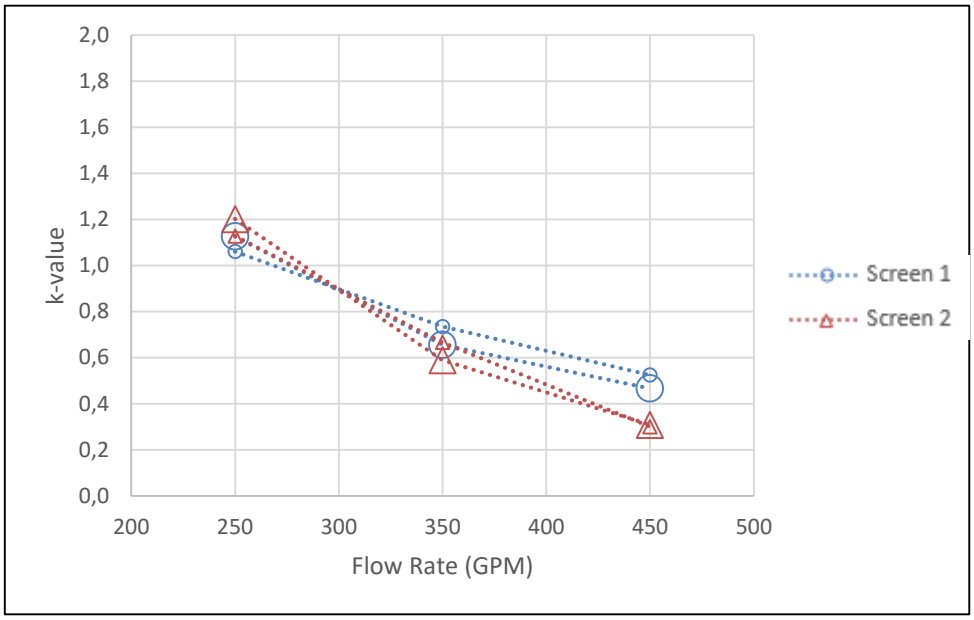

Figure 46: Variation of the Minor Loss Coefficient (k-value) as function of the flow rate. The small and large symbols refer to the 45 and 55 RPM, respectively.

The chart in Figure 46 shows the aforementioned negative relationship between the minor loss coefficient and the flow rates for the two different cutter head speeds on the water-only tests. The research conducted by Girani (2014) showed that for low specific gravity sediments there is a positive relationship between the k-values and the flow rates. Lewis (2014) disagreed with this trend and found out that actually there is a negative

relationship between those two parameters. This author found that for even higher flow rates, the trend presented by Lewis (2014) becomes more pronounced and the k-values smaller. For high flow rates operations, the opening area of the cutterhead screen has a smaller influence over the minor loss coefficient than for operations with lower flow rates. The author also observed that the magnitude of the k-values presented by the 55 RPM points was smaller than for the 45 RPM, which suggests that the higher the cutterhead rotational speeds, the smaller is the minor loss coefficient absolute value, fact attributed to the inherent induced turbulence.

More studies should be done for high flow rate values so their influence over the system losses could be better comprehended. A hypothesis for the presented trends could rely on the turbulence around the cutterhead caused by the high RPMs, which are enhanced when associated with the high suction velocities induced by the high operating flow rates.

Analysis of the K-values for Slurry Tests with Different Cutterhead Speeds

Evolution of the K-values Varying only the Cutterhead Speed for an Averaged Flow Rate

The data obtained for screen 1 with sand tests showed a relatively small spread for high rotational speeds for an averaged flow rate, which is a proof of the low correlation between variations of both k-values and cutterhead speeds. However, screen 2 showed to be more sensitive to variations in the rotational speed of the cutterhead, which resulted in a positive relationship between the k-values and an increase in the cutter speeds. The

strong inclination of the line will be better explained further on, since the k-values associated with each cutterhead speed were plotted for each individual flow rates.

The low values of the minor loss coefficients for both screens can be explained by the amount of turbidity produced during the operation, which is an indicator that sediment spillage was taking place and as already explained in this thesis, resulted in a production loss and therefore a smaller k-value.

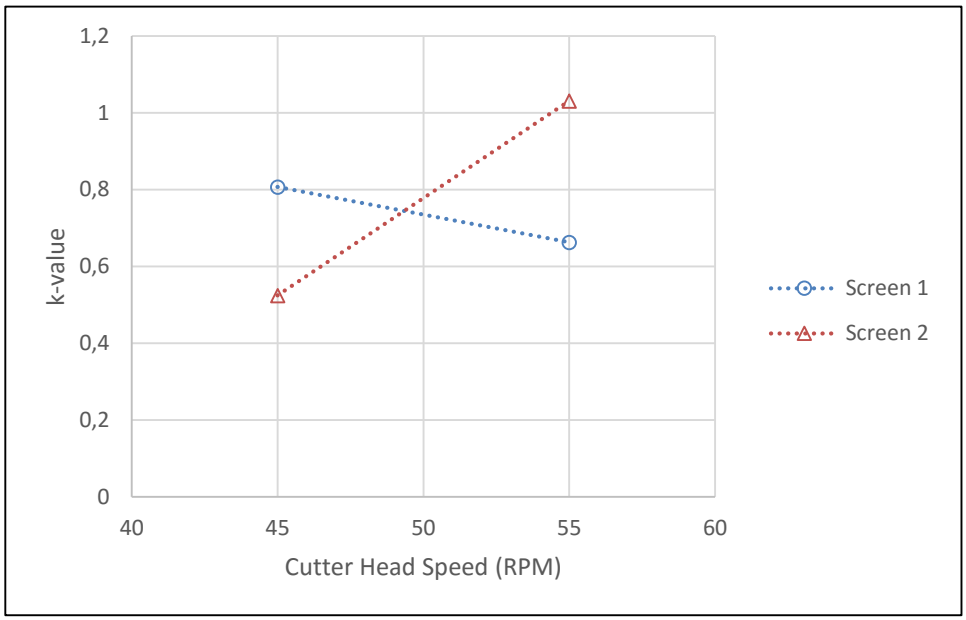

Figure 47: Variation of the Minor Loss Coefficient (k-value) as function of the cutterhead rotational speed for an averaged flow rate.

The results provided by the set of data agrees with those obtained by Lewis (2014), which also showed that the losses due to the screen are not sensitive for increasing values of the cutter head's rotational speed.

The fact that the turbidity increases with a greater RPM had already been confirmed by Henriksen (2009), where he stated that spillage and the rotational speed of the cutter are positively correlated. According to Mol (1977c) and Moret (1977), there's an optimum ratio between the rotational speed and the suction intake velocity, which is directly proportional to the flow rate and was presented in Equation (42) (Dismuke, 2011). This optimum ratio acts as a threshold, which if exceeded, would result in a scenario, whose centrifugal forces dominate the flow around the cutterhead, i.e. the centrifugal forces (represented by the numerator) outweighs the axial forces (responsible for driving the material into the suction line and is represented by the denominator). This event would result in higher spillage and turbidity. For this research, this non-dimensional value ranged from to 0.22 to 0.47.

Henriksen (2009) further analyzed the influence of the cutter's speed and studied the losses for both the overcutting and undercutting modes. His research showed that overcut tests at high RPMs would generate greater turbidity levels, while when undercutting the operation would reach a maximum turbidity and decrease afterwards. More investigation is needed to confirm the influence of the cutter speed, for both cutting methods, on the aforementioned qualitative observation.

Evolution of the K-values Varying the Cutterhead Speed for each Different Flow Rate

In this section, the author compared the evolution the k-values for each flow rate, which enabled a better understanding of the related phenomena for a variation of the cutter

head rotational speeds. The plot in Figure 48 confirmed the trend suggested before that the k-values are not highly sensitive for variations of high RPMs. Besides the circled data point, the rest of the tests resulted in a more or less small spread of data.

The point with a green circle around it depicts a situation where the values of *k* skyrocketed and can be explained by the fact that tests 70; 71; and 72 might have experienced clogging. This observation would have been responsible for blocking part of the suction entrance, contributing to bigger losses due to the screen, since its formation is closely related to the net opening area, i.e. the smaller the opening area, the higher the odds of clog formation. The associated k-value for that set of test was the highest seen throughout the experiments performed at the Haynes Laboratory and equal to 2.34. This author is confident that if the tests were to be re-run values within expected ranges would be achieved.

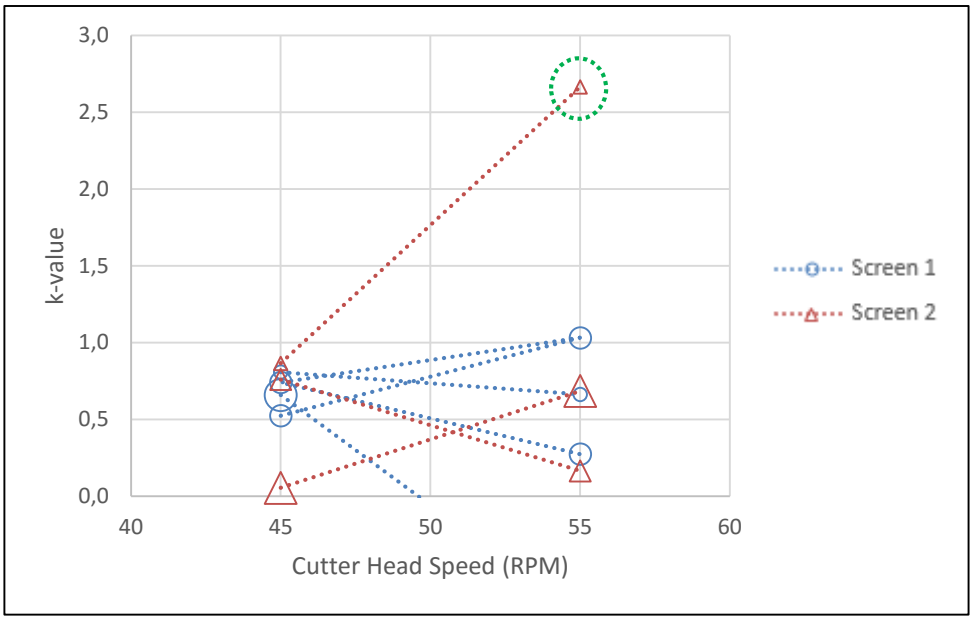

Figure 48: Variation of the Minor Loss Coefficient (k-value) as function of the cutterhead rotational speed for each nominal flow rate. Small, medium and large symbols refer to the 250, 350 and 450 GPM flow rates, respectively.

Although it might be counterintuitive that for greater flow rates there's a smaller associated k-value, it can be explained by the induced turbulent state of the environment around the suction entrance, which was responsible for reducing the specific gravity of the slurry (which is an indicator of production) and consequently the apparent losses throughout the system.

The plot in Figure 48 is a proof that little is known about the behavior of the minor loss coefficient due to the screen with high rotational speeds and high flow rates. From Figure 48 the author was able to conclude that, due to the little variation of non-outliers-data, the k-value shows no correlation with variations in the cutterhead speeds, whereas

the low magnitude of k-values are explained by the elevated spillage caused by the high RPMs and high flow rates.

Evolution of the K-values Varying the Cutterhead Speeds across the Different Flow Rates

In an attempt to compare the influence of the operating flow rates on the variation of the minor losses due to the placement of the screen, this author compared the rotational speeds for both screens across the range of the three different flow rate. The outlier mentioned previously can be seen on the plot of Figure 49 with relatively high k-values.

Although unclear, a general trend can be observed in which the k-values tend to decrease and converge to a point as the flow rate increases for the same rotational speed. The same pattern was observed in Girani (2014) and later confirmed by Lewis (2014), which supports the concept that for high flow rates, the flow velocities and the k-values show a weaker relationship.

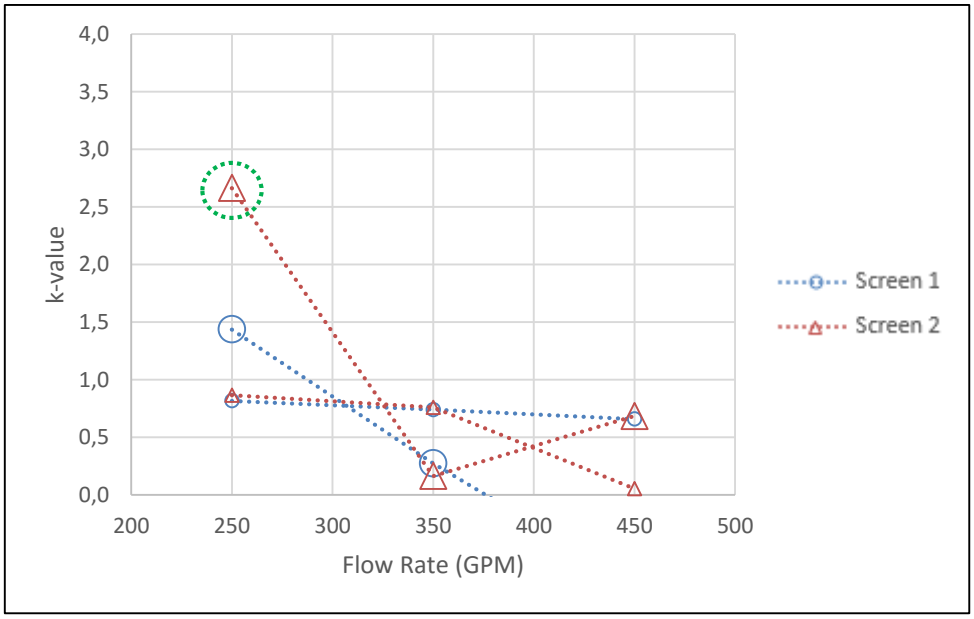

Figure 49: Variation of the Minor Loss Coefficient (k-value) as function of the flow rate. The small and large symbols refer to the 45 and 55 RPM, respectively.

Once again, the fact that the observed k-values happen to be much lower than those found by Lewis (2014) is explained by the turbulence level caused by the high velocities flow field around the cutterhead. This phenomenon is responsible for reducing the overall production and, consequently, masking the real effect of the placement of fixed screens at the suction entrance on the total minor losses total across the system.

Although the author was able to draw a conclusion, the inconsistent trends presented in Figure 49 showed the necessity of further studies on this area. Likewise more investigations are needed on the effect of this turbulent field on not only the influence of operating parameters, involved in dredging operations, on the overall production, but also on the real effect of screens fixed at the entrance of the suction inlet.

Analysis of the K-values for Water Tests with Different Ladder Arm Swing Speeds

Evolution of the K-values Varying only the Swing Speed for an Averaged Flow Rate

Results obtained for different values of ladder arm swing speed for water tests showed that the parameter under analysis had little correlation with the k-values for an averaged flow rate, as shown in Figure 50. This fact was better observed in the plots for each individual flow rate and swing speed.

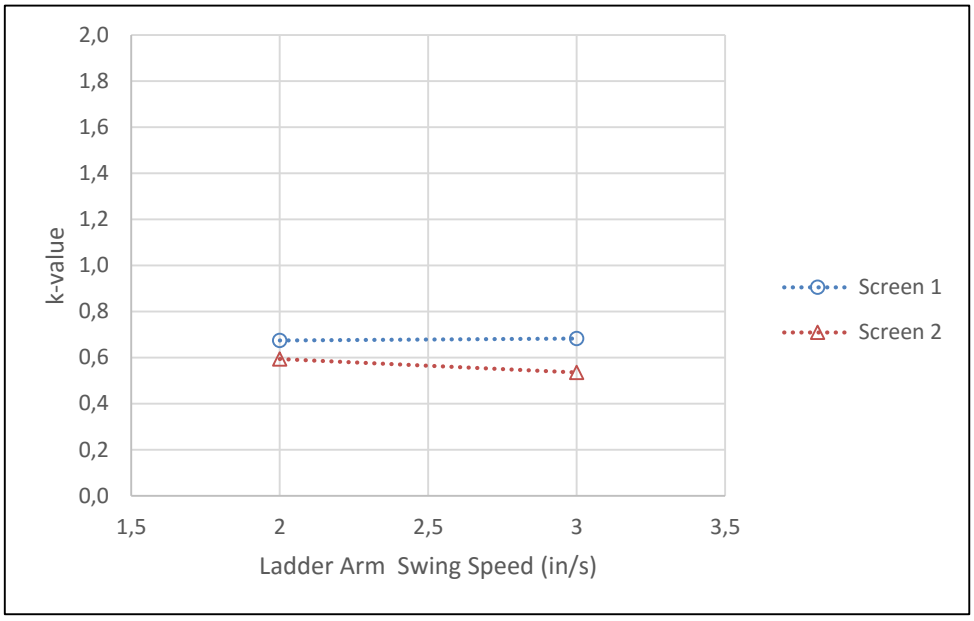

Figure 50: Variation of the Minor Loss Coefficient (k-value) as function of the ladder arm swing speed for an averaged flow rate.

According to the data obtained from the tests, the k-value for both screens is relatively smaller than the result obtained from Lewis (2014), which was already attributed to the smaller production given the high level of turbulence induced by the high rotational speeds of the cutterhead and the flow rates. A study conducted at the Lavaca Bay (part of

the Texas Gulf Coast, located between Galveston and Corpus Christi) reported higher levels of spillage as a result of a greater summation of the cutter speed and the swing speed (Henriksen, 2009). Miltenburg (1983) conducted a set of experiments with sand and showed that a decrease in the cutterhead rotational speed and an increase in the flow rate would actually be beneficial for the production. These studies suggest a strong relationship with the cutter speed and sediment loss that can be pointed out as a reason why variations of the k-values proved not be sensitive to changes in the ladder arm swing speed. It is important to keep in mind that the lowest rotational speed used in this research (45 RPM) was actually the upper limit in the research performed by Lewis (2014) and was reported to result in a high level of spillage.

Evolution of the K-values Varying the Swing Speed for each Different Flow Rate

Figure 51 was used to compare the trends demonstrated by each flow rate at each of the employed swing speeds. The reader can notice that a variation in the k-values for changes in the ladder swing speed is not pronounced for any flow rate, which is a consequence from the lack of relationship between the k-value and the ladder arm swing speed.

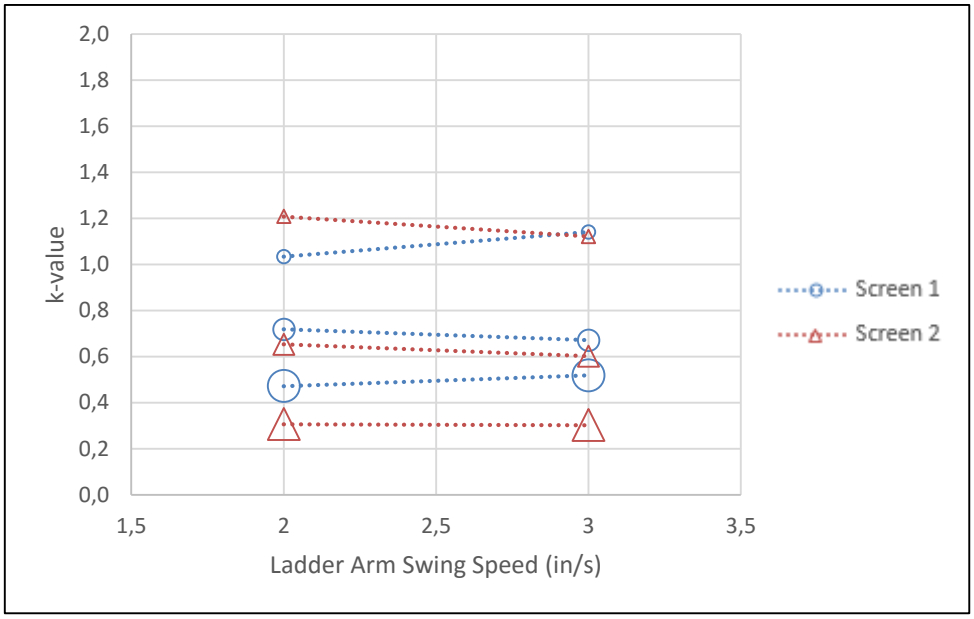

Figure 51: Variation of the Minor Loss Coefficient (k-value) as function of the ladder arm swing speed for each nominal flow rate. Small, medium and large symbols refer to the 250, 350 and 450 GPM flow rates, respectively.

The same pattern was observed by Lewis (2014) in which he evaluated the variation of the minor losses for ladder arm swing speeds equal to 2.54, 3.81 and 5.08 cm/s (1, 1.5 and 2 in/s). The behavior of the k-values with increasing values of swing speeds kept the same trend for greater flow rates. Interestingly, the author also observed a relatively large spread of data every group of two flow rates (for screen 1 and for screen 2). Their separation was of roughly 0.4 and 0.6 within the 450 GPM and 350 GPM lines and the 350 GPM and 250 GPM lines, respectively. This suggests that the k-values are more sensitives to changes of flow rates, which is then investigated in the following section.

Evolution of the K-values Varying the Swing Speeds across the Different Flow Rates

The evaluation of the k-values for both ladder arm swing speeds across the three different flow rates showed a more sensitive trend than observed by changes in the swing speed themselves, which suggests a greater importance of the flow rate in comparison to the swing speeds. This may be a result of the level of significance of each operating parameter within the dredging operations. A superficial analysis of the velocities points out the overwhelming influence of the suction velocities induced by the operating flow rates in comparison to the ladder arm swing speeds. The velocities generated by the 250, 350 and 450 GPM flow rates were equal to approximately 6.3, 8.9 and 11.4 ft/s, which are way higher than the swing speeds of the ladder arm (2 in/s or 0.166 ft/s and 3 in/s or 0.25 ft/s).

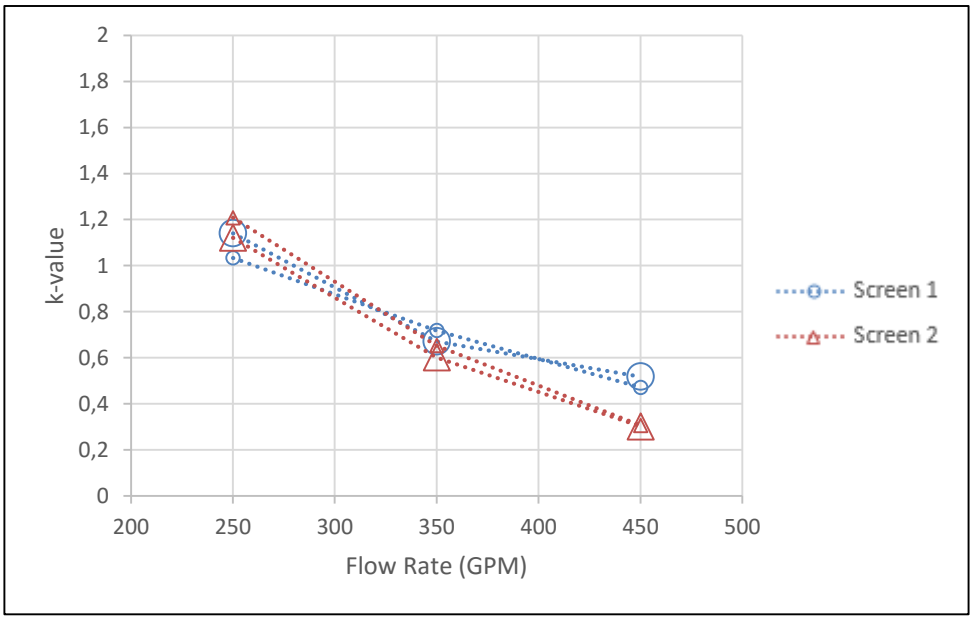

Figure 52: Variation of the Minor Loss Coefficient (k-value) as function of the flow rate. The small and large symbols refer to the 2 and 3 in/s, respectively.

It can also be observed that the spread of data across the flow rates is small, which backs the idea of the overwhelming significance of the flow rates in comparison to the swing speeds.

In comparison to the research conducted by Lewis (2014), the curves in both studies show the same trend for the increasing flow rates, however, the results for the k-values shown herein differ from those obtained by Lewis (2014) regarding the influence of the screen on the changes of the k-values. This trend has been shown valid for all the comparisons and will be further analyzed in the followig sections of this thesis.

Analysis of the K-values for Slurry Tests with Different Ladder Arm Swing Speeds

Evolution of the K-values Varying only the Swing Speed for an Averaged Flow Rate

The research conducted by Girani (2014) showed a good relationship between the specific gravity of the slurry and the variation of the ladder swing speed, i.e. it suggested that an increase in the swing speed would result in a greater production. Lewis (2014) also reported that increasing values of ladder arm swing speeds would also result in a higher production, which theoretically contributes to higher k-values.

The data obtained by this author in the set of experiments done at the Haynes Laboratory showed a more consistent dependence between changes in k-value and ladder arm swing speeds, but further analysis was required for a better understandings of the real patterns.

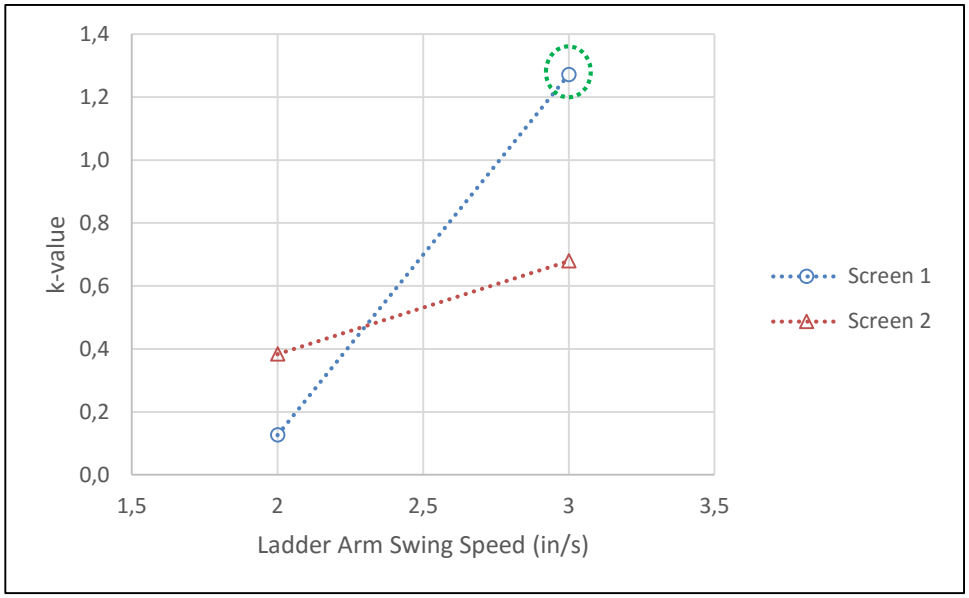

Figure 53: Variation of the Minor Loss Coefficient (k-value) as function of the ladder arm swing speed for an averaged flow rate.

Although the positive relationship between the two parameter could be observed in Figure 53, the data point circled in green seems to be a bit off than what has been observed over the comparisons. Further evaluation of the hypothesis that led to this phenomenon will be discussed over the next sections, where the k-values were compared against variations in the swing speed and in the flow rates.

Evolution of the K-values Varying the Swing Speed for each Different Flow Rate

Figure 54 shows the plot of the k-values against the two different swing speeds for each of the three flow rates. More details about the behavior of the k-values with variations in the swing speed of the ladder arm could be observed from these results.

The large spread of data and the excessively steep curve inclinations between each set of tests showed an inconsistent relationship between an increase in the swing speeds and variation in the k-values, which is counterintuitive concerning its positive relationship with the production.

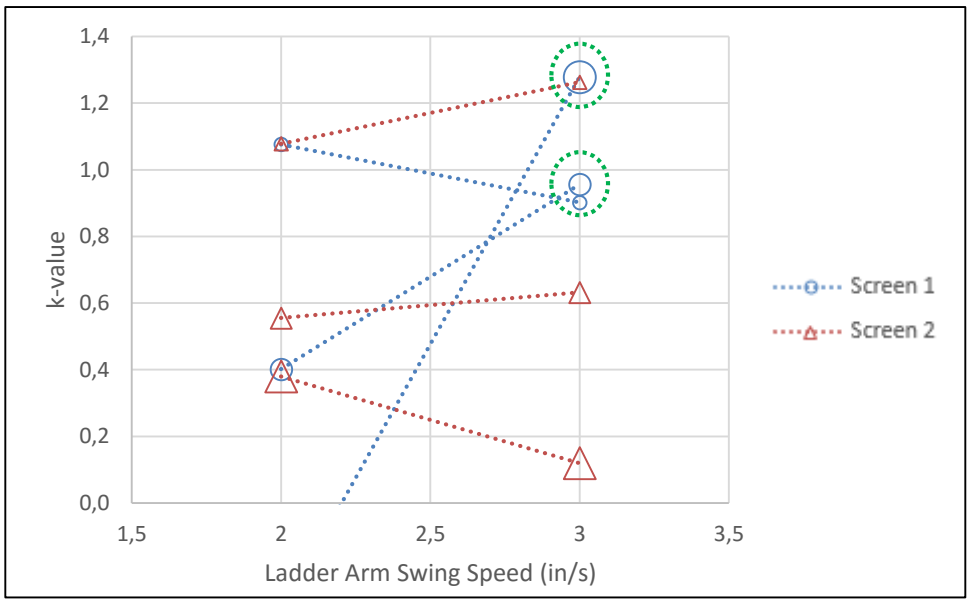

Figure 54: Variation of the Minor Loss Coefficient (k-value) as function of the ladder arm swing speed for each nominal flow rate. Small, medium and large symbols refer to the 250, 350 and 450 GPM flow rates, respectively.

The points circled in green were considered outliers given the general pattern followed by the other curves and might be disregarded for comparisons herein. If more time was available, the author would have them re-run, which would certainly result in more reliable data. The extremely high values for the screen number 1 for a flow rate equal to 450 GPM and 350GPM might have been caused due to clogging, but it could not be confirmed given the impossibility of a visual inspection.

Like previously observed for the behavior of the k-values with variations of the cutterhead rotational speed, the absolute values of the minor loss coefficient are relatively low compared to those obtained by Girani (2014) and Lewis (2014). This can be explained by the hypothesis that the high velocities employed on the model dredge created a turbulent field that affected negatively the production (decrease in the slurry's specific gravity) and resulted in lower k-values.

If the tests corresponding for the outliers (circled in green) were re-done, the author is confident that the results obtained would follow the trend displayed in Figure 55 for non-outliers, which shows lower k-values for increasing values of flow rates. This phenomenon will be better evaluated and investigated in the following section, where the two different swing speeds were compared across the three flow rates for both screens.

Evolution of the K-values Varying the Swing Speeds across the Different Flow Rates

As already suggested by previous plots, the k-values showed to have a negative relationship with increasing values of the flow rate for both screens.

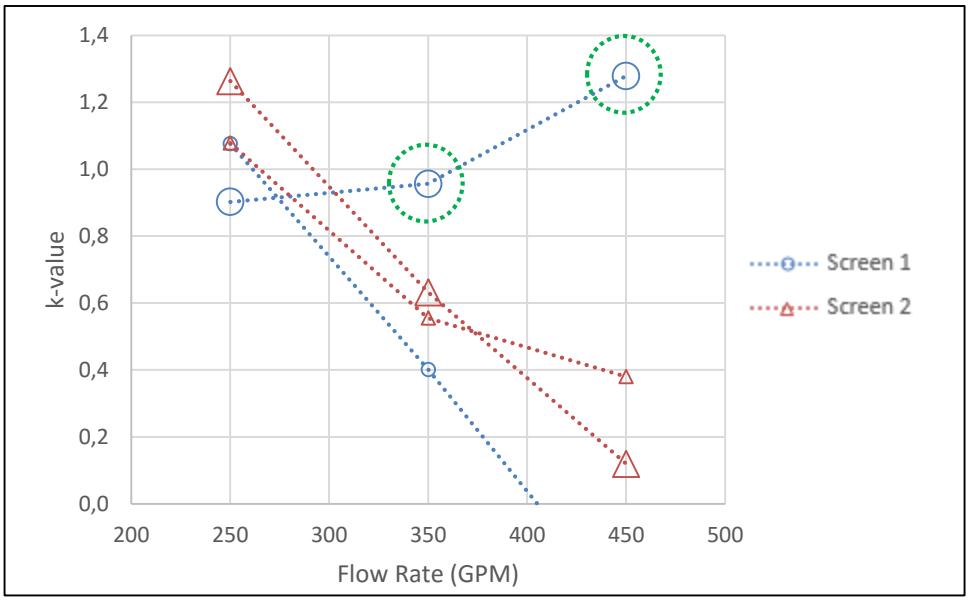

Figure 55: Variation of the Minor Loss Coefficient (k-value) as function of the flow rate. The small and large symbols refer to the 2 and 3 in/s, respectively.

The points circled in green correspond to the aforementioned outliers and were not considered for the swing speed trend analyses. Figure 55 suggests that the k-values decreases for increasing values of flow rates, which is consistent to what has been shown throughout this research. Conversely, Lewis (2014) found that the increase of the suction velocities would actually lead the k-values to converge to a common point for screen 1 (also used on his research) and spread out for a screen with a smaller opening area. However, screen 2 (smaller opening area) showed to have a more consistent pattern than screen 1. Not enough data points were obtained from the experiments and a conclusion could not be reached. Further investigations on the behavior of the k-values for a high velocity flow field is needed in order to attain a better understanding of the involved phenomena.

Comparison of the Screen Properties and the K-values

An evaluation of the screen shapes was not attempted due to the fact that the author compared the performance of two screens with different opening areas. Although Lewis (2014) reported that the results obtained from the rectangular screen showed a better performance than the curved ones, this author believes that the screen proposed on this research would perform better than the rectangular screen proposed by Lewis (2014), since its concept was to integrate both rectangular and curved features. This author would recommend for future studies, the investigation whether the hybrid screen (proposed by this research) would outperform the rectangular one proposed by Lewis (2014) for the same dredging conditions, given the fact that the curved shapes would follow somehow the motion of the cutterhead blades, which hypothetically would be beneficial for the overall production. It is also recommended the study of the near-flow field around the cutterhead, so that a pattern could be reached and a design that would maximize the production could be attempted.

Evaluation of the Screen Opening Area and the K-values

In this chapter, the author evaluated the relationship between the suction inlet net opening area, i.e. the actual area whereby the flow occurs, and the k-values. The studies conducted by Girani (2014) and Lewis (2014) show that the smaller the opening area, the higher the k-values are expected to be. This fact is widely accepted under regular conditions and extensively backed by correlated literature. Conversely, it has been shown

in this research that under turbulent conditions, the net screen opening net and the k-values have an inconsistent relationship. It is suggested more studies in this area so a better understanding of the behavior of the k-values with variation of the fixed screen opening area, or the suction inlet net area, could be established. Changes of the minor loss coefficient were evaluated for different values of cutter head rotational speeds, ladder swing speeds and flow rates in an attempt to identify how the k-value would behave with not only different screen opening areas, but also variations of these operating parameters.

Evaluation of the Behavior of the Minor Loss Coefficient for each Cutterhead Fixed Screen for Water Tests

The comparison of the behaviors of the minor loss coefficient and fixed screen opening areas was of great importance to provide reliable information on how a variation of the suction mouth β-coefficient would lead to changes in the k-values for such flow field dominated by high velocities.

The results obtained from the experiments showed that screen 1 ($\beta = 61.7\%$) had a higher average minor loss coefficient due to the placement of the fixed screen (k-value) than screen 2 ($\beta = 55\%$) for all tests with different cutterhead RPMs and ladder arm swing speeds across the three nominal flow rates employed in this research

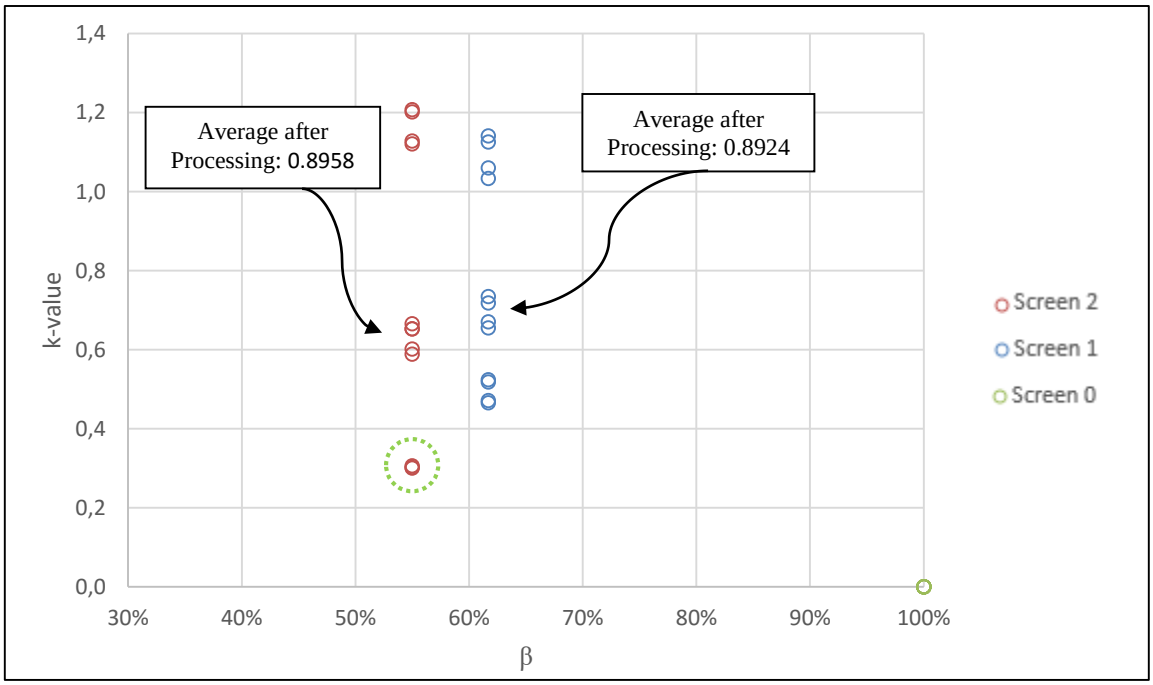

Figure 56: Plot of the Minor Loss Coefficient (k-value) as function of the screen opening area (β) for all screen configurations investigated.

At first, before any kind of processing, the plot in Figure 59 showed unexpected results for the average k-values of both screens, since it is intuitive to relate a smaller screen opening to higher k-values. Conversely, the aforementioned trend was not observed on the preceding figure, which actually indicates a higher average k-value for the screen with the largest opening area. This phenomenon can be explained by the existing turbulence at high velocities that was responsible for concealing the actual effect of a given fixed screen, by means of reducing the specific gravity of the dredged material, which is directly linked to the k-values (Girani, 2014). The point circled in green was considered to be an outlier affected by this induced turbulence.

This effect of the high velocities field was evidenced in Figure 56, which shows the average of k-values for each screen. However, intending to reduce the effect of the induced field disturbance, the data points related to the highest flow rate of 450 GPM (circled with a green dashed line), were excluded from the calculations. Because of this filtering, screen 2 presented higher k-values for the 250 GPM and 350 GPM flow rates.

The removal of these high velocities showed an increase on the k-values associated with screen 2, whose minor loss coefficient average turned to be higher than the k-values associated with screen 1. This fact strengthens the hypothesis that for high velocity flow fields the real effect of the fixed screen on the minor losses is masked by the surrounding turbulence. The study of such a pattern through a CFD analysis would be of great importance and highly recommended for a better understanding of the mentioned phenomenon.

Equation (57), developed by Lewis (2014), represents the k-value as function of the fixed screen opening area and velocity, which, when used to predict the minor loss coefficient associated to the conditions at which this research was conducted, did not match the real values found in the experiments the way it was expected.

$$k(\beta, V') = 24.5 \cdot (1-\beta)^{3.5} - (1.42 \cdot V' - 1.916) \cdot \left(\frac{0.66}{\beta}\right)^{1/3} \qquad (57)$$

where V' refers to the non-dimensional velocity and β is attributed to the screen opening area.

Table 4 summarizes the data points that presented the highest differences (in percentages), considered to be those with a deviation of 100% or more between the predicted data using the model proposed by Lewis (2014) and the measured observations in this research. Although the model did not match perfectly the conditions for screen 1, with the highest difference equal to 28%, the predictions were found to deviate more from the experimental results when screen 2 was being investigated.

Table 4: Deviation (%) of the model proposed by Lewis (2014) from the results observed.

	Condition	**Difference (%)**
Screen 2 ($\beta = 55\%$)	45 RPM and 350 GPM	117%
	45 RPM and 450 GPM	304%
	55 RPM and 350 GPM	145%
	55 RPM and 450 GPM	293%
	2 in/s and 350 GPM	121%
	2 in/s and 450 GPM	295%
	3 in/s and 350 GPM	140%
	3 in/s and 450 GPM	301%

Some major conclusions could be drawn from Table 4. Firstly, the magnitude of the differences are extremely higher than what is acceptable for usual mathematical models used for predicting purposes. Secondly, considering the fact that the greatest percentages are ascribed to the highest velocities, the hypothesis of the induced turbulence eclipsing the real effect of a smaller screen opening area gains more validity. Lastly, given the fact that the 250 GPM flow rate did not result in a difference greater than 100% and the relative difference between the 350 GPM flow rate and 450 GPM are much more significant, this author concluded that the increase in the induced suction velocity is linked to greater deviations from the data points predicted by Lewis (2014).

Evaluating the difference between the predicted data and the real values made evident that the equation does not hold true for velocity flow fields induced by higher rotational speeds and flow rates. This author did not attempt to come up with a model for predicting k-values as function of the screen opening area and velocity for dredging under a complete turbulent flow field. A deeper study of the environment around the cutterhead in an attempt to generate a model with capabilities to take into consideration variables imputed to turbulent scenarios is recommended.

However, in order to compare the trends observed in this research for water-only tests, against the behavior of the k-values in the set of experiments conducted by Lewis (2014), with minimum effect of the turbulence, this author fitted an exponential curve to the existing and reliable data, i.e. excluding outliers likely derived from the turbulent

operating conditions. The form of the curve was found using CurveExpert™ and further modified to meet existing the experiment's intrinsic physical characteristics.

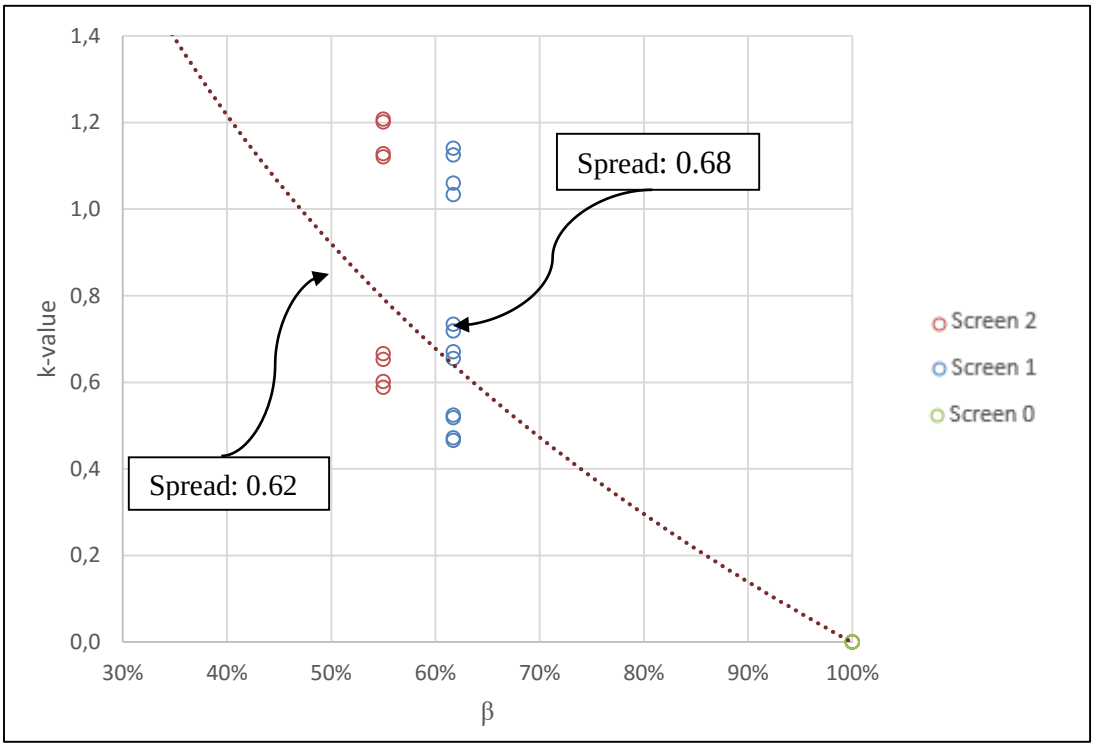

Figure 57: Exponential decay observed across the data for all screen configurations.

Given the exponential nature of the phenomenon, the curve fitted to the data points has the form of Equation (58).

$$k(\beta) = \ a \cdot (1 - \beta) \cdot e^{-b\beta} \tag{58}$$

where a and b refer to the inherent parameters of an exponential curve, and 'β' refers to the fixed screen opening area. The parameter a determines the scale of the vertical axis and b is relative to the shape's curvature. This author suspects that these parameters are associated to the level of turbulence induced by the high velocity flow field around the

cutterhead. Supplementary studies involving detailed CFD analyses of the induced flow field are recommended in order to elaborate a method to compute the value of these curve-fitting parameters as function of the parameters involved in the observed turbulence.

Intending to find a general decay solution for both researches, this author also took into consideration the results from the prediction model developed by Lewis (2014), using Equation (57), for the three nominal flow rates investigated in this research and a screen with 45% opening area (also investigated in Lewis (2014)). The exponential decay, represented by Equation (58), was fitted for all the observations, plotted and analyzed so the constants could be calculated. The resulting chart was plotted and it is shown in Figure 58.

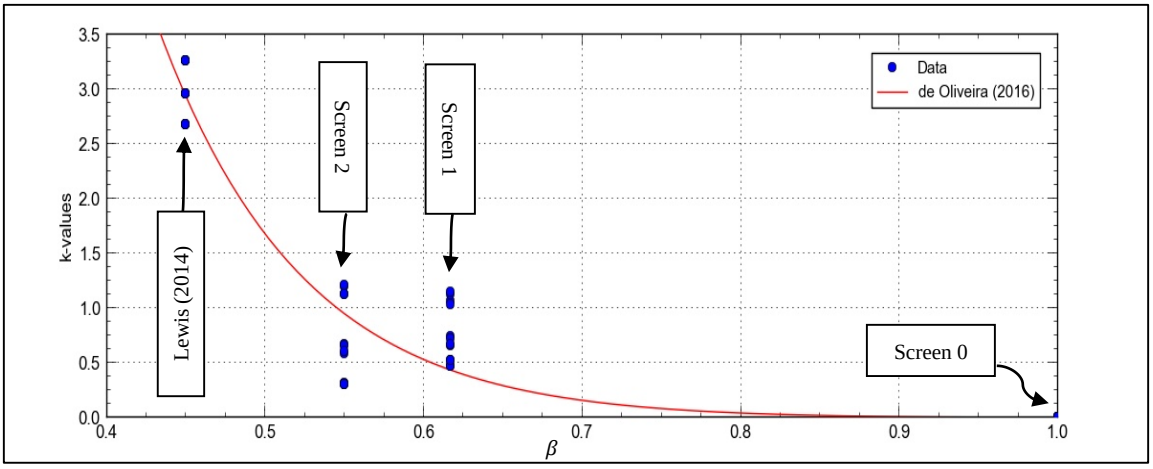

Figure 58: Resulting exponential decay when considering data from Lewis (2014) and de Oliveira (2016). Fitted with CurveExpert™.

Through an iterative method, this author computed the values of a and b, which resulted in a best-fit for the data set and incorporated the results from both experiments. The final version of the equation for water tests is given by Equation (59).

$$k(\beta) = 347.096 \cdot (1 - \beta) \cdot \ e^{-9.281 \cdot \beta} \tag{59}$$

It is also important to state that the limited time at the Haynes Laboratory and, consequently, limited amount of data, contributed for a rough computation of the aforementioned constants.

An extra term to account for the velocity-dependent nature of the k-values was calculated in which the suction velocity was put in a non-dimensional form in the same way done by Girani (2014), i.e. dividing the induced suction velocity (V_s) by the critical velocity (V_c) (minimum velocity capable of transporting sediment). The non-dimensional velocity (V_n) is, then, given by Equation (60).

$$V_n = \frac{V_s}{V_c} \tag{60}$$

where V_s is the induced suction velocity; and V_c is the critical velocity, which for this research was considered to be equal to 6.17 ft/s. This is the same value used by Lewis (2014), since the sediments used for the experiments and the suction line found on the dredge remained unchanged. The critical velocity was taken visually from the nomograph proposed by Wilson, et. al. (2006) for a 4-inch pipe and sand.

Table 5 shows the three nominal flow rates next to their correspondent non-dimensional values, which were averaged across all set of experiments to provide more reliable results.

Table 5: Averaged non-dimensional flow rate with its respective nominal flow rate.

Nominal Flow Rate	Averaged Non-Dimensional Flow Rates
250 GPM	1.01
350 GPM	1.44
450 GPM	1.85

As shown in previous chapters, variations of both cutterhead rotational speeds and ladder arm swing speeds showed little relationship with changes in the k-value. Additionally the turbulent flow field created by the high velocities concealed the real effect of a reduction in the suction mouth net opening area that led to smaller magnitude k-values in comparison to former researches. Given the nature of the set of experiments, the model proposed in this section is not only a function of the fixed screen opening area and suction intake velocity induced by the flow rate, but is also limited to water-only dredging operations.

To account for the velocity-induced spread of data for each screen, a correction term had to be employed, in which the average of the spread was scaled according to the suction velocity. The spread of the reliable data is also displayed on the plot of Figure 57.

The spread of the k-values for screen 1 is equal to 0.68, while the spread for screen 2 is equal to 0.62. Thus, the average spread of k-values for both screens is equal to 0.65. The other terms on the velocity correction term refer to the median value of the non-dimensional velocities ($V_{nmedian} = 1.45$ ft/s) and the spread of theese non-dimensional

velocities ($V_{nspread} = 0.84$). The final term relative to the suction velocity correction is given by Equation (61).

$$Induced - Velocity\ Spread\ Correction\ Term = 0.65 \cdot \left(\frac{1.45 - V_n}{0.84}\right) \quad (61)$$

To account for the theoretical, although not seen, effect of decrease of k-values data spread with increasing values of the screen opening area this author came up with a scaling term, which is denoted by Equation (62).

$$Spread\ Scaling\ Term = \ c \cdot e^{d/\beta} \quad (62)$$

Equation (62) has an exponential form and features the coefficient β on the denominator of the power-term, given the nature of the aforementioned decay-phenomenon. The values found in this research for *'c'* and *'d'* were 0.035 and 1.74 and refer to the vertical scale of the decay function and to its shape. This scaling term was then multiplied by Equation (61) to result in the final equation.

$$k(\beta, V_n) = \quad (63)$$

$$347.096 \cdot (1 - \beta) \cdot \ e^{-9.281 \cdot \beta} + (1.122 - 0.774 \cdot V_n) \cdot 0.035 \cdot e^{(1.74/\beta)}$$

It is important to remember that outliers associated with the flow field turbulent characteristics were not considered for the development of the proposed equation, which presents a reliable way of predicting k-values under turbulent and normal conditions, even though it is not a function of variables used to model turbulence.

Figure 59 shows a plot of both models next to each other. It is evident that in each model the behavior of a change in the fixed screen opening area is different. In the curve plotted from Equation (63) the reader can notice that a much flatter trend is presented for the current dataset. The proposed function is different from the equation proposed by Lewis (2014) mainly at the mid-section of the plot, i.e. when evaluating smaller screen opening areas. It was one of the objective of this thesis to fulfill the former existing gap between the 45% and 61.7% opening areas. The reader can observe that the presence of the data points for an opening area equal to 55% were responsible for shifting the curve downward. To guarantee the accuracy of the proposed model, the author also incorporated the results obtained by the equation proposed by Girani (2014) for 50% opening area, which was also used in Lewis (2014) for the same purpose.

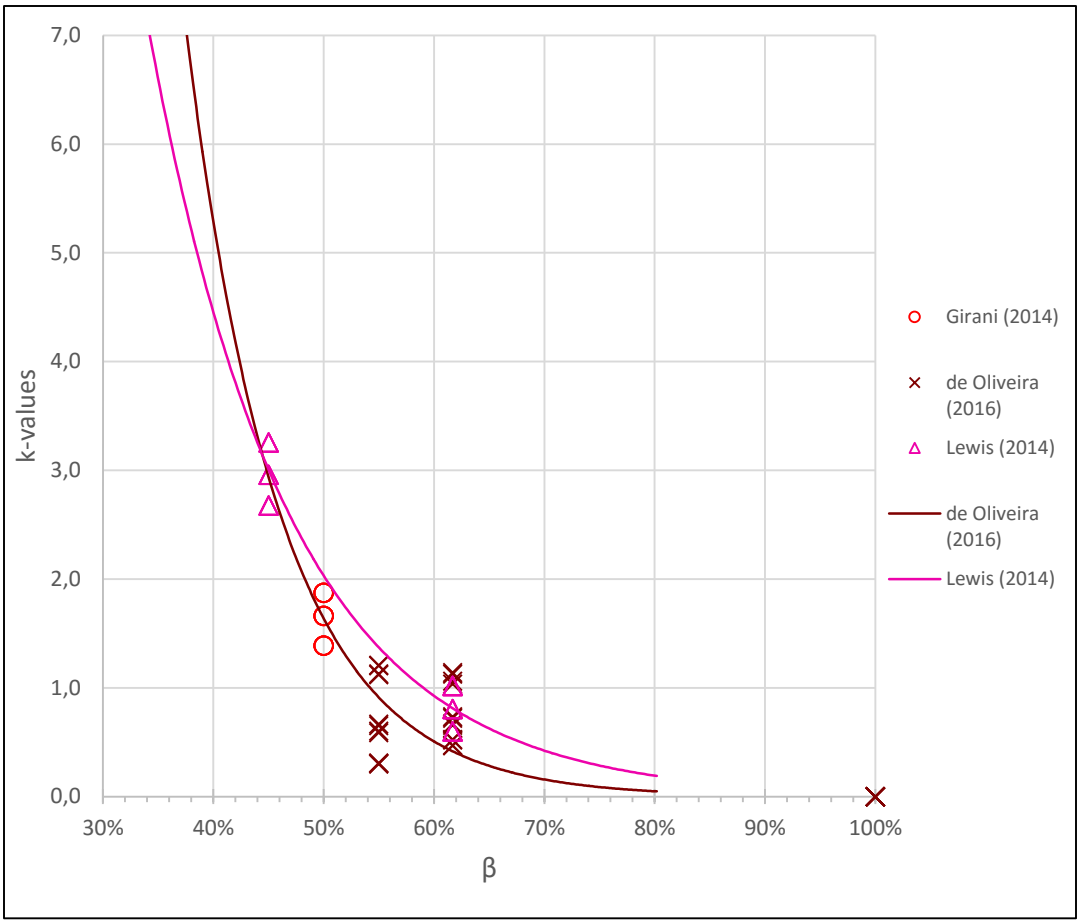

Figure 59: Plot of both Minor Loss Coefficient prediction models ranging from β=0.35 to β=0.80 for averaged results of k-values of all flow rates.

The curve plotted by this author also seems to be a better fit to all data points investigated across these three researches. The reason why the curve proposed in this thesis presents a flatter shape for the region comprehended between β equal to 50% and 61.7% could be directly linked to the other operating parameters involved and will be better explained over the next sections.

Intending to have a better way to compare the models for each investigated flow rate the author plotted Figure 60 and Figure 61, which display individually the result obtained from the models for each of the three flow rates studied in this research.

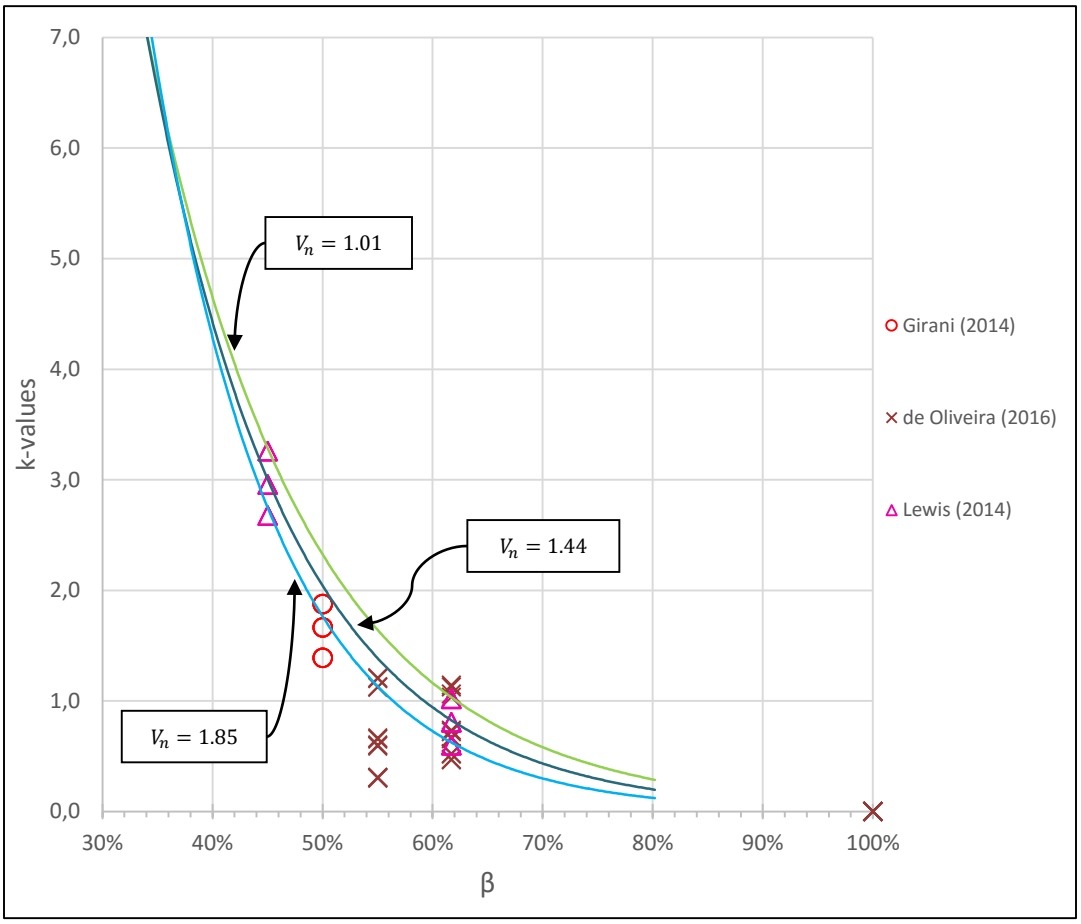

Figure 60: Plot of the prediction model proposed by Lewis (2014) for each of the three investigated flow rates.

In Figure 60 the author plotted the prediction curves from the model proposed by Lewis (2014) for each of the three operating flow rates investigated in this research. As expected his model has a good agreement with the predicted data by its function (pink

triangles), however the same level of agreement is not reached when using it to predict the results for neither the 55% screen, nor the one with 50% opening area modeled with the equation present in Girani (2014). This disagreement with the results from Girani (2014) was also reported in the research conducted by Lewis (2014) and also confirmed by this author. Nevertheless, the prediction model this author came up with presented a better correlation with the investigated data and was plotted in Figure 61.

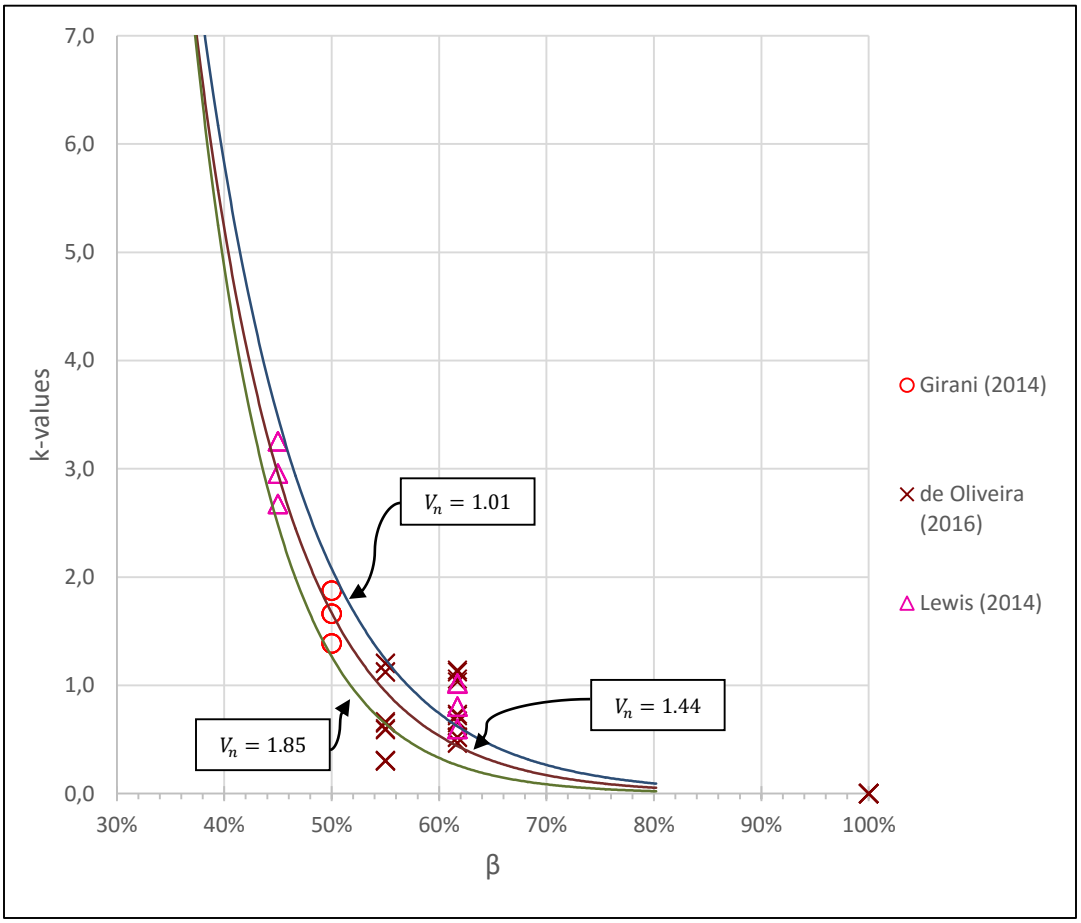

Figure 61: Plot of the prediction model proposed by de Oliveira (2016) for each of the three investigated flow rates.

The chart plotted in Figure 61 shows a strong correlation with all results investigated and data observed from the models proposed by Girani (2014) and Lewis (2014). This level of agreement and the fact that the major differences in the prediction equation formulations was regarding the decay function led this author to conclude that the phenomenon under observation is better fitted with the exponential decay proposed in this research rather than with the power law function proposed by Lewis (2014). This hypothesis could only be formulated since the gap (between 50% and 62%) covered by this research is now fulfilled.

Both models seem to agree on the fact that the presence of a fixed screen on the suction inlet of the cutterhead dredge has almost no influence on the losses across the systems for β-coefficient over 70%. It is recommended more studies regarding the behavior of different screen opening areas amidst turbulent flow fields should be conducted, so their relationship with dredging operating parameters could be better understood. It is also needed the investigation of larger screen opening areas in order to evaluate the behavior of the curve after the point where $\beta = 0.62$ to confirm the trend shown by both models for increased values of the fixed screen opening area.

Besides the form of the equation predicting the phenomena decay, the function parameters a and b are essentially what distinguish both proposed models. These constants were found to possibly be a function of the system's level of turbulence and are likely to vary according to the scenario under investigation. In an attempt to verify this hypothesis, this author swapped the values proposed for these constants in this research for those used

in Lewis (2014) power law function ($a = 24.5$ and $b = 3.5$), and plotted the results in Figure 62.

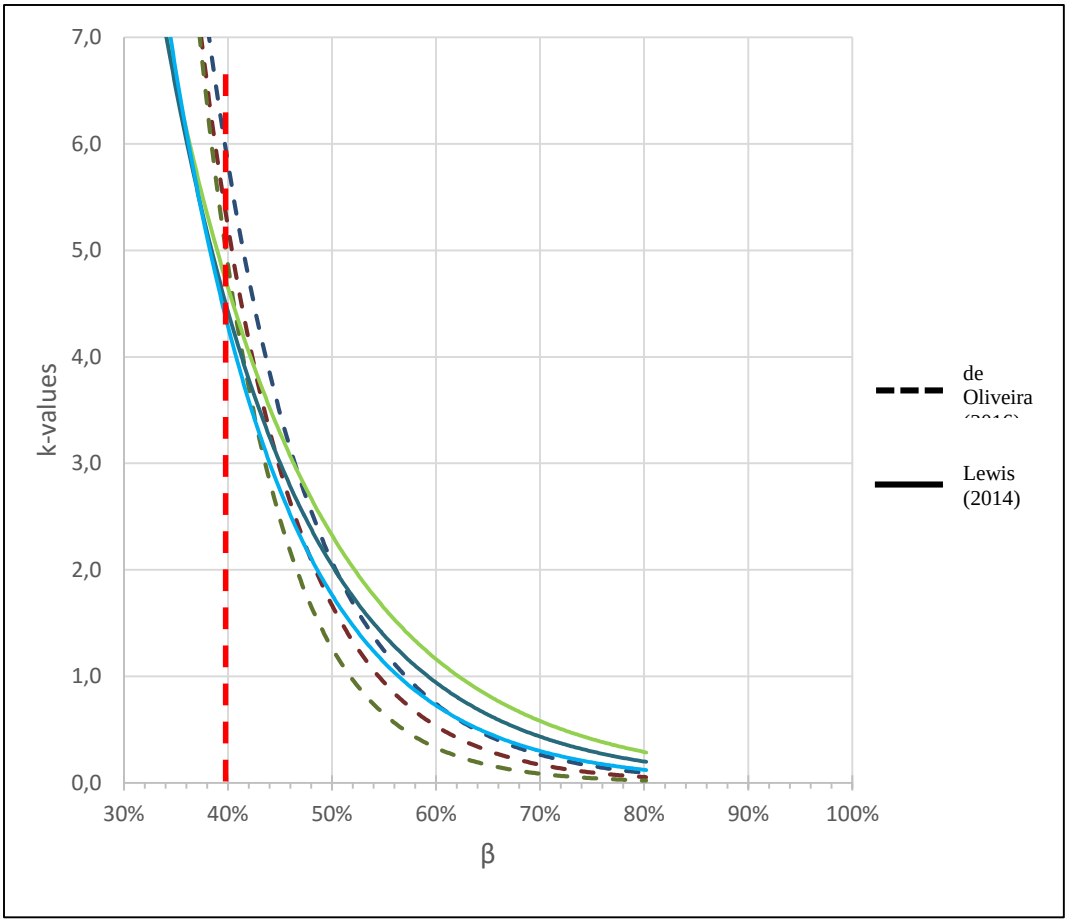

Figure 62: Plot of both models overlapping for each of the three flow rates when under the same values for a and b. The meaning of different colors are the same of Figure 60 and Figure 61.

Although the results do not match the observations made on the experiments, it is useful to reach some important conclusions given the nature and difference of both set of experiments. Based on the fact that the experiments conducted by Lewis (2014) were done for flow rates ranging from 250 GPM to 400 GPM, cutterhead rotational speeds going

from 15 RPM to 45 RPM and ladder arm swing speeds from 1.0 in/s to 3.0 in/s, i.e. for different operating conditions, it is evident that the results would be also different. However, the fact to be highlighted is the possibility to predict the results obtained in Lewis (2014) by means of changing the constants of the prediction model proposed for the set of experiments performed in this research, even with the different decay equation form. What can be also gleaned from the chart is that the model's capability is only valid for β-coefficients greater than 40%.

On the other hand, changing the constants in the model predicted by Lewis (2014) did not result the same overlapping effect as seen in Figure 62. Thus, this phenomenon suggests that the previously mentioned parameters, a and b, are closely related to the conditions under which the dredging operation is being executed and that the phenomenon investigated features a rather exponential decay in comparison to the power-law function. Studies on this area are strongly recommended to understand the relationship between these parameters and dredging operating variables so these hypotheses could be further investigated.

The reader must be careful when using Equation (63), since there is a possibility of forecasting negative values, which are not valid for this kind of study. It is recommended the use of the equation along its graphic, so a more reliable information could be withdrawn.

Evaluation of the Behavior of the Minor Loss Coefficient for each Cutterhead Fixed Screen for Slurry Tests

For this set of comparisons, the author studied the evolution of the k-values for both screens for experiments with slurry. The data points consist of averaged data obtained from the experiments, in which, in this particular comparison, the operational flow rate and the specific gravity of the mixture were the parameters under investigation, since likewise the scenario for water tests, variations of the rotational speeds of the cutterhead and the swing speeds showed no major relationship with variations in the k-values.

Given the turbulent nature of the flow field around the entrance of the suction mouth and a possible effect of clogging, the plot in Figure 63 displays some extreme points that should not be considered for drawing major conclusions.

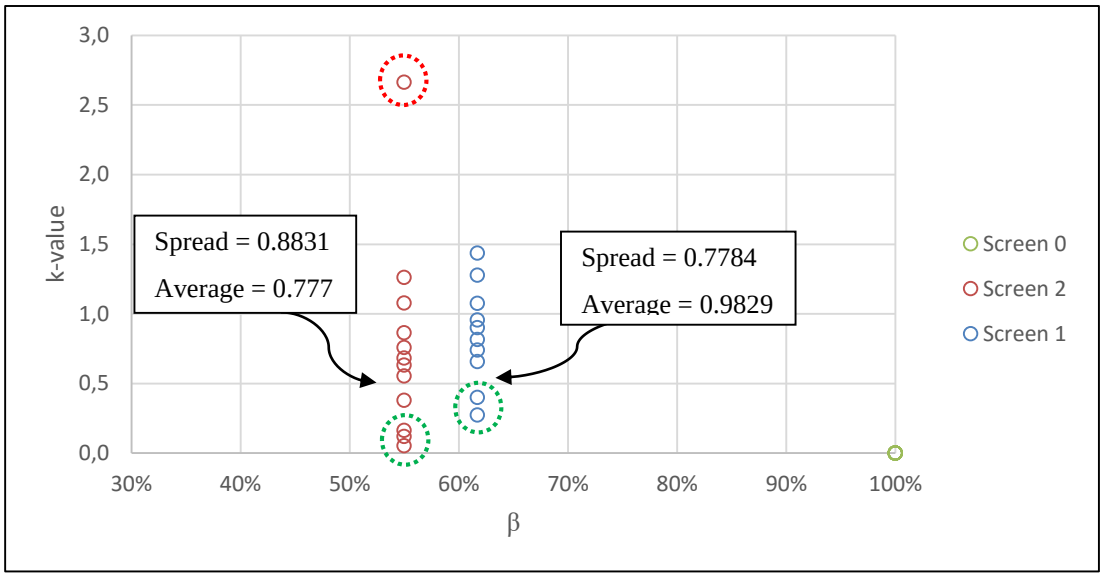

Figure 63: Plot of the observed k-values for slurry tests

The points circled with dashed lines refer to outliers, which were not taken into consideration given their natures. The point circled in red presents an extremely high minor loss coefficient, which is likely to have happened due to clogging of the screen. The points circled in green were also excluded from the calculations given their association with the turbulent environment induced by the high velocities. Even though this pre-treatment was done, the reader can observe that this high velocity flow field was responsible for masking the real effect of the fixed screen opening area, shifting downwards the expected results for screen 2 by a significant amount. The average k-value for each spread of data, before their treatment, was also plotted in Figure 63 and shows this counterintuitive phenomenon caused by the flow field characteristics. Interestingly, out of the 8 points deleted for the curve fitting (including points with negative k-value, which would make no sense considering and displaying on the plot), 4 were related to the

450 GPM and 55 RPM. This observation is useful to show the inherent correlation between a flow field dominated by high velocities and disturbances that do not follow a predicted pattern.

After the data processing, the author was capable of coming up with a relationship for the k-values and the fixed screen opening area. The curve relating the data points was then plotted following the same modified exponential decay presented in the previous section by Equation (64). Their similarity are explained by its non-dependence from the mixture specific gravity, which will be handled by the other terms and better detailed further on.

$$k(\beta) = \ a \cdot (1 - \beta) \cdot e^{-b \cdot \beta} \tag{64}$$

It is important to understand that this equation does not correspond to a best-fit curve of the set of experiments. This modified exponential decay was chosen given the theoretical nature of the phenomenon and takes into consideration other conditions related to the physics involved in the operation. The parameter a and b are two constants, which were also present in Equation (57) proposed by Lewis (2014) and already explained in this thesis and refer to the magnitude of the k-values and the shape of the decay. Throughout this research, the author observed that the k-values associated to the dredging operating parameters were relatively small when compared to previous studies; this difference was associated to the high velocity flow field at which the experiments were performed. Hence, this author suggests that the constants a and b are actually values dependent on the flow

field characteristics, once Equation (64), proposed in this thesis, is a better fit for the experiment's dataset than the power-law decay proposed by Lewis (2014).

Intending to best fit the proposed function within the set of data obtained, a non-linear regression was performed and the values for a and b were found to be equal to 371.398 and 9.281, which resulted in Equation (65).

$$k(\beta) = \ 371.398 \cdot (1 - \beta) \cdot e^{-9.281 \cdot \beta} \tag{65}$$

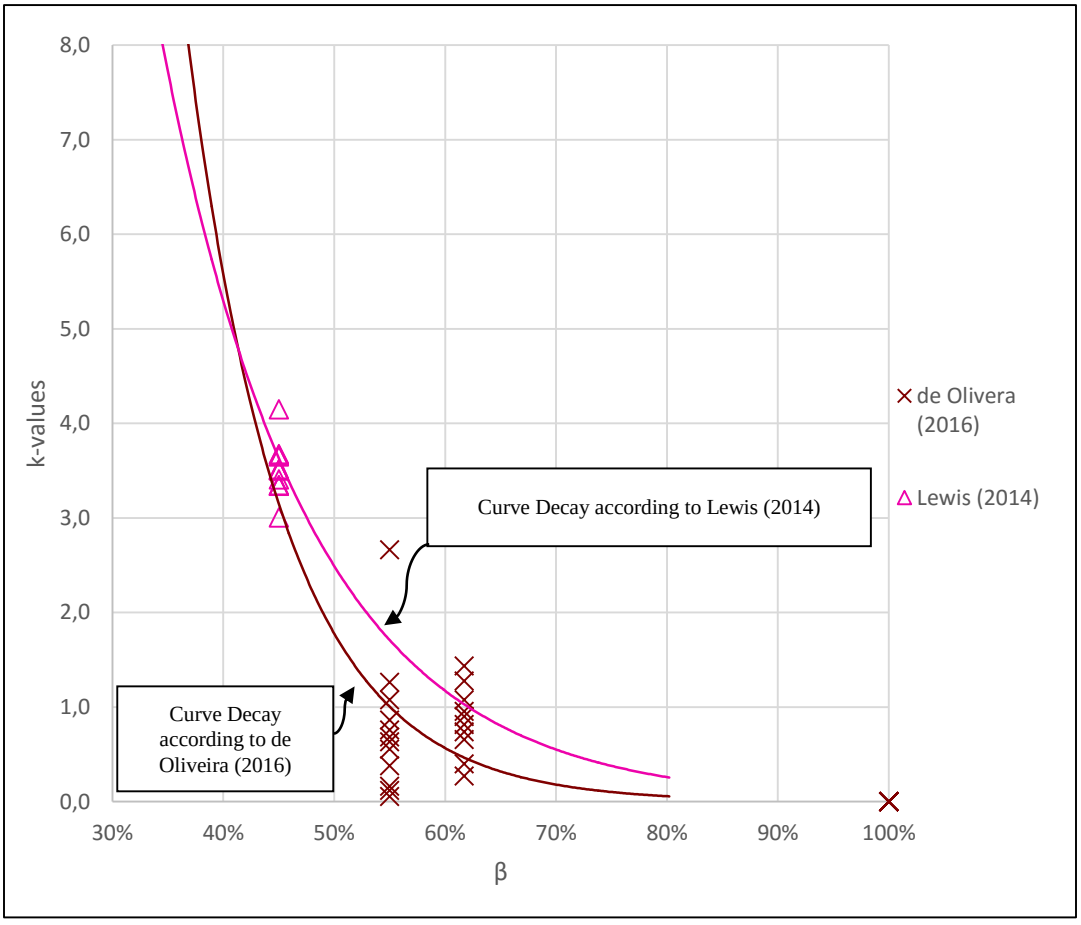

Figure 64: Curve decays according to de Oliveira (2016) and Lewis (2014).

The plot displayed in Figure 64 shows the curve correspondent to Equation (65), along the considered data points used to generate its function, and the curve originated from the model proposed by Lewis (2014).

Due to the increased specific gravity of the slurry in comparison with the water-only tests, given the nature of the experiments, it is needed to couple Equation (65) with Equation (66) for the k-values as function of the suction velocity and specific gravity previously proposed by Girani (2014).

$$k(V_s, SG) = \frac{2g}{V_s^2} \cdot (-0.694 - 0.442 \cdot V_s + 1.302 \cdot SG + 0.0468 \cdot V_s^2 + 0.187 \cdot V_s \cdot SG) \quad (66)$$

where V_s is the suction intake velocity induced by the flow rate over the 4-inches suction line and SG is the specific gravity of the slurry. According to the fact that this author proposed a new screen format to be investigated under different conditions than the ones employed by Girani (2014) in his experiments, it was necessary to evaluate the spread of data for predicted k-values of his set of experiments using the points across the three different and individually averaged flow rates for all tests of this experiment, which were 250 GPM (average of 6.25 ft/s), 350 GPM (average of 8.9 ft/s), and 450 GPM (average of 11.4 ft/s). In the same manner, the spread of k-values for the range of values of specific gravities found in this research (from 1.0 to 1.11) had to be calculated.

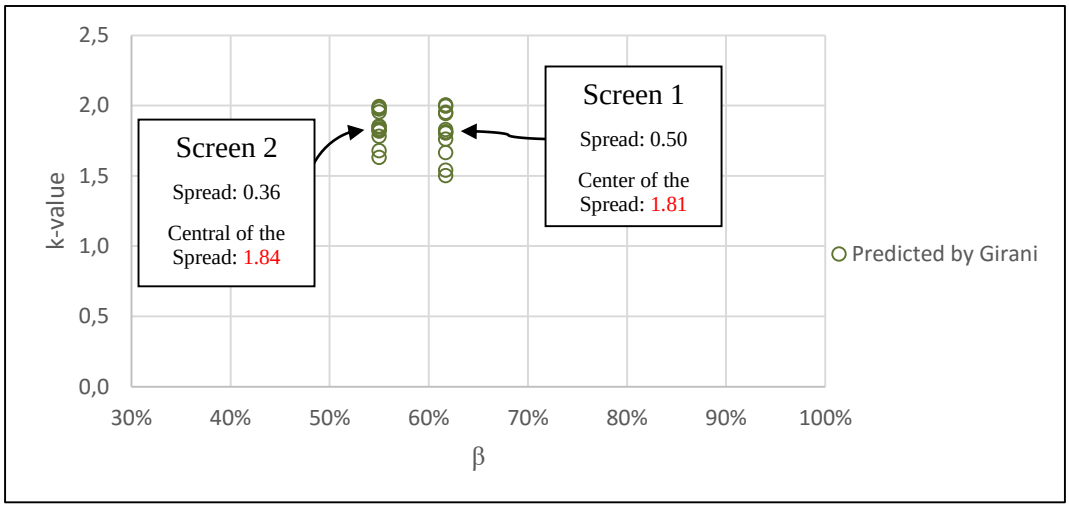

Figure 65: Predicted results by Girani (2014) for investigated screen openings.

The plot in Figure 65 shows that the spread of data encountered by Girani (2014) on his set of data was relatively small and close to one another. The central value for both screens was almost the same and their average (1.83) was taken for further processing. Before coupling Equation (65) and Equation (66), it was necessary to account for the previously mentioned spread of data in Girani (2014). Thus, a spread correction term, given by Equation (67), was introduced.

$$Spread\ Correction\ Term = \frac{2g}{V_s^2} \cdot (-0.694 - 0.442 \cdot V_s + 1.302 \cdot SG + 0.0468 \cdot V_s^2 + 0.187 \cdot V_s \cdot SG) - 1.83 \quad (67)$$

where the additional term (-1.83) refers to the distance of each point from the center value of the spread in Girani (2014) and was subtracted from his model.

Coupling the decay model proposed in this research with the spread correction term modified from Girani (2014), the general dimensional equation used to predict k-values for operations under similar flow field conditions is given by Equation (68).

$$k(\beta, V_s, SG) = \tag{68}$$

$$371.398 \cdot (1-\beta) \cdot e^{-9.281 \cdot \beta} + \left[\frac{2g}{V_s^2} \cdot (-0.694 - 0.442 \cdot V_s + 1.302 \cdot SG + 0.0468 \cdot V_s^2 + 0.187 \cdot V_s \cdot SG) - 1.83\right].$$

It is important to highlight that given the empirical nature of Equation (66) and its relationship with dimensional values, its non-dimensionalization cannot be easily performed. Considering this constraint, the proposed model works fine with the range of velocities induced by usual flow rates handled at the Haynes Laboratory. A better use of this model can be achieved by means of a visual interpretation of Figure 66, in which the respective fitted curve was plotted not only for the non-dimensional velocities investigated in this research, but also for the range of specific gravities resulted from the experiments.

Once again the model proposed by Lewis (2014) and the one proposed by this author are different from each other due to, not only the decay form, but also the constants a and b, which, when matched, resulted in almost overlapping prediction curves.

Figure 66 displays the plot of the prediction models for both slurry and water, represented by the maximum achieved specific gravity throughout the experiments and even though the velocities used as input for the second model were applied in their dimensional form, the author plotted their non-dimensional values (averaged velocities across the experiments) in order to grant the chart a more realistic use.

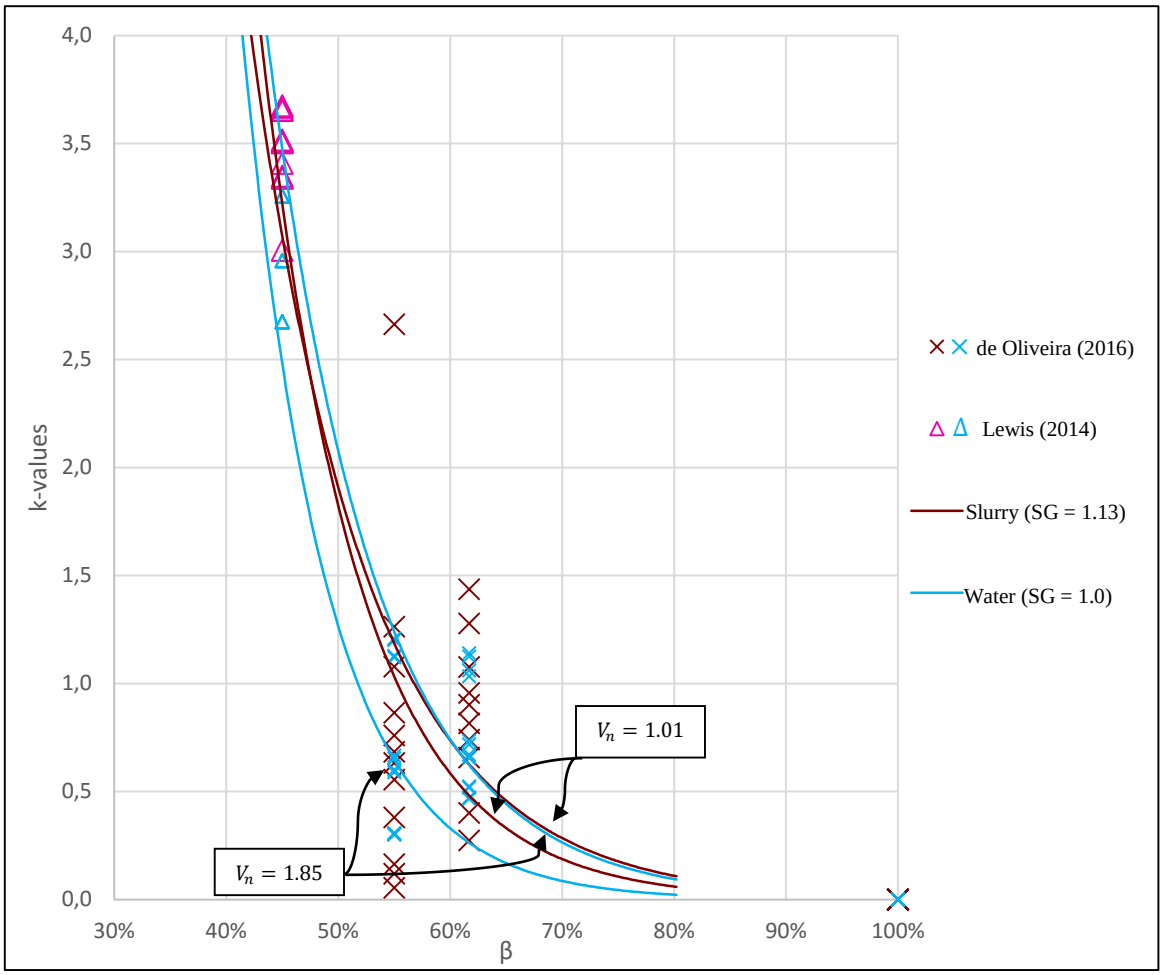

Figure 66: K-values prediction curves for the smallest and the greatest non-dimensional flow rates and maximum and minimum specific gravities.

The model proposed in this section can be used to predict the minor loss due to the placement of a fixed screen on the cutterhead suction inlet with opening areas ranging from 40% to 80% and should be used with care along its visual representation plotted in Figure 66 given the function's mathematical constraints, i.e. negative k-values prediction. In Figure 66 the author decided to plot the model for k-values up to 4.0 in an attempt to better detail the function for β-coefficient values ranging from 40% to 80%.The reader should keep in mind that minimizing the k-values magnitude by means of increasing the fixed screen opening area, may be not the best idea for the desired dredging operation, since pipeline plugging would be likely to occur. Thus, this author proposes the user of the model to apply a safety factor on his or her analyses. Moreover, considering the minor loss coefficient investigated in this research was regarding the fixed screen on the suction inlet, the reader should also take into consideration the inherent minor loss induced by the suction line entrance itself. Thus, it would be worthless the use of the model to evaluate minor losses induced by screen openings greater than 80%, since the k-values associated would be equal to the suction entrance minor loss for water tests. The suction mouth at which the fixed screen is mounted on has also an inherent minor loss coefficient, which this author included in Figure 67 as a straight line. The value of 0.3, at which the line was drawn, was taken as an assumption for water operations, since Randall (2016) shows minor loss coefficients that range from 0.1 for funnel type suction entrances to 1.0 for a plain end suction. This lower limit serves as the minimum threshold of k-values, the user of the model should account for. Hence, the reader should keep in mind that screens with

opening areas greater than 80% of the total suction mouth are pointless to be investigated given the primary reason for the installation of such fixture. Furthermore, results from the model smaller than 0.3 should not be considered, since this value is the inherent suction intake minor loss coefficient.

The reader should also take into consideration the environment in which the set of experiments was performed. The high velocity flow field caused by high rotational speeds of the cutterhead and suction velocities was found to be responsible for creating a turbulent environment, which resulted in a low production and due to the low values of specific gravity, small k-values were observed. Figure 67 provides reliable information on the behavior of the minor loss coefficient across the range of operating parameters handled in this research. Extrapolation of this data is possible, but should be done with care, given the limited dataset available for the phenomena modelling.

Considering the fact that Equation (66) was empirically developed by Girani (2014) and can accurately predict k-values for slurry with specific gravities up to 1.4, this author plotted in Figure 67 results for specific gravities related to both water-only and

sand tests. By doing it, the author sought to grant the graphic a broader use, which would enable the user of the model to investigate a larger range of slurry specific gravities.

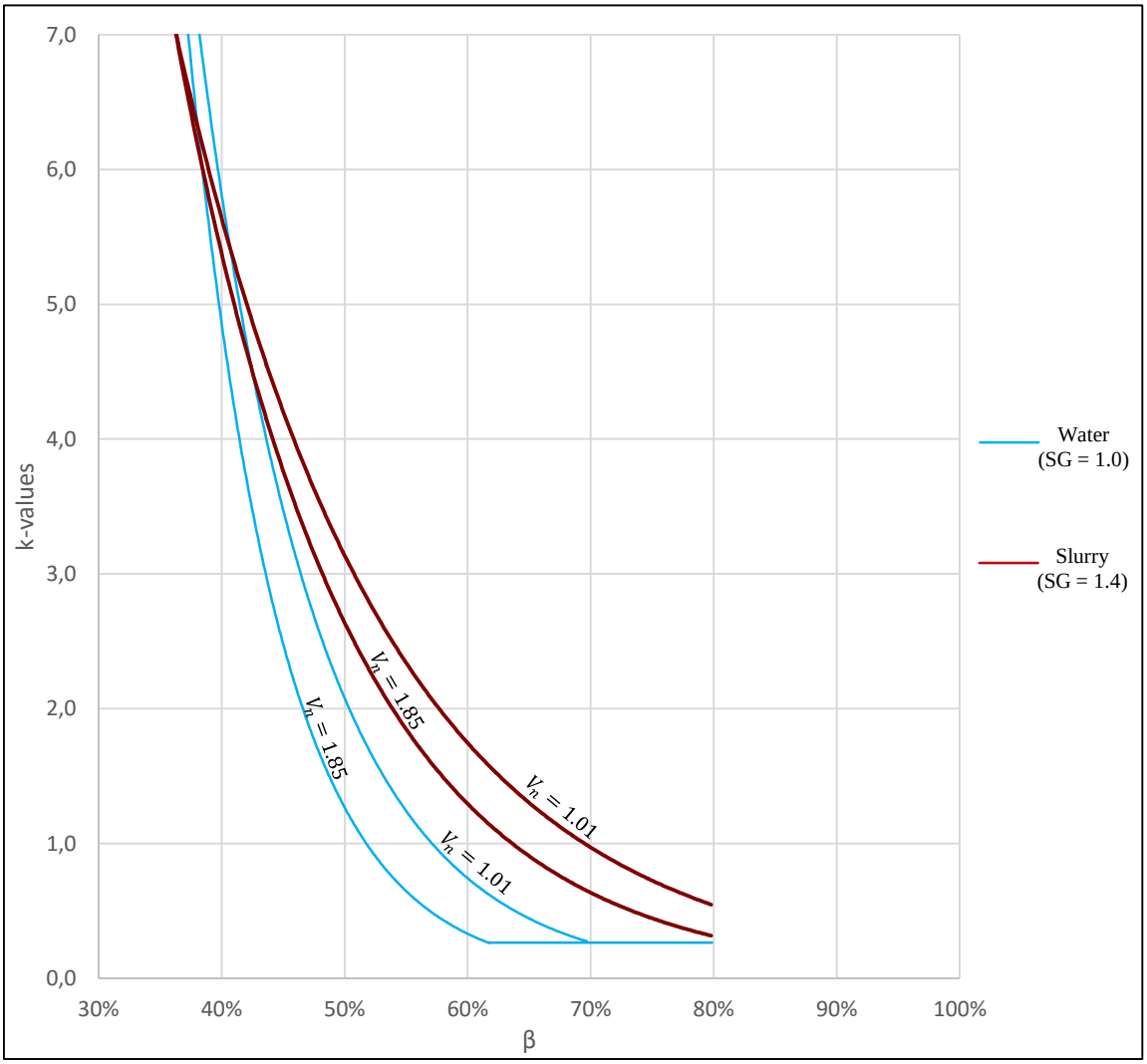

Figure 67: K-values prediction curves for the smallest and the greatest non-dimensional flow rates and specific gravities equal to 1.0 and 1.4.

Important observations can be gleaned from the plot in Figure 67. First, the author noticed that the curve for the slurry shifted upwards when the specific gravity was

increased. It can also be seen that for screen opening areas less than 45% the k-values variation skyrockets and therefore screens with such small opening areas are not recommended. It is suggested the use of the model given by Equation (68) along the plot in Figure 67, since negative values are computable on account of the mathematical formulation. This author does not recommend the use of screens with opening areas smaller than 40% or greater than 80%. Extremely small fixed screen opening areas (less than 40%) presented a minor loss coefficient over 5.0, and although β-coefficients over 80% would resulted in k-values almost equal to the lowest k-values achievable, the fixture would not meet the overall objectives of a fixed screen at the suction inlet of the cutterhead suction dredge.

Comparative Analyses between both Models

Two main reasons were to be responsible for the differences between both models and were further investigated and analyzed in this section. The high velocity flow field associated mainly with the high cutterhead rotational speeds seems to play a major role in the difference shown by both models. The RPMs investigated in Lewis (2014) went up to 45 RPM, whereas the RPMs investigated in this research started at that value. Thus, intending to investigate the data the author compared the results obtained in this thesis for 45 RPM with the ones from the model proposed Lewis (2014) for the same cutterhead rotational speed. Considering the fact that the model is not a function of the rotational speed, its effect was evaluated indirectly with regards to the specific gravity in the produced slurry for the observed experiments, since as already mentioned in this thesis,

the cutterhead rotational speed and production are positively related for the usual dredging operating parameters.

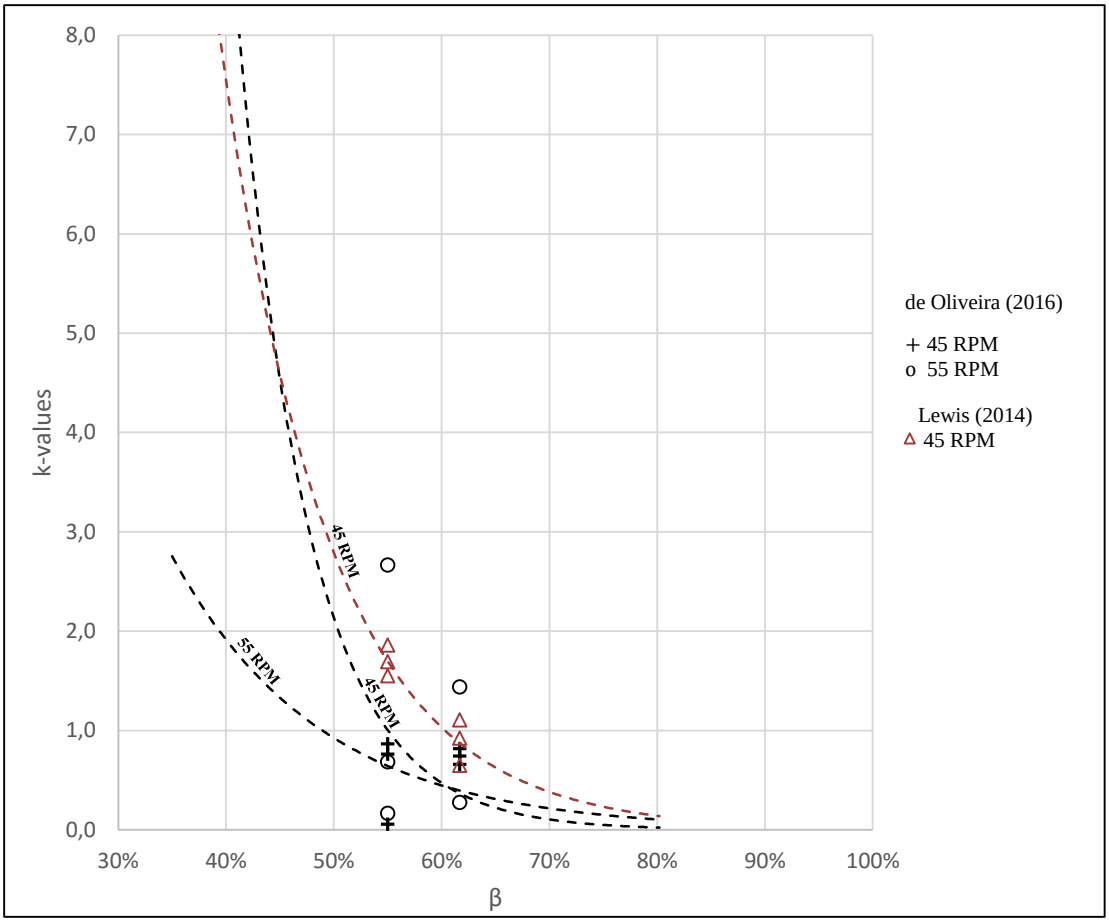

Figure 68: Plot of the de Oliveira and Lewis models for the 45 and 55 RPMs predicted k-values.

In Figure 68, the author essentially compared the influence of increasing the cutterhead rotational speeds on the prediction model and how it relates to the differences with Lewis (2014) shown in the previous sections. Considering that experimental results will never be the same for two different set of experiments, the prediction curves for the 45 RPM present a good agreement and displays almost the same trend across all the fixed

screen opening areas investigated. However, the curve showing the results for the 55 RPM predicted by this author with the model proposed in this research evidenced the already explained turbulent phenomenon responsible for flattening the curve, which is the most important difference between both models. The percentage difference between both models is equal to 61% and 32% for sand and water-only tests respectively, which as previously mentioned was mainly attributed to the cutter rotational speed values. The difference between the prediction curves increases in the region between the 50% and 70% opening areas. For water-only tests, the difference between the models in that region is equal to 53%, whereas for sand tests the curves differ in approximately 63%.

Intending to confirm this hypothesis the author plotted in Figure 69 the prediction models for the 2 in/s ladder arm swing speed, since the same configuration was also investigated by both researchers. Likewise done for the cutterhead rotational speed comparison, the results from the prediction proposed by this author for the 3 in/s swing speed was plotted on the same graph in an attempt to identify the influence exerted by the increase of the ladder swing speeds on the aforementioned disagreement.

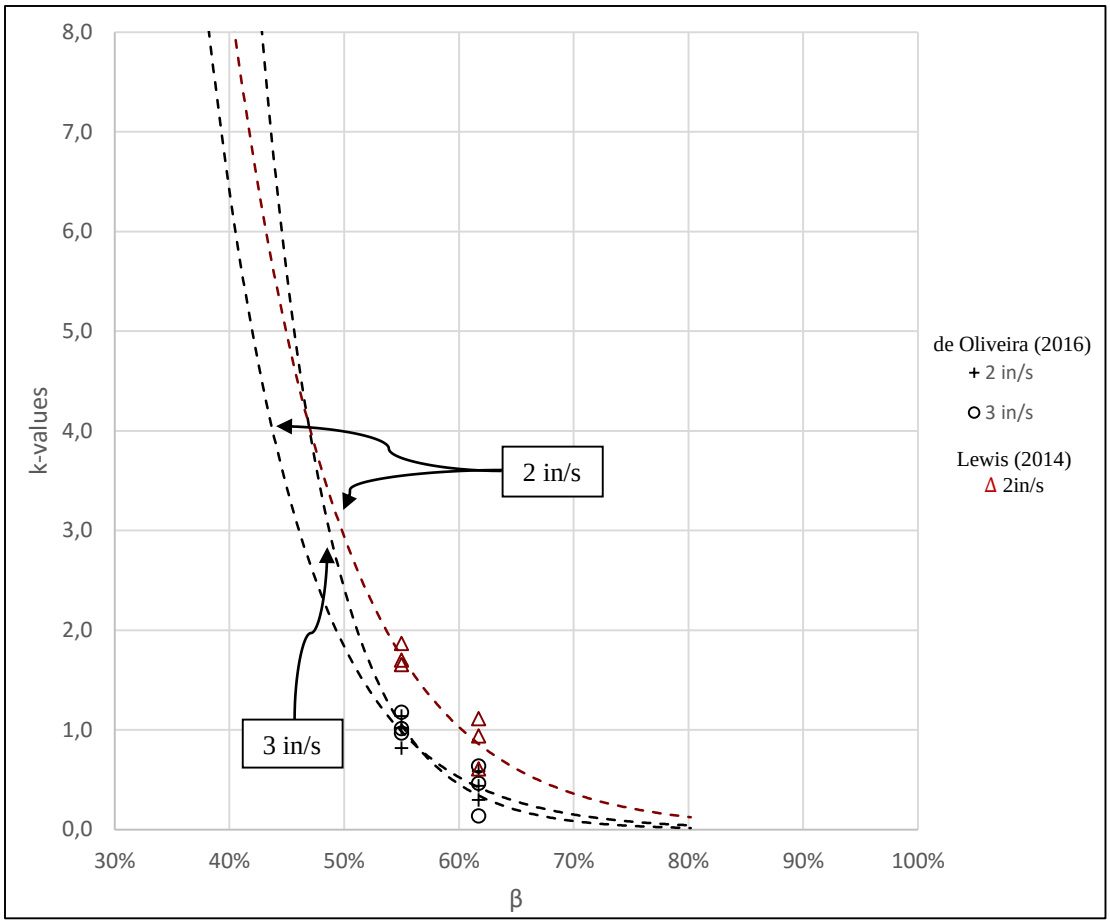

Figure 69: Plot of the results observed from de Oliveira (2016) and Lewis (2014) for ladder arm swing speeds equal to 2 in/s and 3 in/s.

From the plot in Figure 69 the author concluded that given the high level of correspondence between both models, the increase in the values of the swing speed did not affect considerably the predictions done by the model proposed by this research, which suggests that the new arm swing speed 3 in/s did not contribute for the dissimilarity observed between both models. This fact led this author to conclude that ladder arm swing speeds investigated in this research did not play a role as big as the cutterhead rotational speed with regards to the turbulent flow field. This hypothesis could be of a great

importance in future experiments, since it evidences the capability of the model dredge to operate under even higher swing speeds.

The reader should keep in mind that what should be comprehended from these curves are their trends rather than their absolute values. Given the limited time available at the Haynes Laboratory this author could not isolate each of the investigated parameters for further and more detailed analysis. These plots serve to show the impact of the turbulent environment in which the experiments were conducted and how they affected the variation of the minor loss coefficient (k). It is also important to consider that the model used to predict the k-values is a function of the fixed screen opening area, suction velocity and specific gravity. Therefore, the only way to investigate the effect of the cutterhead rotational speed and the ladder arm swing speed was by means of an indirect the evaluation of the specific gravity of the slurry associated to each of these specifications, which turned to be a reliable source given the direct relationship between these parameters.

Experimental Uncertainty

Whenever experimental tests are conducted, uncertainties of this nature should be expected. It must be kept in the reader's mind that calculating uncertainties does not mean measuring errors, instead it states what the possible error (the uncertainty) is, which is normally due to the coarseness of the measuring tools used. Regardless of the care taken throughout the experiments, errors are certainly going to creep into all experiments and

will have, at some extent, some kind of influence over the observed results. Holman (2012) defines *uncertainty* as the possible value the error may have, which in the case for theoretical methods is equal to the maximum error in any parameter used to compute the investigated function.

The method developed by Kline and McClintock and further detailed in Holman (2012) determines the inherent uncertainty of calculations, i.e. the inherent possible error, given the nature of the measurements and the tolerances of those measurements. Let us consider w_R to be the uncertainty in the results analyzed and $w_1, w_2, w_3, \dots, w_n$ to be the possible errors in the independent variables. As per Holman (2012), if the uncertainties in these independent variables are given with the same odds, then the uncertainty in the result having these odds is given as

$$w_R = \left[\left(\frac{\partial R}{\partial x_1} w_1\right)^2 + \left(\frac{\partial R}{\partial x_2} w_2\right)^2 + \left(\frac{\partial R}{\partial x_3} w_3\right)^2 + \cdots + \left(\frac{\partial R}{\partial x_n} w_n\right)^2\right]^{1/2} \tag{69}$$

where

$$R = R(x_1, x_2, x_3, \dots, x_n) \tag{70}$$

is a given function of the independent variables within parenthesis.

In the present study, the variable *R* is the minor loss coefficient of the system due to the placement of a screen at the suction entrance, whereas the independent variables are related to the part of the system we are investigating. In this research, the aforementioned variables are the specific gravity, the pressure of the pump, the velocity, the depth of the

cutter head, among others, whose terms in the equation above refer to the rate of variation of the minor head loss, per unit change of the intrinsic independent variable

Considering that

$$\Delta h_{screen} = \frac{k_{screen} \cdot {V_s}^2}{2g} = \left[\frac{\Delta P_{2n} - \Delta P_{1n}}{\gamma_{mixture}} + \frac{\Delta({V_{2n}}^2)}{2g}\right] \tag{71}$$

the function that represents the minor loss coefficient due the screen at the suction entrance can be written as Equation (72).

$$k_{screen} = \left[\frac{2g}{{V_s}^2} \cdot \left(\frac{\Delta P_{2n} - \Delta P_{1n}}{SG_{mixture} \cdot \gamma_{water}}\right) + \frac{\Delta({V_{2n}}^2)}{{V_s}^2}\right] \tag{72}$$

Taking all variables that induce, at some extent, influence over the minor head loss behavior into consideration and plugging them into Equation (69), we can, then, re-write

$$w_{k_{screen}} = \left[\left(\frac{\partial k_{screen}}{\partial V_s} w_{V_s}\right)^2 + \left(\frac{\partial k_{screen}}{\partial \Delta P_{2n}} w_{\Delta P_{2n}}\right)^2 + \left(\frac{\partial k_{screen}}{\partial \Delta P_{1n}} w_{\Delta P_{1n}}\right)^2 + \left(\frac{\partial k_{screen}}{\partial SG} w_{SG}\right)^2 + \left(\frac{\partial k_{screen}}{\partial \Delta V_{2n}} w_{\Delta({V_{2n}}^2)}\right)^2\right]^{1/2} \tag{73}$$

To calculate the general uncertainty of the calculations for the k-values related to the given screen condition (denoted by the subscript *n*), the author had to plug all the intrinsic uncertainties for each of the given variables. This information was generally provided by the maker of each of the sensors responsible for the data acquisition. First, the uncertainty of the flow meter was introduced in the equation. According to the Khrone

IFC 090K specifications, the gauge has an uncertainty of 0.3%. Considering the fact that the flow rate and its induced velocities are correlated by a constant, which is the area of the suction and discharge lines, the author found the uncertainty of the suction velocity measurements to be equal to 0.5%. These calculations were done taking into consideration the coarseness of the measuring tools that led to an uncertainty of 0.1 mm for pipe radius measurements, which corresponds to an uncertainty of 0.1% and around 0.2% for measurements of the cross-sectional area. Converting the flow rates to the same units used for usual velocity representation and relating it to the pipe dimensions uncertainty resulted in an overall uncertainty equal to 0.5%, as previously mentioned. The uncertainty for the suction pressures are given by the intrinsic accuracy of the pressure sensors that is equal to 0.25%, which yields an uncertainty for the ΔP_{2n} equal to 0.5%. The hydrostatic pressure is a function of the depth of the tank and the respective uncertainty for the ΔP_{1n} is simply equal twice the uncertainty of the measurements for the dimensions, which, as already mentioned, is given by the coarseness of the tools and equal 0.1% of the measurements. Hence, the maximum uncertainty for the variation of the hydrostatic pressure is equal to 0.2%. Regarding the uncertainty of the specific gravity measurements, the nuclear density gauge is the sensor to be investigated. The uncertainty of such device is equal to 0.71%, according to the specifications provided by its maker. The last term to be evaluated is the variation of the square of the velocity at point 2. For practical reasons point 2 was taken at a point where $V_s = V_2$, which means that the uncertainty for the suction velocity and the velocity at point 2 are the same and resulted in an uncertainty equal to 0.98% for both

squared velocities that, following the same logic as the other velocity variations, resulted in an uncertainty equal to 1.95%. This term was found to be the most influencing term for the overall uncertainty computed for the k_{screen}.

These values, along the partial derivatives of k_{screen} with respect to all investigated variables, served as input for Equation (73) that resulted in a maximum uncertainty of 0.07% and corresponded to an uncertainty of 0.0019 in absolute values for the maximum k-values observed in this research ($k = 2.663$).

Bathymetry Measurements Analysis

The ADV used for the bathymetry measurements was connected to computers placed atop of the carriage and the recorded data was stored for further processing. As mentioned in previous sections of this thesis, although two different runs were made for the seabed screening, before and after screens 1 and 2, just the second one came out in good conditions for an appropriate processing and analysis.

The profiler output data consisted of information about: the x-axis, which was used to compute the distance from the starting point until the end of the run; the velocity; and the z-distance, which was used to calculate the seabed bathymetry.

This data served as input for further processing in MATLAB®, which was used for data filtering and profile curve smoothing through the usage of a code written by one of the assistants at the Haynes Laboratory.

The ADV was run before and after the dredging operation took place. Figure 70 shows the recorded profiles for both probes before the seabed excavation for screen 2.

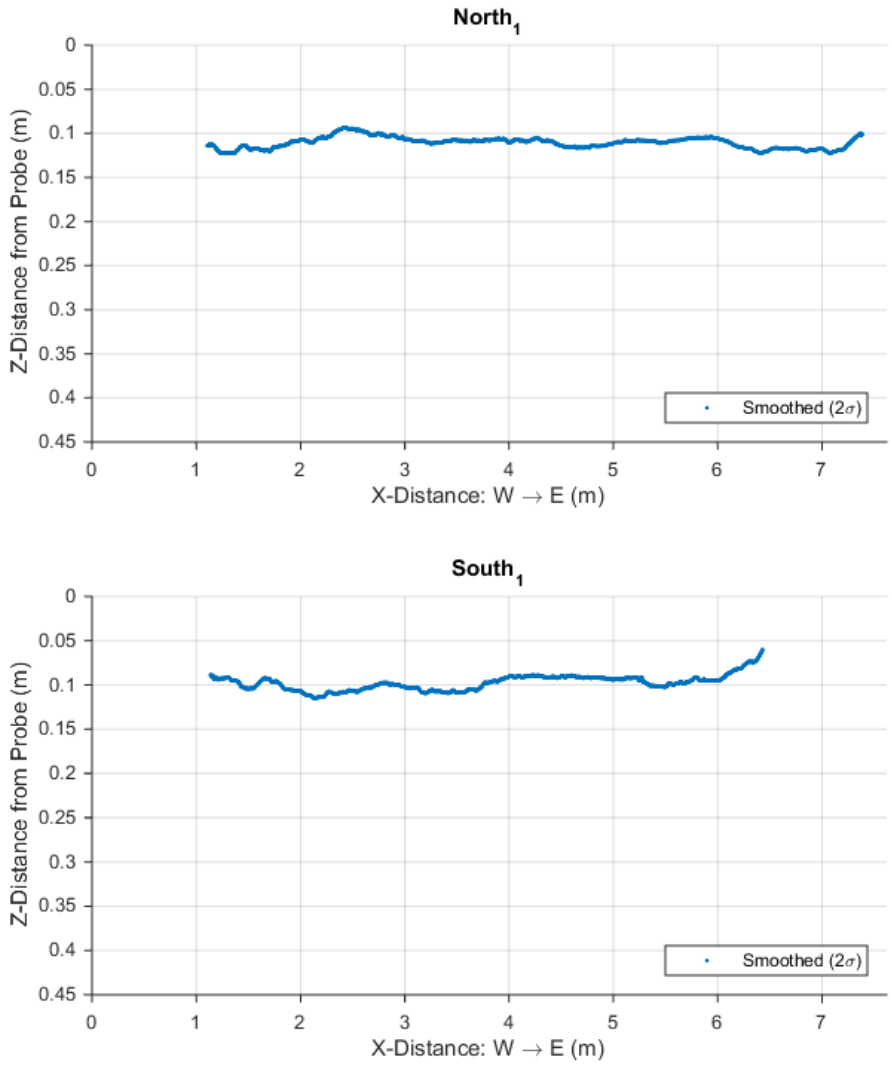

Figure 70: Seabed configuration before dredging operations took place.

Intuitively, it was already expected that the profiles followed the pattern above, since no disturbances occurred at that point and the sediment pit had been previously refurbished for subsequent experiments. The subscript 1 denotes the moment the measurements were taken, which in this case refers to the moment before the excavation

of the pit. The chart titles ‘North’ and ‘South’ refer to the location of the respective probe and are equal to ‘Port’ and ‘Starboard’, respectively. The screening direction is detailed on the x-axis, whose label indicates the carriage was moving from West to East, i.e. the same direction travelled by the dredge during its regular operations. The y-axis shows the distance measured from the beams to the seafloor, which, as displayed, was at about 0.1 m (4 in). This data on the y-axis should be carefully analyzed, as the values refer to the distance to the beams and not the real depth of the excavated spots.

The results for the seabed scanning after its excavation by the dredge is presented in Figure 71.

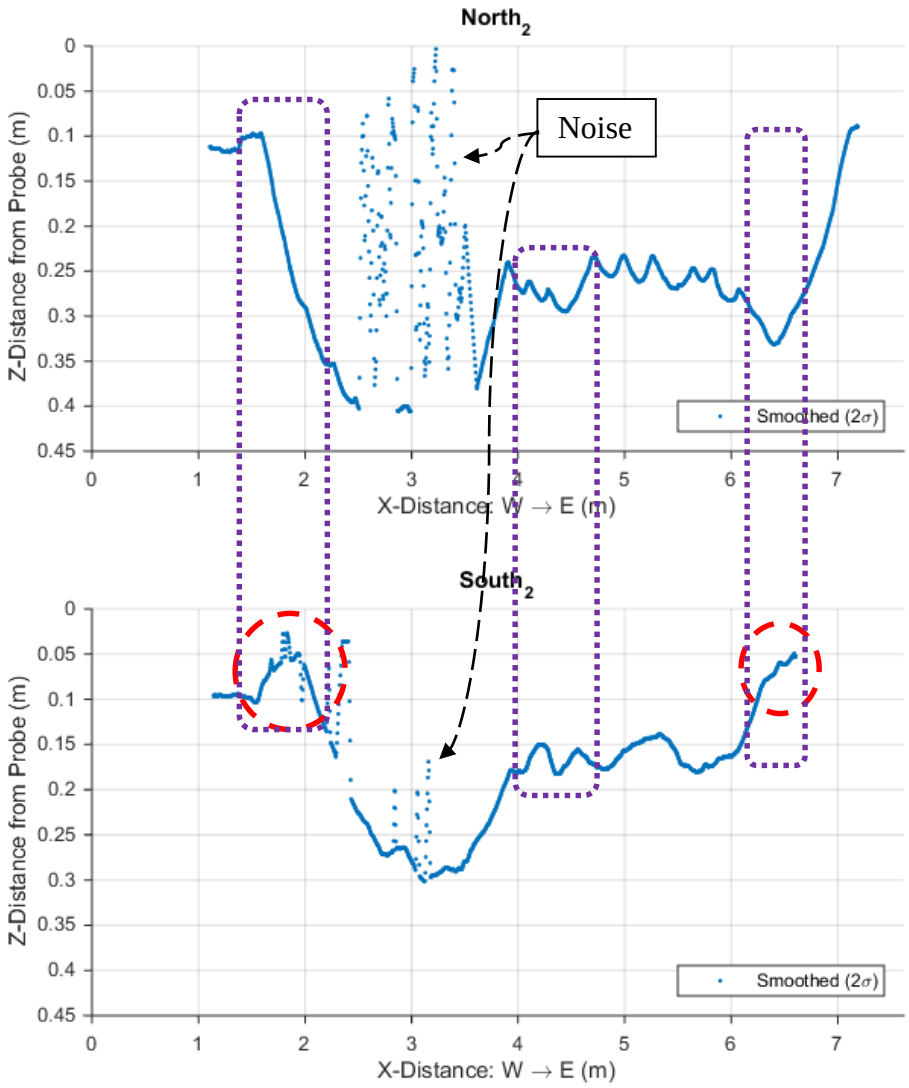

Figure 71: Seabed configuration after dredging took place.

In Figure 71, the subscript 2 refers now to the seafloor screening after it was excavated by the dredge. Some interesting, however limited, information can be gleaned from the chart. Comparing the two moments, the author noticed that for $South_2$, the peak values for both ends (circled in red) are greater than for the moment before the excavation,

suggesting a possible accumulation of sediments at that points. This hypothesis gained more strength after the author compared the results, for the second moment, of both probes to each other. It was observed that not only the greatest excavated depth was found to be related with the North probe, but also the mean distance from that probe was greater than the mean distance for the south probe. According to these results, this author was led to infer that might exist an induced current by the rotation of the cutterhead that was responsible for transporting sediment from the port side of the dredge to its starboard side. Another strong evidence of the existence of a cross-current in the y-direction is the almost direct correlation between peaks (south) and minima (north) outlined by the purple rectangles.

This author suggests that this phenomena might be closely related to the direction which the cutterhead rotates and, even though these are preliminary analyses of the single data available to be investigated, this author is confident on the finding's repeatability and recommends that more experiments of this nature be performed, not only to validate these assumptions, but also to find other trends.

This evidence can be also explained at some extent by the path followed by the ladder arm. The swinging arm was first set to travel from port to the starboard side, move forward and then back to the new origin, from where the whole carriage would advance for the starting point of the new cut, as shown Figure 36. According to the position of the installed probes, a possible reason for this offset in the peaks and troughs are possibly due to the forward movement of the carriage for the subsequent cuts.

Overall, the author observed that a reasonable amount of trends could be found and hypotheses could be attempted from the generated results, which may grant this kind of observation a great level of importance on any kind of fluid dynamic analysis and specially on dredging operations. The choice of different screening paths is also highly recommended with regards to the reliability of the results and accuracy of the data.

CHAPTER VIII

CONCLUSIONS AND RECOMMENDATIONS

In this research the author observed the behavior of a screen with opening areas (β) equal to 55% and 61.7% of the total suction mouth inlet area across different values of three of the most important parameters in dredging operations when a cutterhead suction dredge is under investigation, which are: the rotational speed of the cutterhead; the ladder arm swing speed and the flow rate.

Results from the experiments showed that an increase in the nominal flow rates would lead to a decrease in the specific gravity of the produced slurry, however a slightly positive relationship with the overall production was also observed. This observation with the fact that the greatest slurry specific gravity (SG = 1.13) was found at the lowest nominal flow rate employed, proved to be consistent with the literature and with the former researches of same nature performed using the cutterhead model dredge at the Haynes Laboratory. The analyses on this research also showed that for higher values of flow rates, the effect of the ladder arm swing speed and the cutterhead rotational speed on the specific gravity were masked. This conclusion could be gleaned through the comparison of Figure 22 and Figure 23, where both specific gravity and production showed to be more sensitive to increases of the cutterhead RPMs at the lowest nominal flow rate of 250 GPM. This observation agrees with the findings in Girani (2014) and Lewis (2014) and was explained by the overwhelming magnitude of higher velocities induced by the operating flow rates in comparison to both the cutterhead and swing speeds. This author also suggests that the

relatively lower values of specific gravity at higher flow rates was a result of the additional turbulence induced by these greater velocities onto the flow field, which was generated by the summation of all investigated parameter's velocities Observations of the same nature were also reported by Henriksen (2009).

Variations of the cutterhead rotational speeds showed no major relationship with production and specific gravity of the dredged material for an averaged flow rate and swing speed, but presented a positive relationship for both parameters when dredging was being performed at the lowest flow rate. The highest specific gravity observed in this research was found to be at the highest RPM value (55 RPM) when the flow rate was set at 250 GPM, which was still much lower than the maximum value found by Lewis (2014) on his dataset. The range of RPMs investigated in this research evidenced the fact that the best operating point for this variable would be for values around 30 RPMs, which was responsible for the highest values of specific gravity found across the three researches (SG = 1.22). The rotational velocities set for the cutterhead in this research were responsible for the significant spillage saw across the 72 tests conducted at the Haynes Laboratory and were associated with the turbulent flow field observed, which was responsible for the low magnitude of the minor loss coefficient values (k-values) found herein, in comparison to Lewis (2014).

Analyzing the data for the variation of specific gravity and production, for the averaged and the minimum nominal flow rates investigated, the author observed that the ladder arm swing speed played no role on these parameters, which disagrees with former

researches conducted by Slotta, et. al. (1977) and Yagi, et. al. (1975). This was explained by the fact that the effect of this parameter was actually concealed due to the dominance of the high cutterhead RPMs on the total y-direction velocities (cutterhead RPMs plus ladder arm swing speed). Higher ladder arm swing speeds are theoretically possible to be set on the model dredge, but practical constraints, such as the tank width, do not allow it to be experimented.

The aforementioned turbidity associated with the high cutter head speeds were considered the main cause for the low specific gravities observed in this research, which has a direct relationship with the minor loss due to fixed screens on the suction inlet of the model dredge, as discussed in Girani (2014). Spillage is likely to occur when the forces in the y-direction, (function of the centrifugal and swing speeds), outweighs the axial forces induced by the suction velocities. This phenomenon was observed to have a major influence on the results for the k-values, which disagrees with conclusions drawn by Lewis (2014). Using all the results obtained by the three researches this author came up with a new prediction model, that differs from the one developed in Lewis (2014) with regards to the decay form employed that corresponds to an exponential function instead of a power-law as formerly proposed. The possibility to predict the results found by Lewis (2014) and Girani (2014) granted the model a great level of confidence. The constants a and b in Equation (64), responsible for the magnitude and curvature of the function's plot, were also found to be indicators of the characteristics of the induced flow field around the dredge's cutter head and consequently an indicator of its level of turbulence, which in this

research was mainly generated by the high cutterhead rotational speeds. These findings left this author with the hypothesis of the aforementioned constants to be actually function of the cutterhead RPMs.

The results from the experiments done for water-only tests showed that variations in the k-values do not have any relationship with increasing values of both the cutterhead speeds and ladder arm swing speeds. The minor loss coefficient actually was observed to decrease for all the range of investigated RPMs and ladder swing speeds with increasing flow rates. The model proposed by this author for water-only tests that is function of the non-dimensional velocities induced by the suction flow rates and the opening area of a given fixed screen, showed a good agreement with the results observed in Lewis (2014) and in Girani (2014).The difference shown by both models was around 32% for water-only tests and approximately 61% for tests with slurry. For the midsection comprehended between the screen with 55% openings and the one with 61.7%, the difference of both models increases to 53% for water tests and 63% for sand tests.

An evaluation of the set of experiments ran for slurry tests showed that the variation on k-values associated to high cutterhead speeds were not pronounced on this research, given the amount of spillage produced by such rotational velocities. The observations also evidenced the overwhelming effect of the losses due to spillage on the magnitude of the k-values found. Moreover, the results for the k-values tended to decrease and converge for both studied cutterhead speeds across increasing values of flow rates. The results for the ladder arm swing speed showed a more consistent relationship with the

observed k-values variations. Although, screen 1 seems to have experienced clogging that led to higher k-values, the minor loss coefficient showed that both parameters had no relationship with each other, which sounded counterintuitive given the extensive literature confirming that the increase in the specific gravity would result in an increase of the k-value for higher swing speeds. This phenomenon was already explained and justified by the fact that the cutterhead speeds outweigh the ladder arm swing speed with regards to the net y-direction velocities. The author proposed a model according not only to the results found in this research, but also to the observations obtained by Lewis (2014) and Girani (2014), which proved to be a better fit to all data points in comparison to the model proposed by Lewis (2014) mainly because of the exponential form of the decay. Once again, the new model was capable of predicting results for both researches, whereas the power-law function proposed by Lewis (2014) was not able to model with an acceptable accuracy the results from the experiments conducted by this author.

In an attempt to evaluate the major reason for the deviations on the two models, the author plotted the respective functions for 45 RPM, which was a common rotational speed employed by both researchers and also the 55 RPM for the equation proposed in this thesis. Figure 68 evidences the theory that the higher cutterhead rotational speeds were responsible for the difference between the proposed models. On the other hand, the plots show a relatively high accuracy for the 45-RPM prediction curve. Intending to confirm the hypothesis, the author also presented a plot of the models for the 2 in/s swing speed that was investigated in both researches, and a plot of the 3 in/s swing speed studied by

this author only for the function proposed herein. Differently from the results for the cutterhead, the change in values of swing speed showed no influence on the disagreement of the models and the curves of both models almost overlapped. Plots for the range of experimented flow rates were not attempted given the fact that Lewis (2014) investigated the minor losses due to fixed screen for flow rates equal to 250, 325 and 400 GPM, which are similar to the ones employed in this research and were therefore already compared and examined throughout previous chapters of this thesis.

Considering the turbulence observed through the high levels of spillage across all set of experiments, the author suggests that the influence of the cutterhead rotational speed to be better examined with a more detailed investigation of the near-flow field around the cutterhead. This would provide valuable data for a possible determination of relation between the cutterhear RPMs and the k-values. It was shown in the thesis that the constants present in the minor loss coefficient prediction equation are actually function of the conditions under which dredging is taking place. Further studies on the influence of these parameters would be of a great importance in finding a relationship between the aforementioned constants and the cutterhead speeds, which would contribute to a reformulation of the proposed model for a more general equation.

Although the range of the swing speeds employed on the set of experiments performed at the Haynes Laboratory did not show a strong relationship neither with the specific gravity nor with the production and considering the fact the model dredge is capable of performing cuts at greater swing speeds, it would be important to see how

greater values of ladder arm swing speeds would affect flow field around the cutterhead. These data would also be significant in the formulation of a relationship for the model constants a and b, since they were seen to be a function of the y-direction velocities.

In this study, the author investigated the behavior of three screen configurations, in which a screen designed by Lewis (2014) and one proposed in this research were evaluated across a set of different flow rates, swing speeds and cutterhead rotational speeds. It was observed that the real effect of the reduction of the opening area on the k-values was eclipsed by the turbulent flow field around the cutter. Thus it is recommended that different fixed screens with different β-coefficients ought to be tested in order to validate the aforementioned observation. Moreover, according to the result from the ADV screening regarding the possible residual cross-flow induced by the cutterhead rotational direction, the author suggests the design of a screen with shapes that would follow this cutter rotation pattern in order to observe whether these configurations would play any role on the overall production and specific gravity of the slurry. Evaluating all results from the experiments performed using the model cutter suction dredge at the Haynes Laboratory, the author believes that screens with opening areas within 30% and 65% should be investigated across even higher values of cutterhead RPMs, flow rates and swing speeds, so the observations seen in this research could be confirmed or denied. This would also provide more data points to be incorporated on the proposed model, which would result in more accurate prediction curves. Considering the presence of a bean-shaped suction mouth, this author suggests future studies to investigate the inherent minor loss

coefficient of the line entrance in order to feed the model with more data points and, this way, to formulate a more general equation to predict k-values for the suction entrance/screen assembly.

In this research, the author made use of an Acoustic Doppler Velocimeter (ADV) for the analysis of the seabed configuration after the sediment pit dredging, which showed to be very reliable in screening the seafloor. The plots generated from the instrument output data showed that during the operations there might have been a residual flow from the carriage's port side towards its starboard side that led the author to come up with the hypothesis of a cross-flow induced by the rotational direction of the cutterhead. Further studies in this area are highly recommended, since the device showed a strong potential in showing the seabed evolution across the sediment pit. The author also recommends the scanning-path to follow the pattern performed by the ladder arm when dredging is taking place. This setting would enable the researcher to better analyze the influence of both undercutting and overcutting methods across the range of values chosen for the dredging parameters.

REFERENCES

Albar, A. (2001). *Modeling of a Bucket Wheel Dredge System for Offshore Sand and Tin Mining,* Ph.D. Dissertation, Ocean Engineering Program, Texas A&M University, College Station, Texas.

Albar, A. (2000). *Effect of Various Terminal Velocity Equations on the Result of Friction Loss Calculation,* Proceedings of the Western Dredging Association 20th Technical Conference and 32nd Texas A&M Dredging Seminar, Warwick, RI, June 25-28.

Basco, D. R. (1971). *Particle Size and Density Effects on Cavitation Performance of Dredge Pumps,* Proceedings of the Third Dredging Seminar, Texas A&M University, Sea Grant Program Report no. TAMU-SG71-109.

Brahme, S.B., and Herbich, J.B. (1986). *Hydraulic Model Studies for Suction Cutterheads,* Journal of Waterway, Port, Coastal and Ocean Engineering, ASCE, Vol 112, No.5, pp. 590-607.

Bray, R. N. (1979). *Dredging: A Handbook for Engineers,* First Edition, Edward Arnold, London, England.

Bridges, T., Ells, S., Hayes, D., Mount, D., Nadeau, S., Palermo, M., . . . Schroeder, P. (2008). *The Four Rs of Environmental Dredging: Resuspension, Release, Residual, and Risk,* Vicksburg, MS, USA: Engineer Research and Development Center.

Craven, J. P. (1951). *A Study of Transportation of Sands in Pipes,* Ph.D. Dissertation, State University Iowa.

den Burger, M., Vlasblom, W. J., & Talmon, A. M. (2005). *Design Aspects for Cutter Heads Related to the Mixture Forming Process when Cutting Coarse Materials, Terra et Aqua,* (98), pp.12–18.

den Burger, M. (2003). *Mixture Forming Processes in Dredge Cutter Heads*, PhD Thesis. Delft University of Technology, Netherlands.

den Burger, M., Vlasblom, W. J., & Talmon, A. M. (1999). *Influence of Operational Parameters on Dredge Cutterhead Spillage*, Proceedings, *CEDA Dredging Days 1999*. Amsterdam, the Netherlands.

den Burger, M., (1997). *Mixture Forming in a Cutterhead*, Proceedings of the Central Dredging Congress, CEDA 1997, Amsterdam, the Netherlands.

Dismuke, C. P., Randall, R. E., & Yeh, P.-H. (2012). *Laboratory Measurements of the Suction Inlet Flow Field of a Model Cutter Suction Dredge*, Proceedings, *WEDA XXXI Technical Conference & TAMU 43 Dredging Seminar* (pp. 97–116). San Antonio, Texas, USA, June 10-13.

Girani, J. (2014). *Experimental Measurement of a Model Pipeline Dredge Entrance Loss Coefficient and Modification of a Spreadsheet for Estimating Model Dredge*

Performance, Master's Thesis. Texas A&M University, College Station, Texas, USA.

Glover, G. J. (2002). *Laboratory Modeling of Hydraulic Dredges and Design of Dredge Carriage for Laboratory Facility*. Master's Thesis. Texas A&M University, College Station, Texas, USA.

Gower, G. L. (1968). *A History of Dredging*, Session A, Paper One, Dredging, Editor: The Institution of Civil Engineers, William Clowes and Sons, London.

Hayes, D. F., Crockett, T. R., Ward, T. J., & Averett, D. (2000). *Sediment Resuspension during Cutterhead Dredging Operations,* Journal of Waterway, Port, Coastal, and Ocean Engineering, Port, Coastal, and Ocean Engineering, 126(3), 153–161.

Herbich, J.B. (2000b), *Handbook of Dredging Engineering*, Second Edition, McGraw-Hill Co., NewYork, New York, USA.

Henriksen, J. (2009). *Near-Field Sediment Resuspension Measurement and Modeling for Cutter Suction Dredging Operations,* Ph.D. Dissertation. Texas A&M University, College Station Texas, USA.

Holman, J. P. (2012). *Experimental Methods for Engineers,* (8th ed.). McGraw-Hill Co., New York, New York, USA.

Joanknecht, L. W. F (1976). *A Review of Dredge Cutterhead Modelling and Performance*, Proceedings of the Seventh World Dredging Congress, WODCON VII, San Francisco, California, pp. 995-1016.

Kline, A., & McClintock, F. (1953). *Describing Uncertainties in Single-Sample Experiments. Mechanical Engineering,* Vol. 75, pp. 3-8

Lewis, J. M. (2014). *Measuring the Effects of Cutter Suction Dredge Operating Parameters on Minor Losses due to Fixed Screens Installed at the Suction Inlet*, Master's Thesis. Texas A&M University, College Station, Texas, USA.

Miltenburg, C. J. M. (1983). *Flow and Mixture Forming in Large Cutterheads,* Laboratory of Soil Transportation, Delft University of Technology, Delft, the Netherlands.

Mol, A. (1977c). *Cutting tests in Sand*, Delft Hydraulics Laboratory, Delft, the Netherlands.

Moret, G.E. (1977). *Flow Around and In a cutter head Part IV. Flow Around a Cutter Head Placed in an Artificial Bank; Injections of Coarse Sand, Fine Gravel and Artificial Pieces of Clay*, Delft Hydraulics, Delft, the Netherlands.

Ogorodnikov, S. P., Mikheev, I. I., & Kulakov, A. E. (1987). *Optimization of the Mud Intakes of Dredges with Submersible Pumps,* Power Technology and Engineering (formerly Hydrotechnical Construction), 21(7), pp. 432-436.

Ohmart Vega Corp. (2006a). Haynes Laboratory Quote No. 6071665. Cincinnati, OH, USA.

Randall, R. E. (2016). *OCEN688 Course Notes: Dredging and Dredged Material Placement,* Texas A&M University, College Station, Texas, USA

Rosemount 1151. (2010). *Rosemount 1151 Pressure Transmitter,* (No. 00813-0100-4360). Chanhassen, Minnestota, USA.

Schiller, R. E. (1992). *Sediment Transport in Pipes*, Chapter 6, Handbook of Dredging Engineering, Editor: J.B.Herbich, McGraw-Hill: New York, New York, USA.

Shen, H. W., & The Committee on Sedimentation, Hydraulics Division. (1970). *Sediment Transportation Mechanics: J. Transportation of Sediment in Pipes.* Journal of the Hydraulics Division, ASCE, vol. 96 (no. HY7), July.

Slotta, L. S. (1968). Flow Visualization Techniques Used in Dredge Cutterhead Evaluation, Proceedings of the 1968 World Dredging Congress, WODCON II, Rotterdam, The Netherlands.

Slotta, L.S., Joanknecht, L.W.F., Emrich, R.K., (1977). *Influence of Cutterhead Height of Dredge Production,* Second International Symposium on Dredging Technology, Texas A&M University, College Station, Texas, USA.

Stepanoff, A. J., (1964). *Pumps and Blowers, Two Phase Flow*, John Willey, New York.

Swamee, P., & Jain, A. (1976). *Explicit Equations for Pipe-Flow Problems. Journal of the Hydraulics Division,* 102(5), 657-664

USACE. (1983). *Dredging Equipment and Techniques,* In U.S. Army Corps of Engineers (Ed.), Engineer Manual (EM 1110-2-., pp. 3.1–3.34). USACE. doi:10.1017/CBO9781107415324.004.

Vallentine, H. R. (1955). *Transportation of Solids in Pipeline,* Commonwealth Engineer, pp.349-354, Australia, April 1.

Vlasblom, W. J. (2003). *Introduction to Dredging Equipment,* In Designing Dredging Equipment (Wb3408b ed., pp. 1–27).

Vlasblom, W. J. (2005). *The Cutter Suction Dredger*, In Designing Dredging Equipment (WB3408b ed., pp. 1–79).

Wiedenroth, W. A. (1968). *An Examination of the Problems Associated with the Transportation of Sand-Water-Mixtures in Pipelines and Centrifugal Pumps,* Proceedings of the World Dredging Conference WODCON II, Rotterdam, The Netherlands.

Wilson, K., Addie, G., Sellgren, A., & Clift, R. (2006). *Slurry Transport Using Centrifugal Pumps*, 3rd Ed. Springer.

Yagi, T., Miyazaki, S., Yashikumi, O., Koreishi, A., Sato. Y., Saito, M., Nakazono, Y., Masuda, K., Koro, S., Shibuya, Y., Kikuchi, K., and Kikuya, T. (1975). *Effect of*

Operating Conditions of Hydraulic Dredges on Dredging Capacity and Turbidity, Technical Note 228, Port and Harbor Research Institute, Ministry of Transport, Yokosuka, Japan.

APPENDIX A – RAW DATA

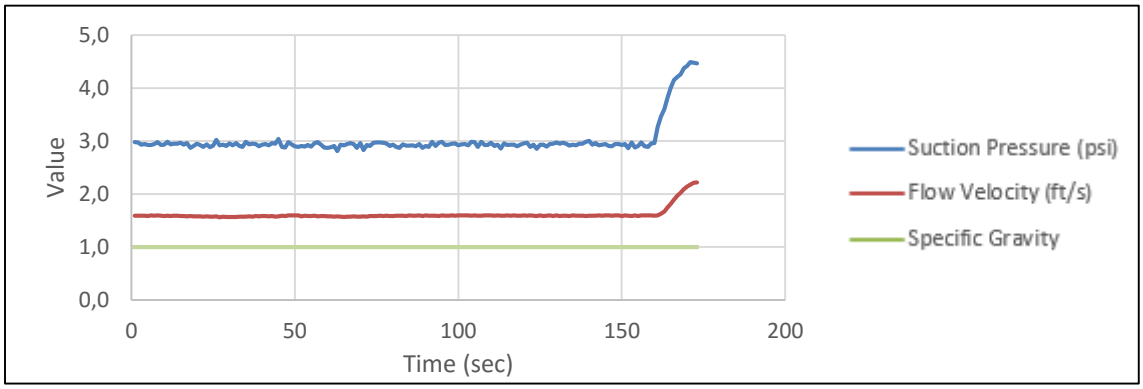

Figure A 1:Test 01.

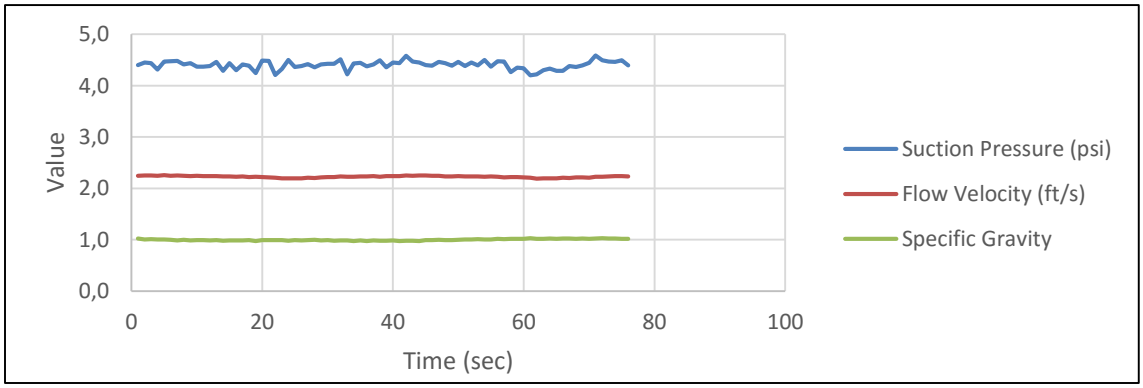

Figure A 2: Test 02.

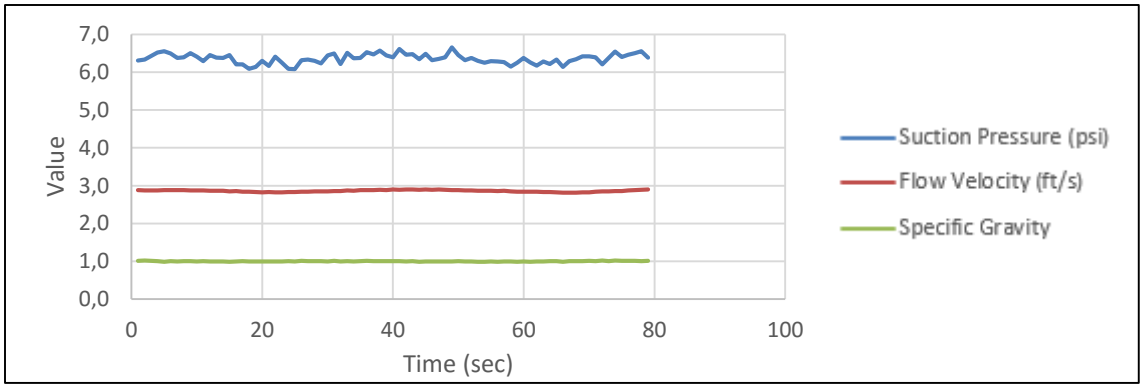

Figure A 3: Test 03.

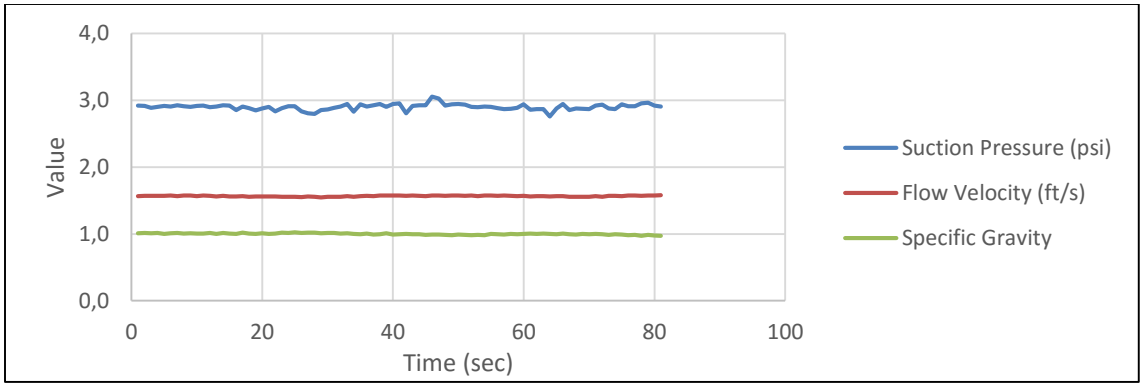

Figure A 4: Test 04.

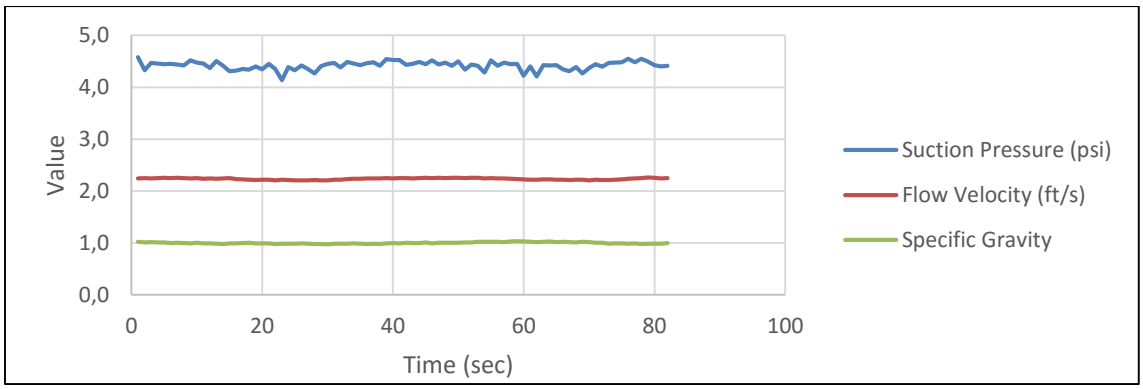

Figure A 5: Test 05.

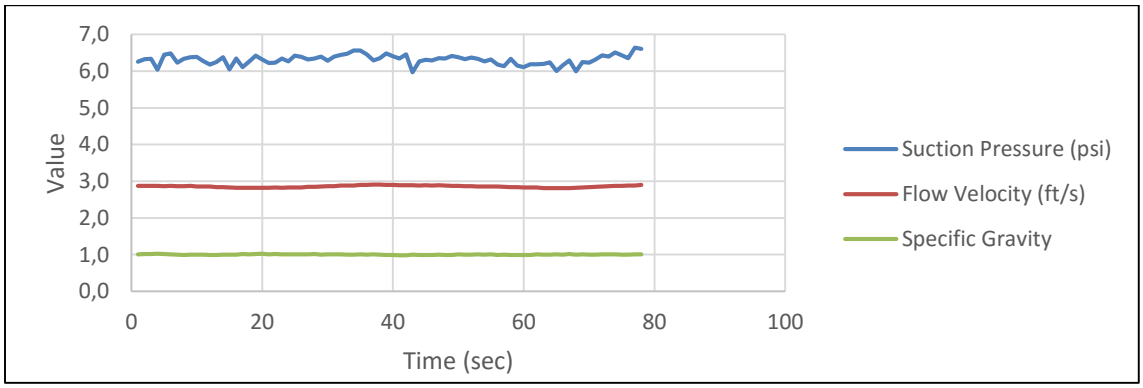

Figure A 6: Test 06.

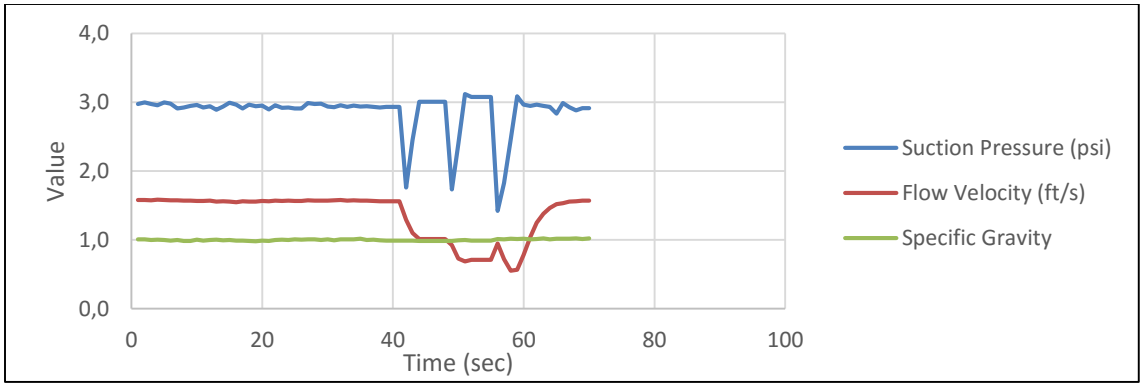

Figure A 7: Test 07.

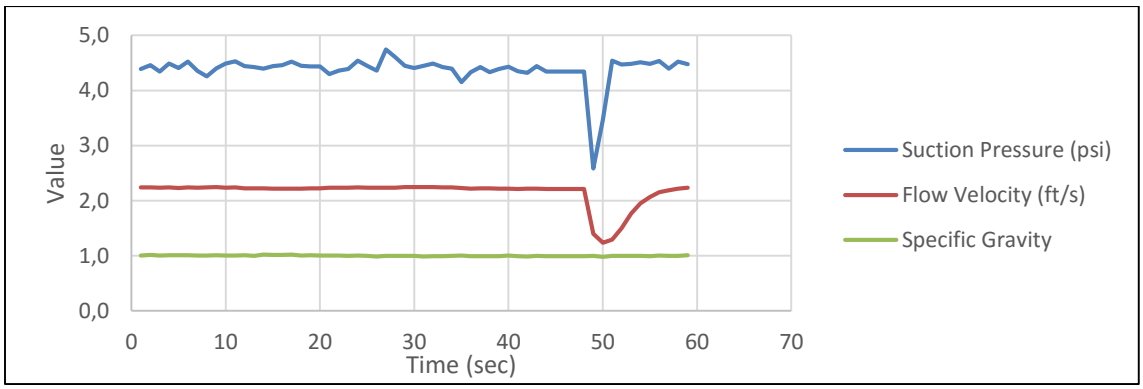

Figure A 8: Test 08.

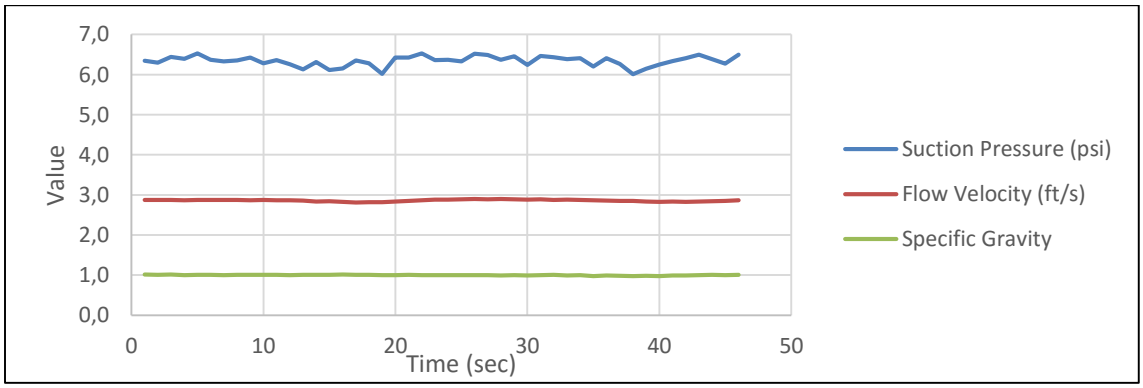

Figure A 9: Test 09.

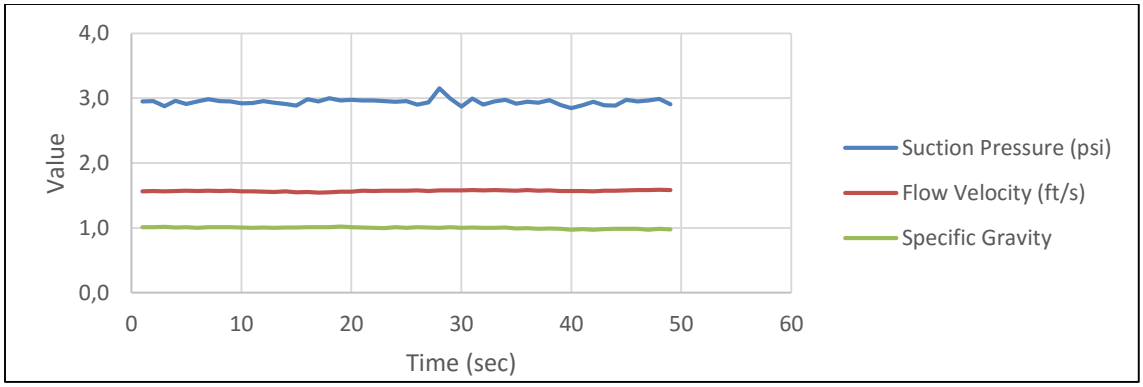

Figure A 10: Test 10.

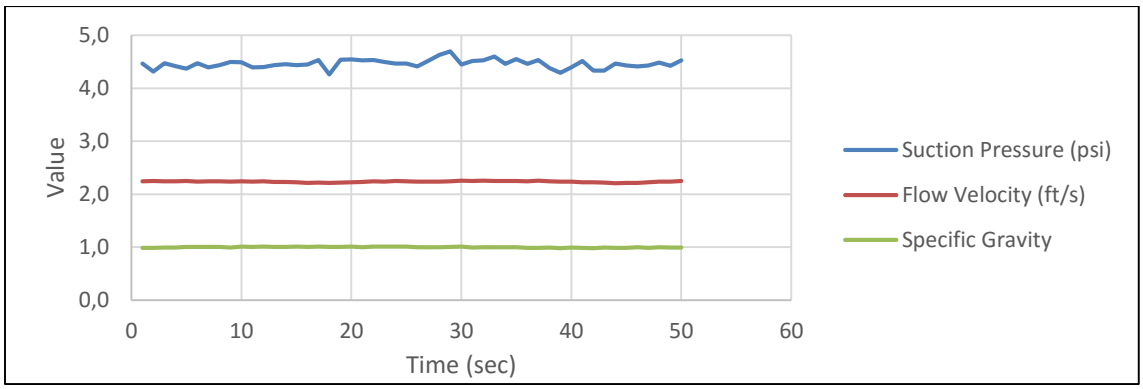

Figure A 11: Test 11.

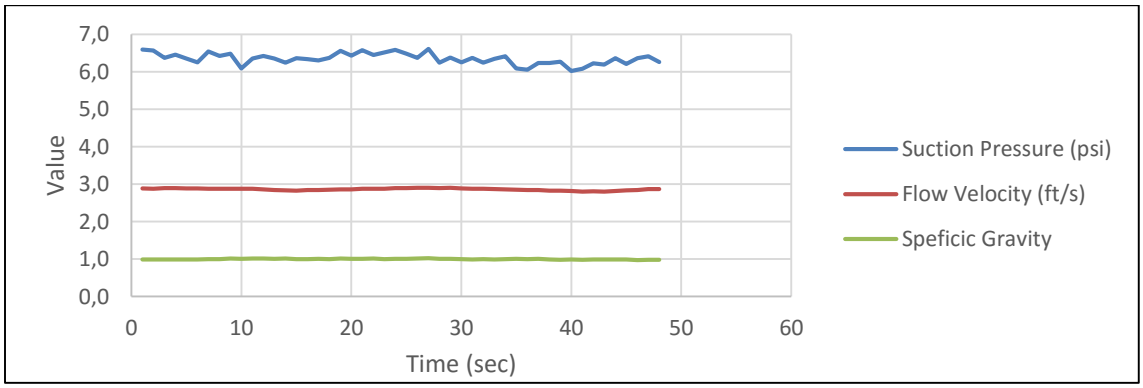

Figure A 12: Test 12.

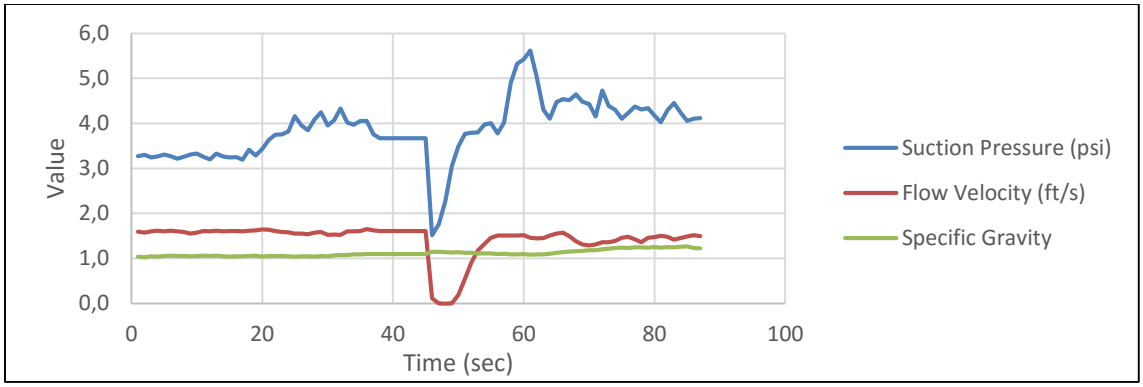

Figure A 13: Test 13.

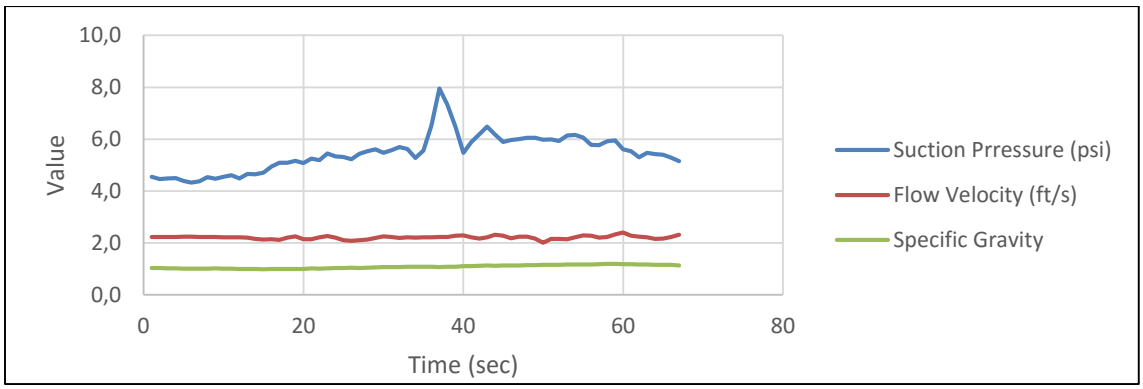

Figure A 14: Test 14.

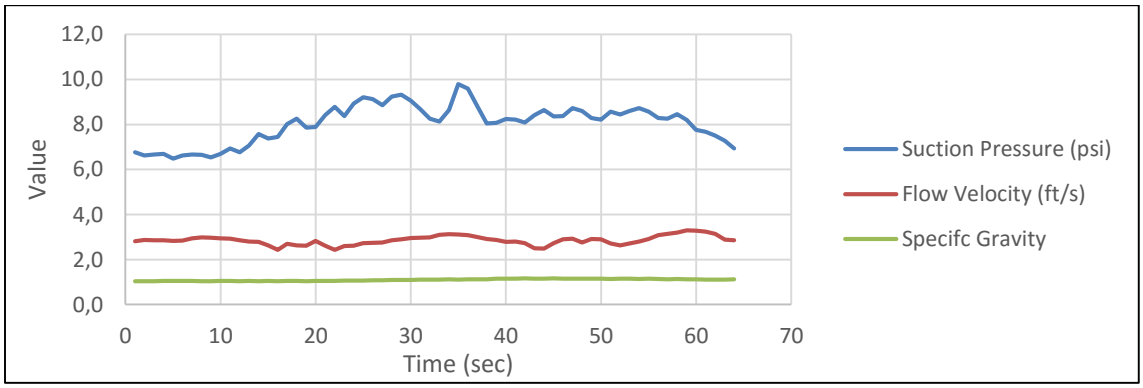

Figure A 15: Test 15.

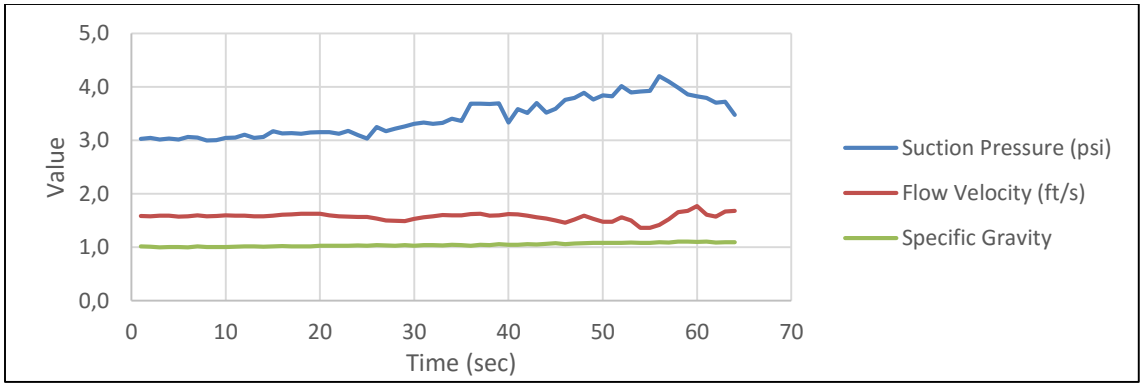

Figure A 16: Test 16.

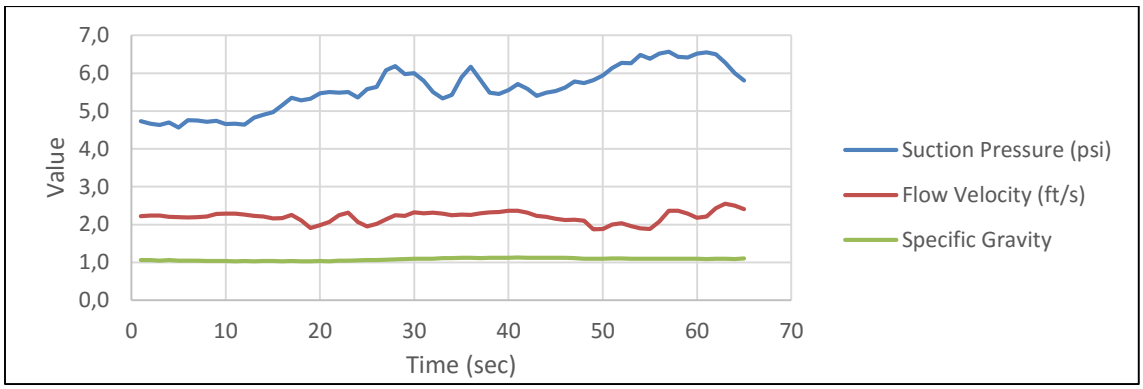

Figure A 17: Test 17.

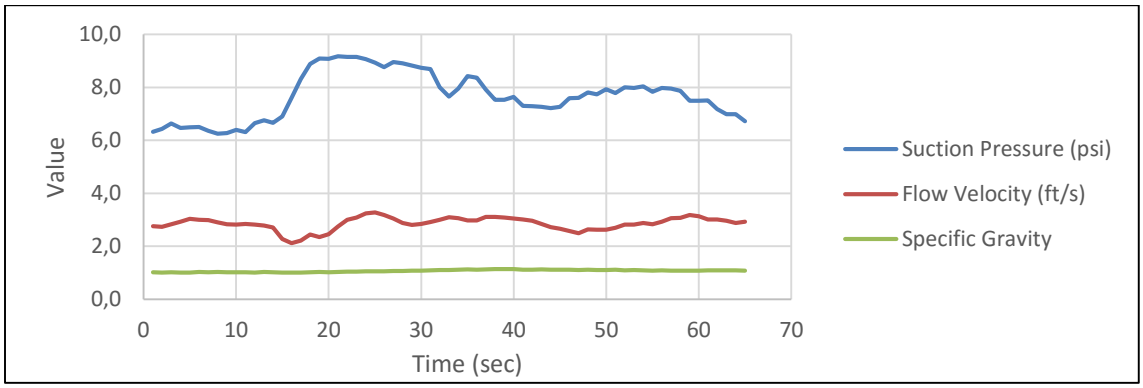

Figure A 18: Test 18.

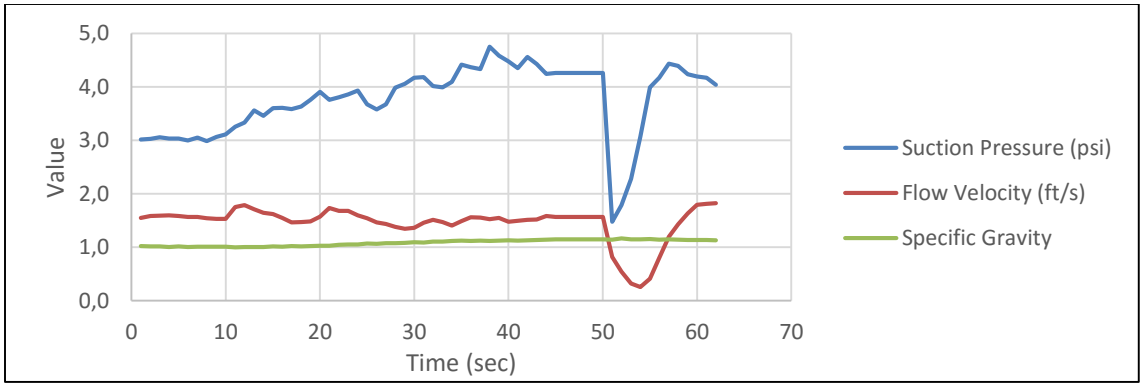

Figure A 19: Test 19.

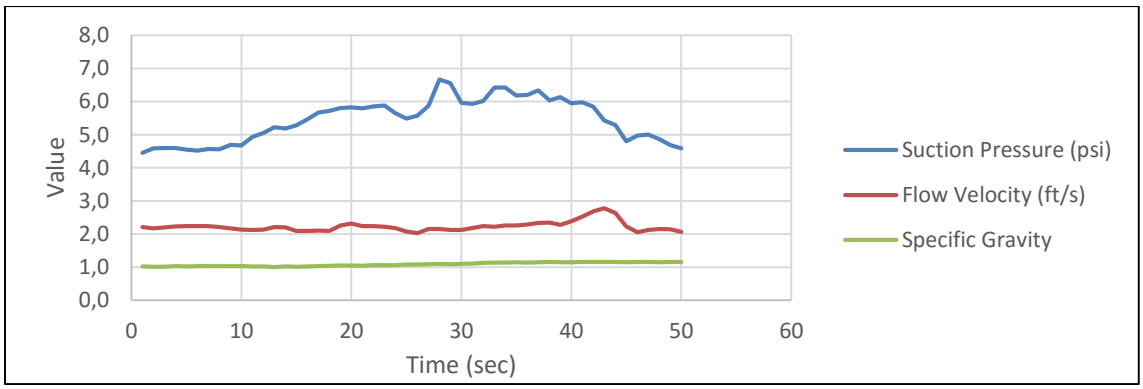

Figure A 20: Test 20.

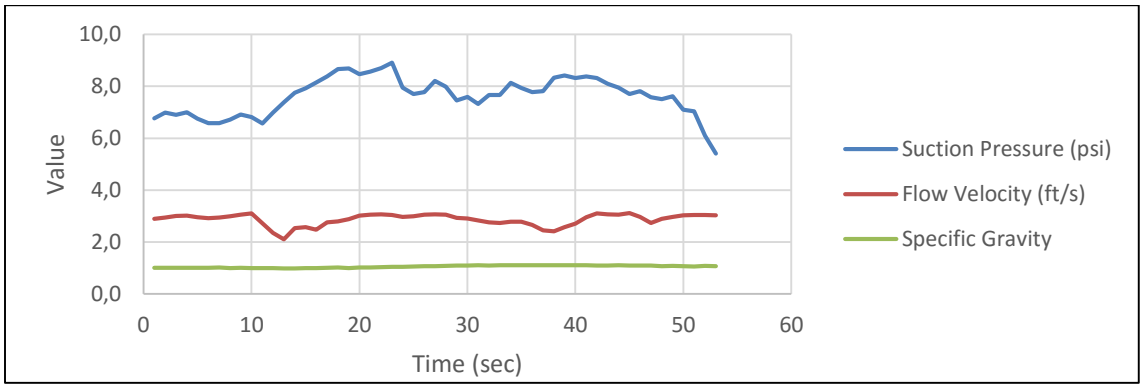

Figure A 21: Test 21.

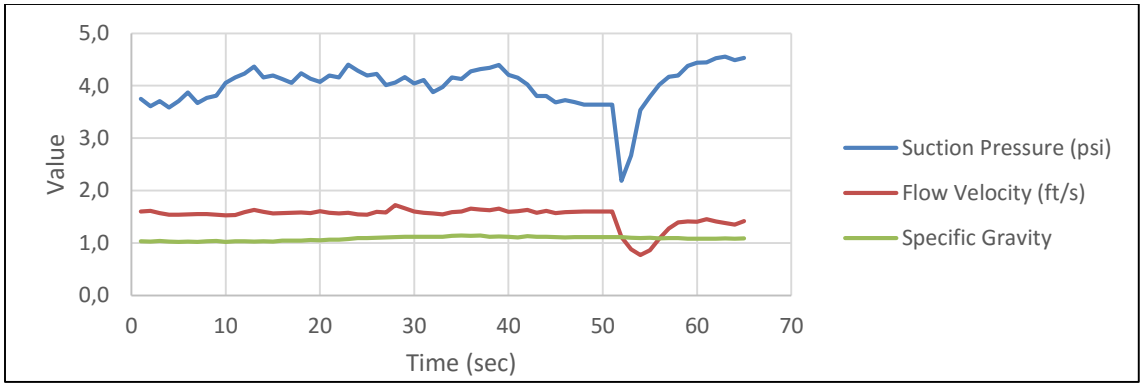

Figure A 22: Test 22.

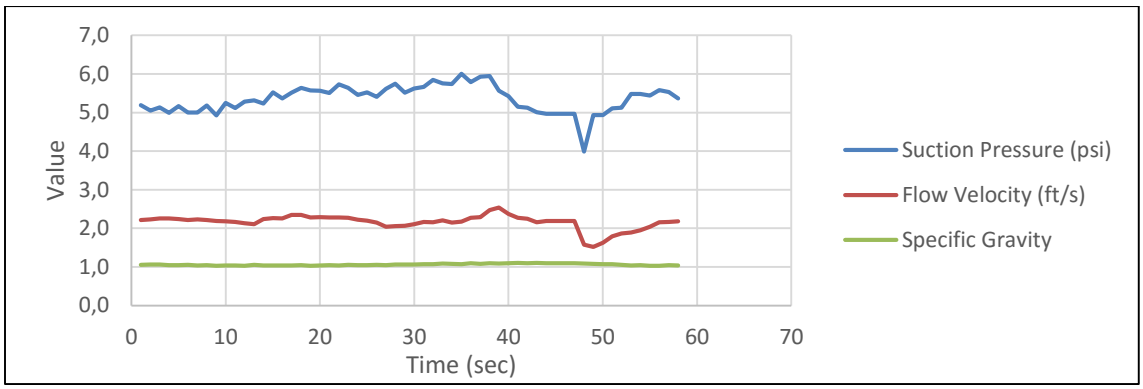

Figure A 23: Test 23.

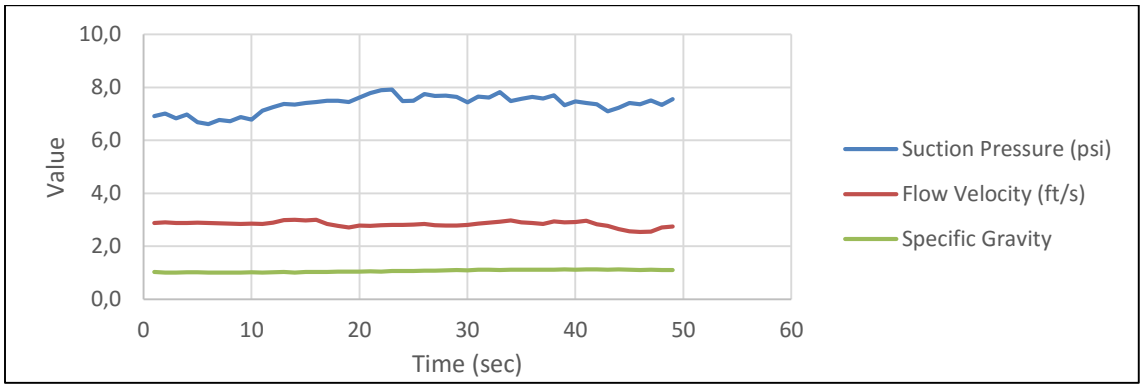

Figure A 24: Test 24.

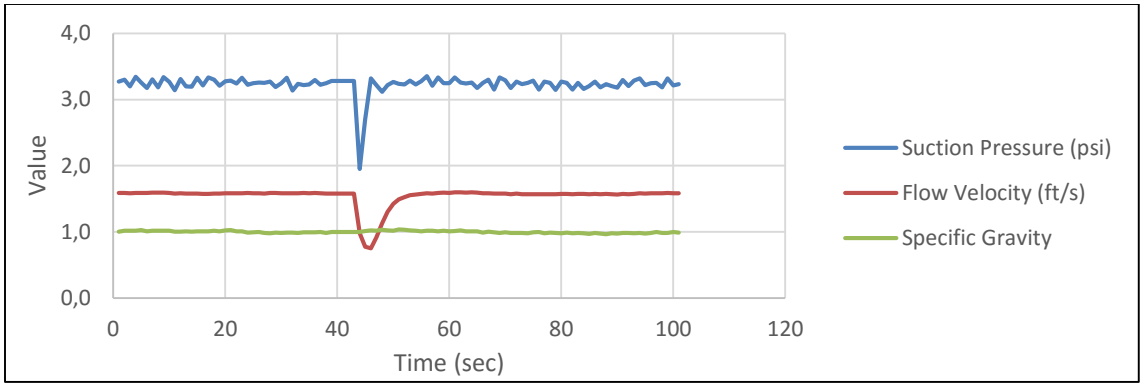

Figure A 25: Test 25.

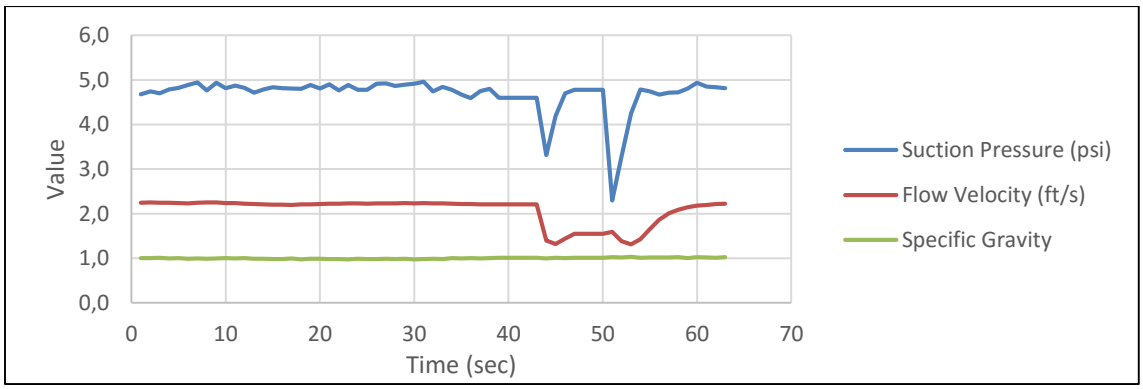

Figure A 26: Test 26.

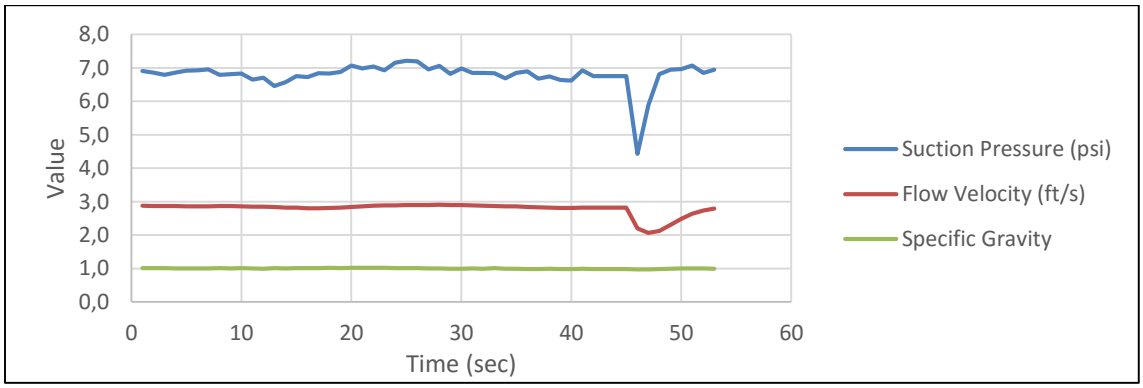

Figure A: 27: Test 27

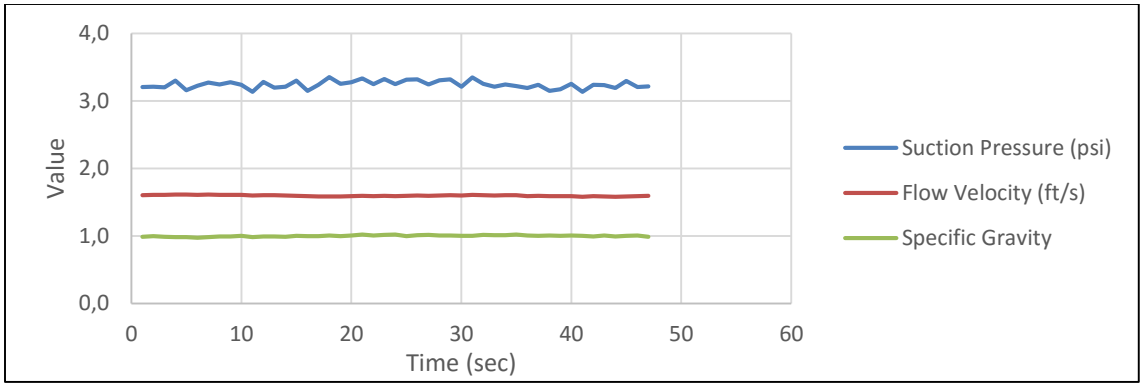

Figure A 28: Test 28.

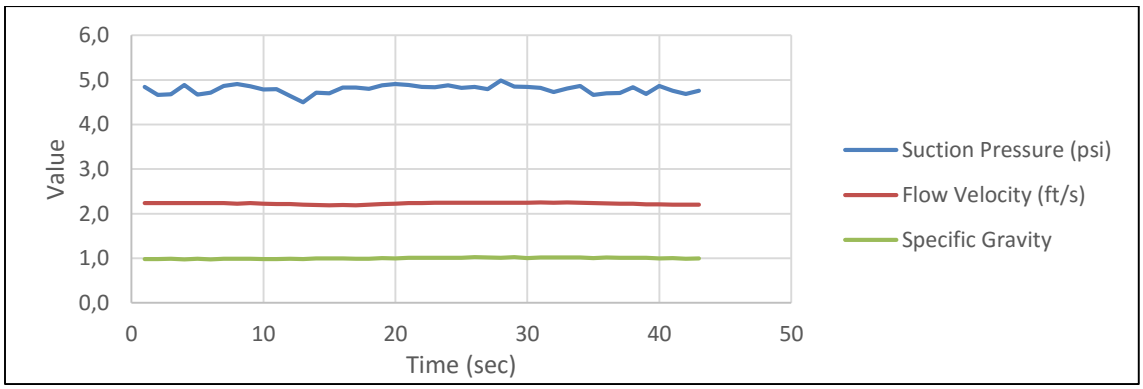

Figure A 29: Test 29.

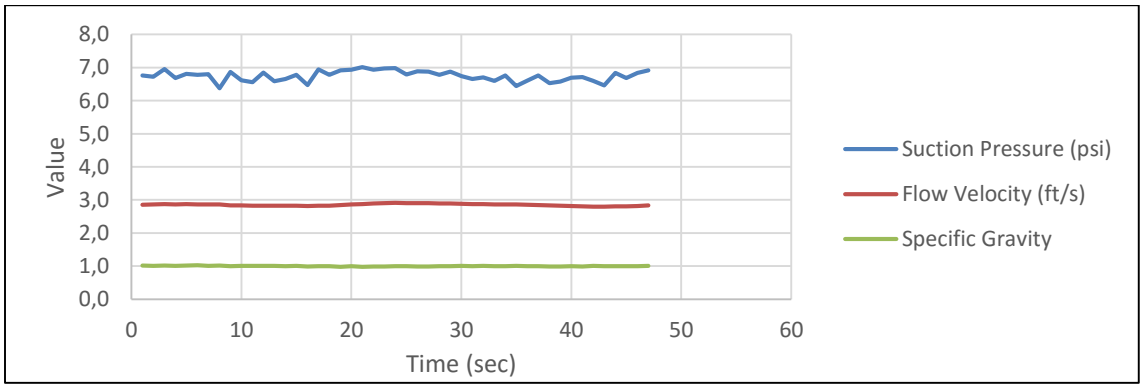

Figure A 30: Test 30.

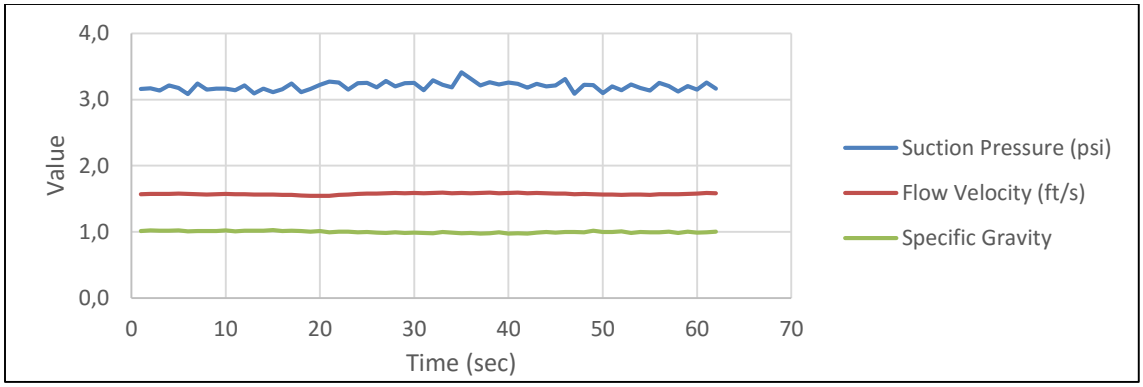

Figure A 31: Test 31.

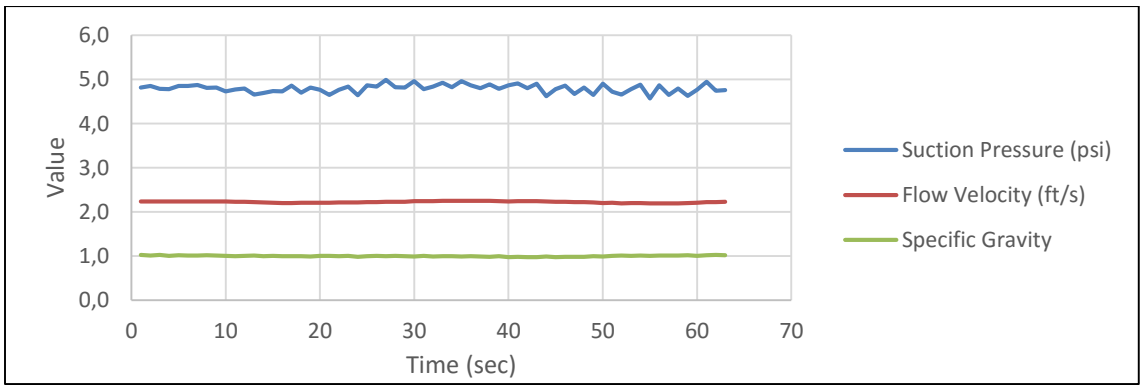

Figure A 32: Test 32.

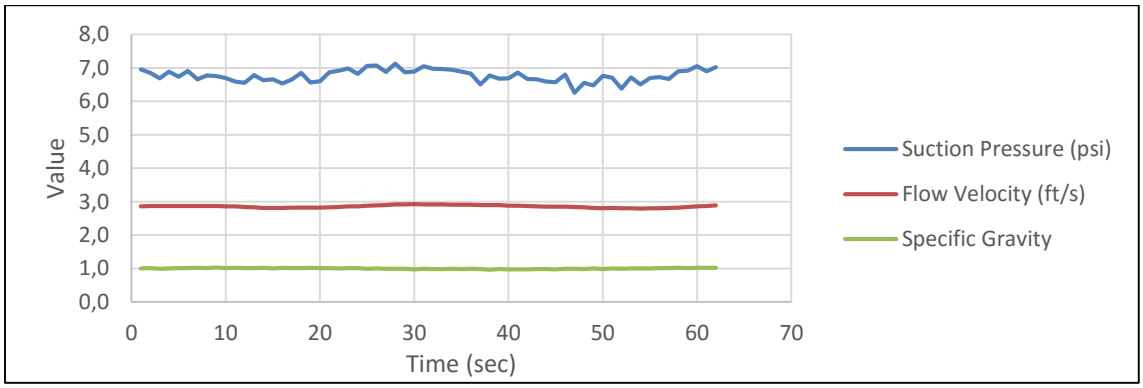

Figure A 33: Test 33.

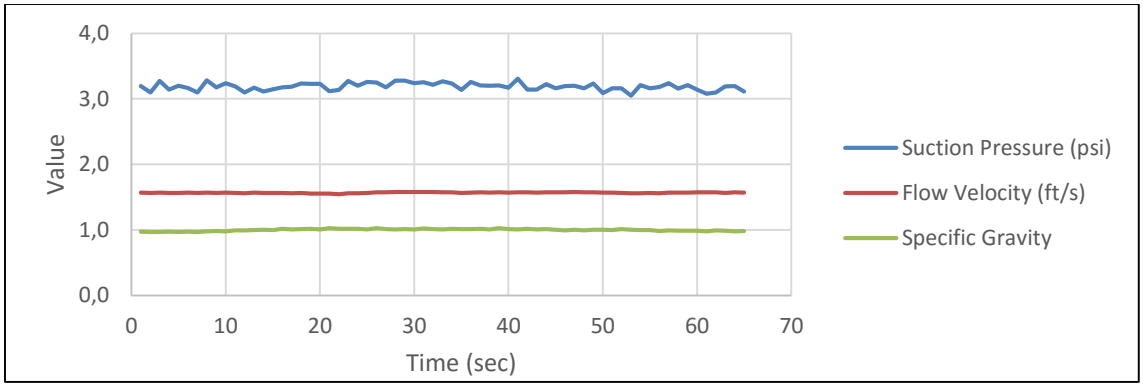

Figure A 34: Test 34.

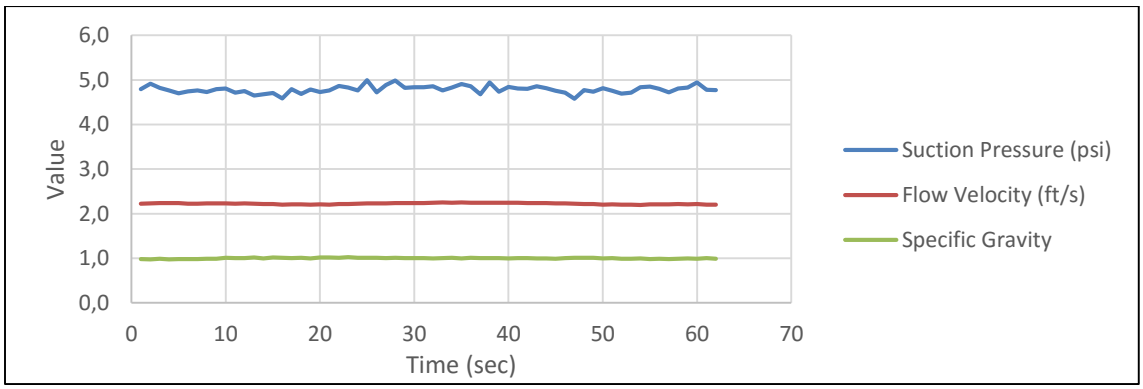

Figure A 35: Test 35.

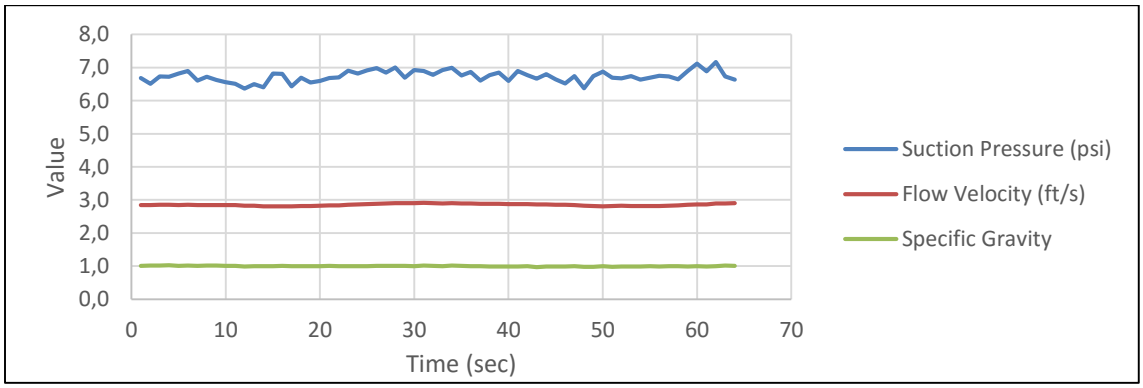

Figure A 36: Test 36.

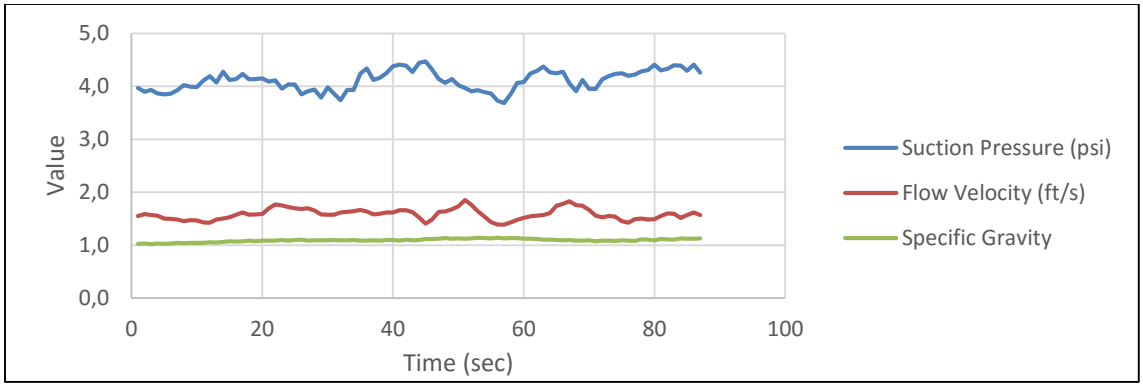

Figure A 37: Test 37.

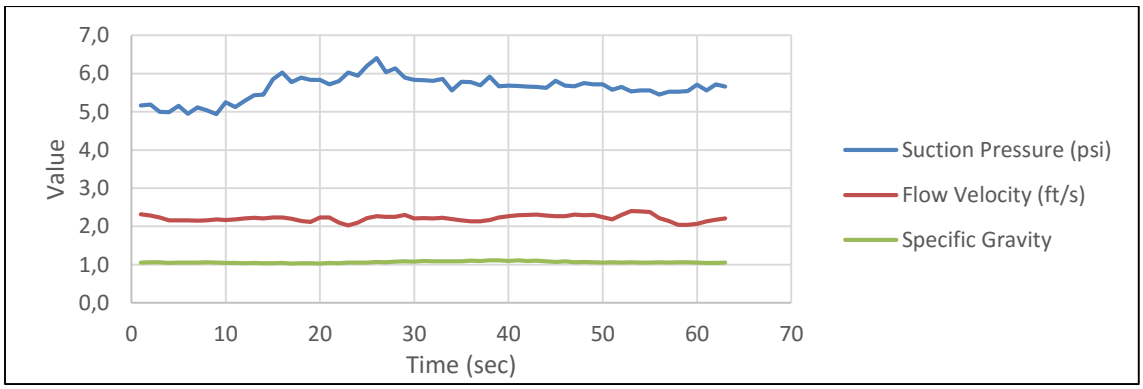

Figure A 38: Test 38.

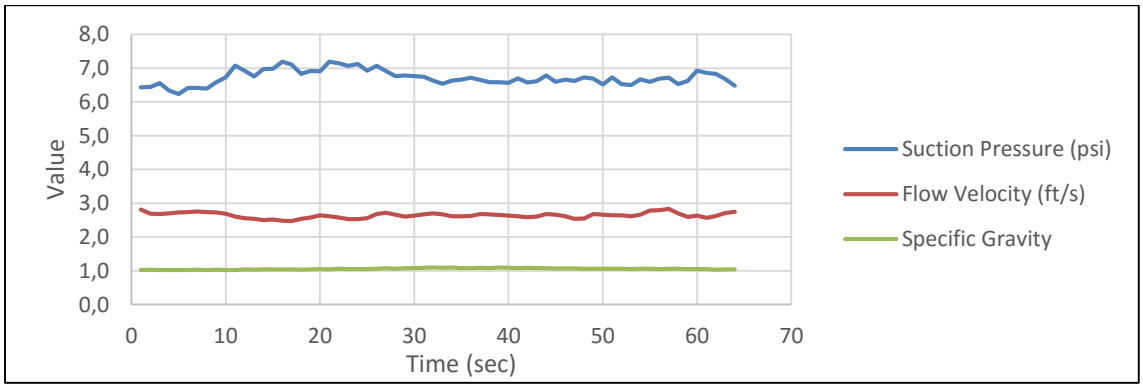

Figure A 39: Test 39.

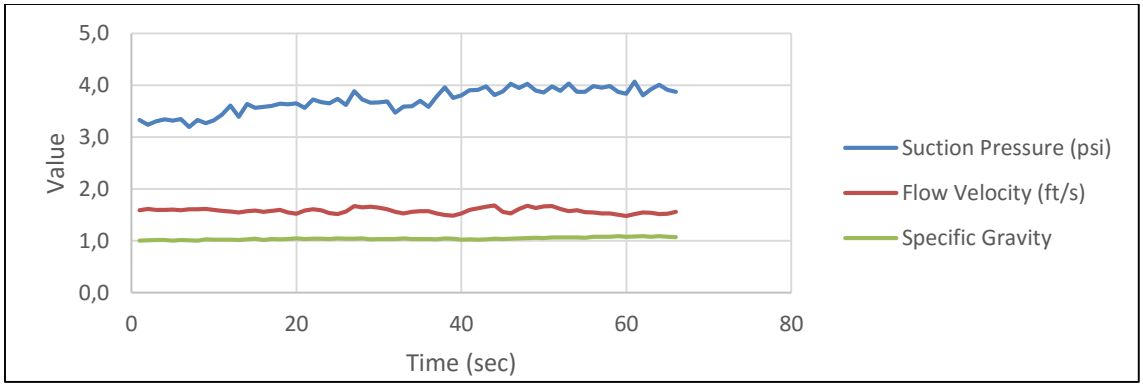

Figure A 40: Test 40.

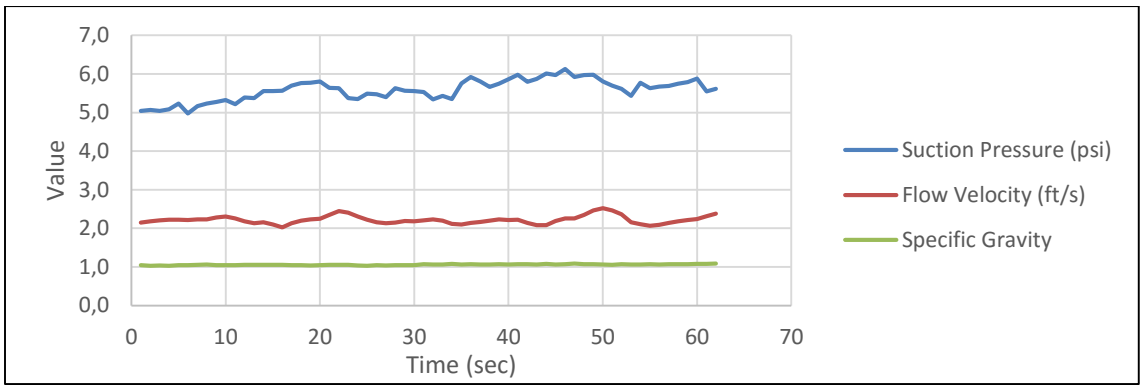

Figure A 41: Test 41.

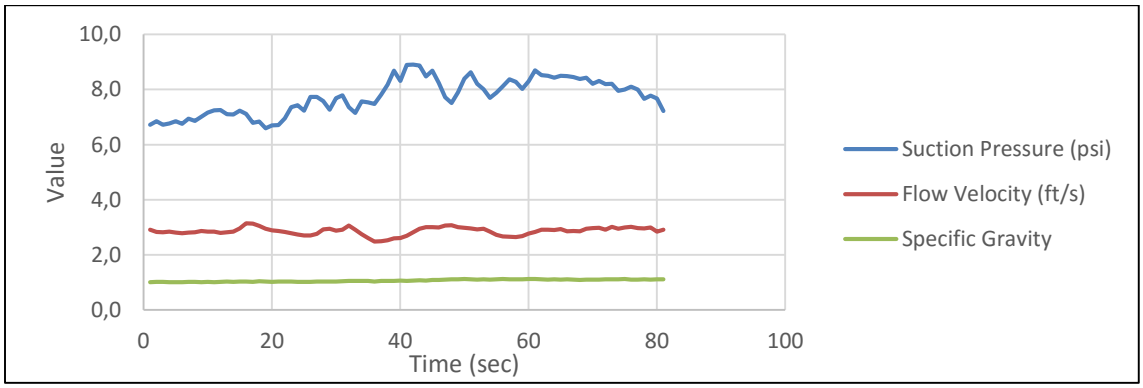

Figure A 42: Test 42.

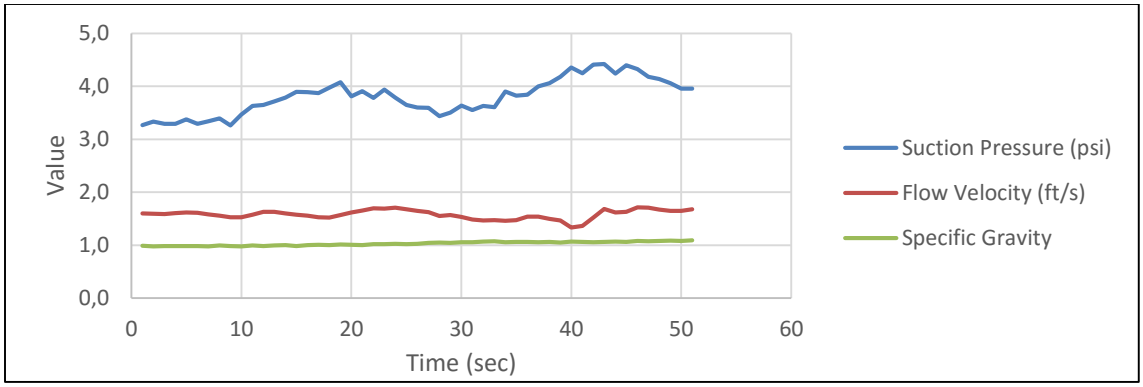

Figure A 43: Test 43.

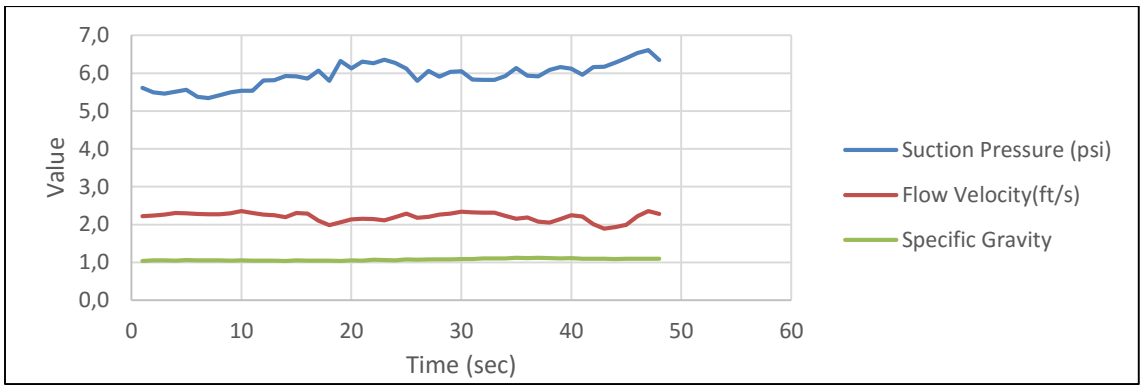

Figure A 44: Test 44.

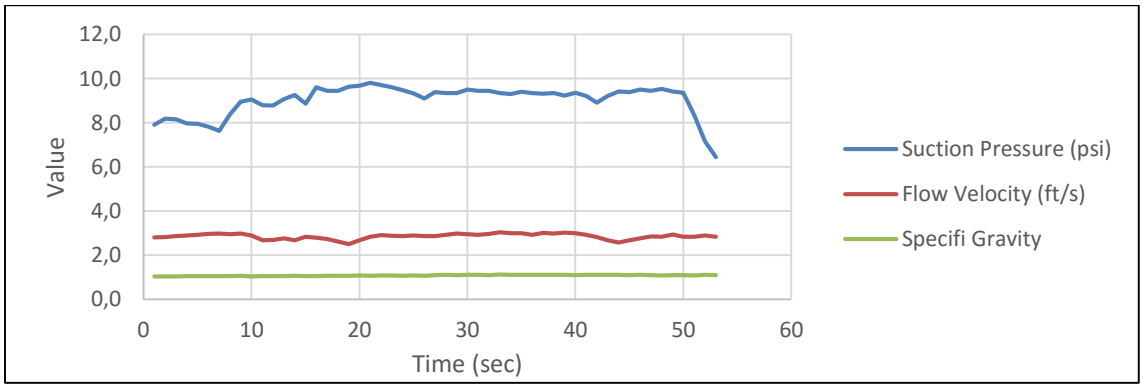

Figure A 45: Test 45.

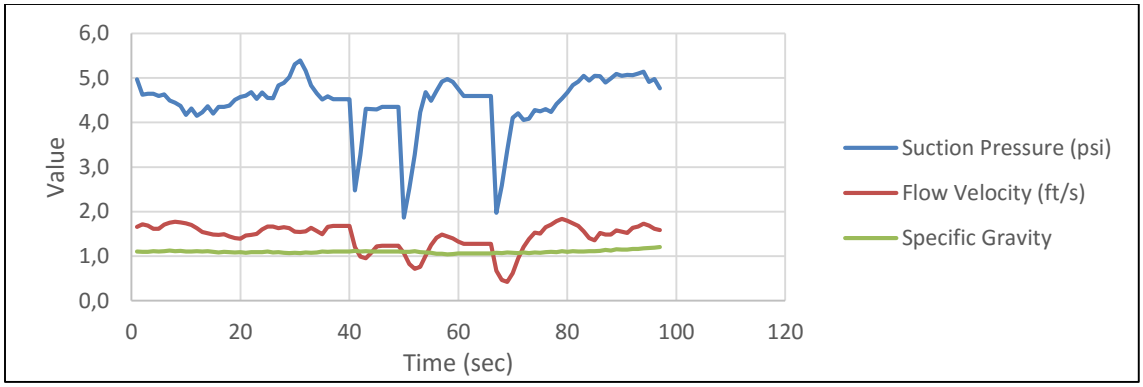

Figure A 46: Test 46.

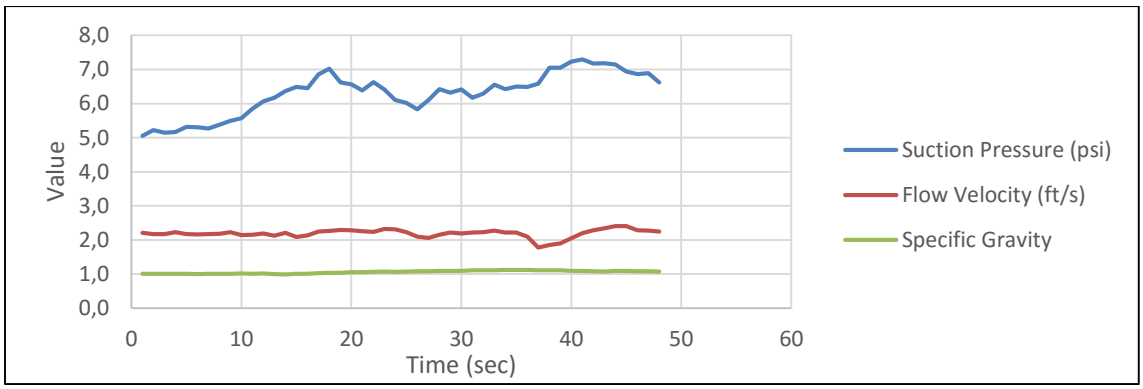

Figure A 47: Test 47.

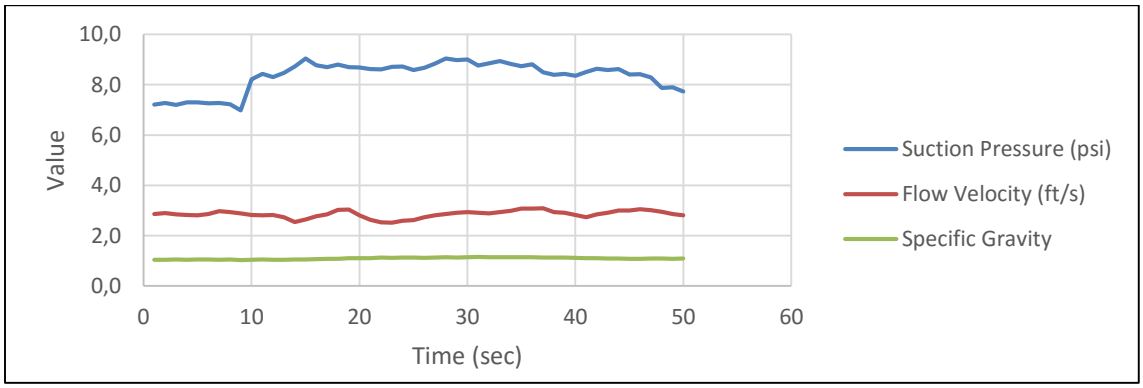

Figure A 48: Test 48.

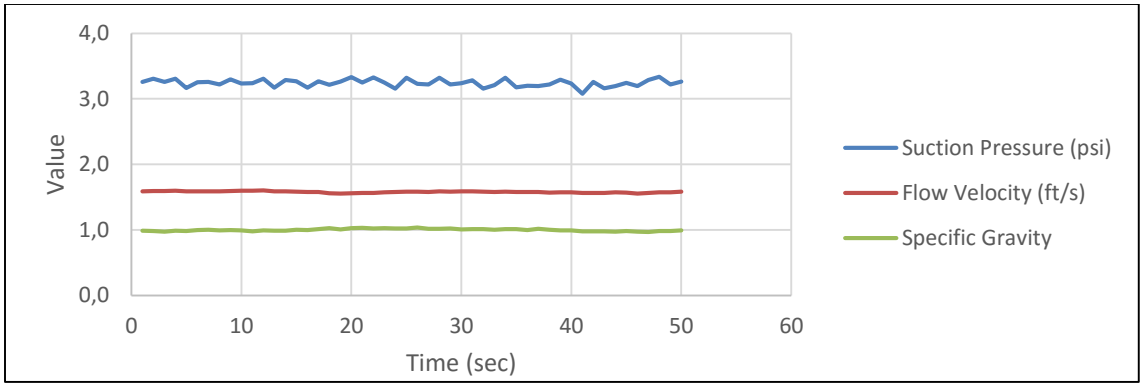

Figure A 49: Test 49.

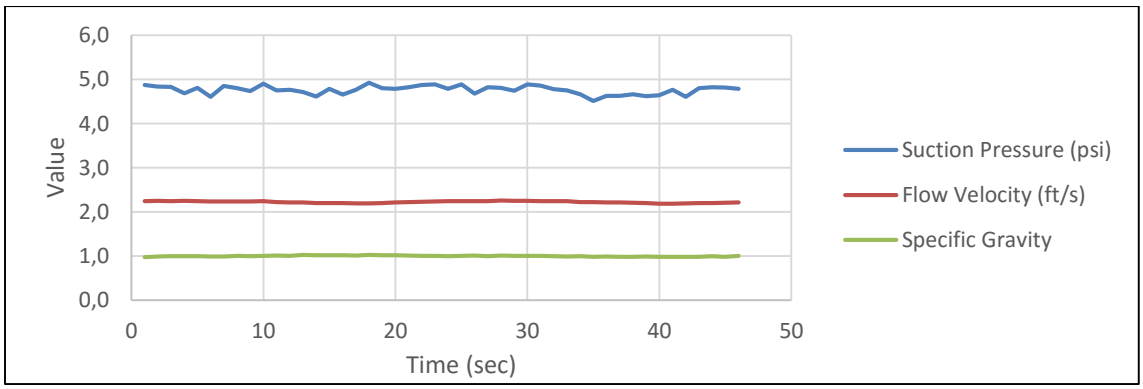

Figure A 50: Test 50.

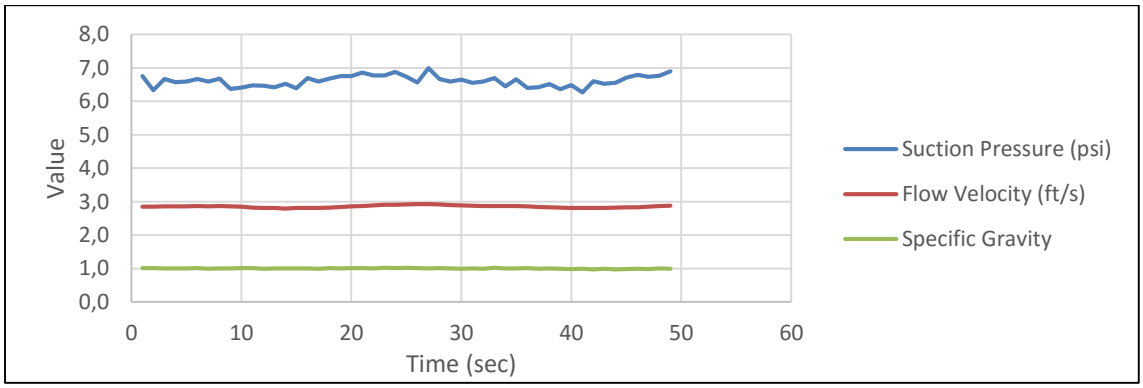

Figure A 51: Test 51.

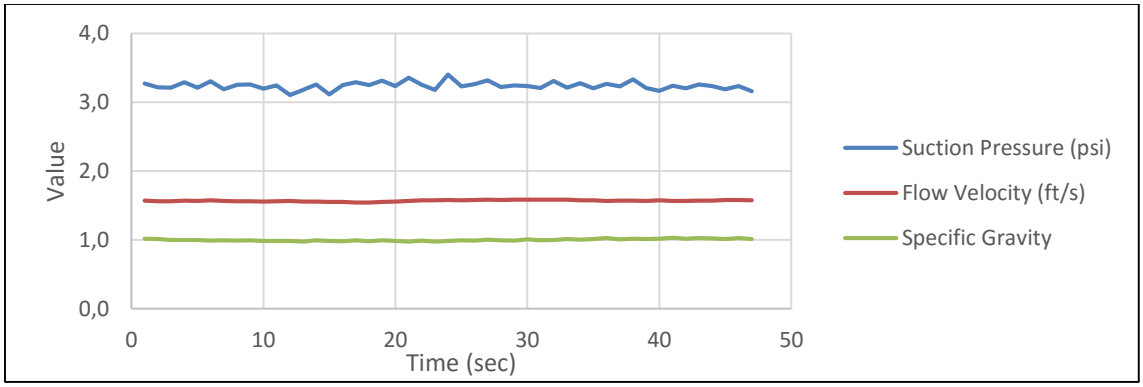

Figure A 52: Test 52.

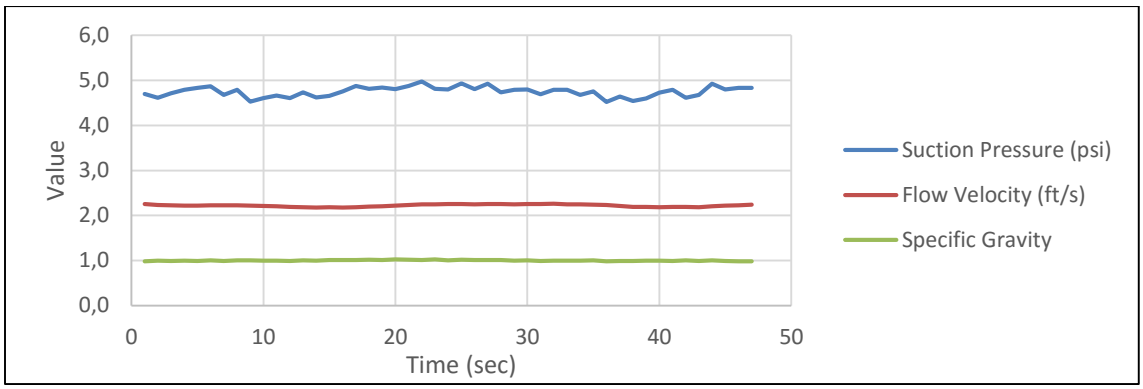

Figure A 53: Test 53.

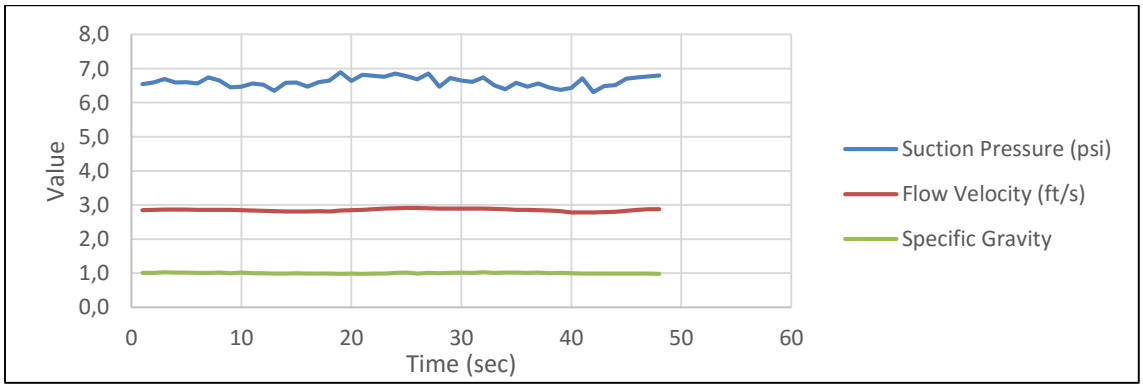

Figure A 54: Test 54.

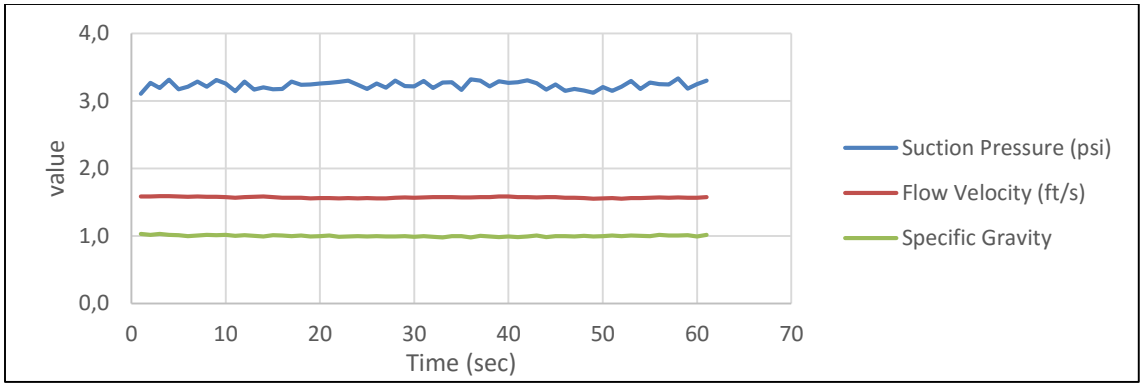

Figure A 55: Test 55.

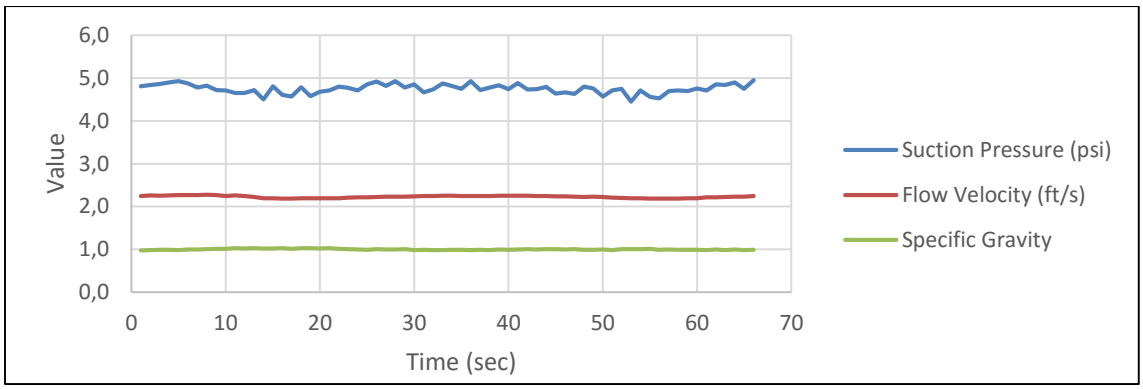

Figure A 56: Test 56.

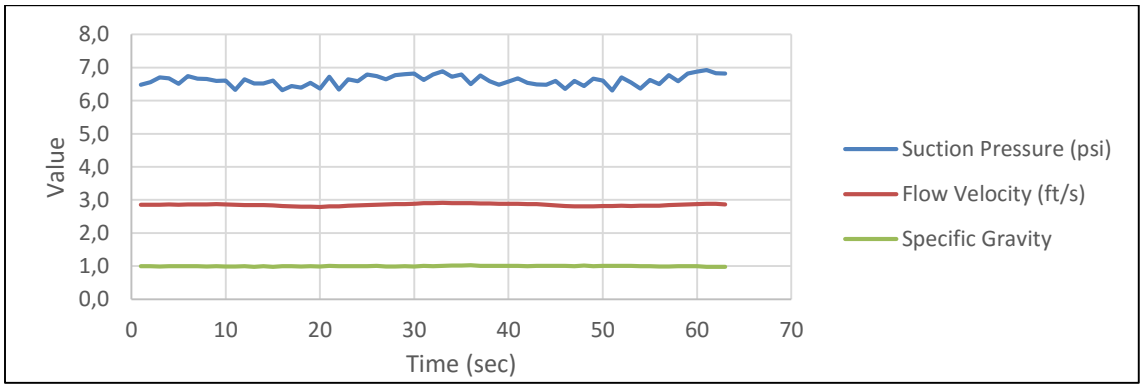

Figure A 57: Test 57.

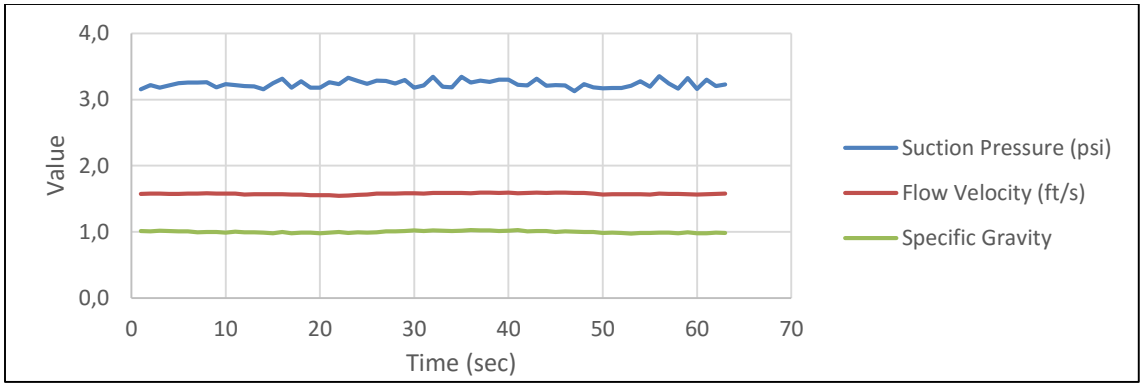

Figure A 58: Test 58.

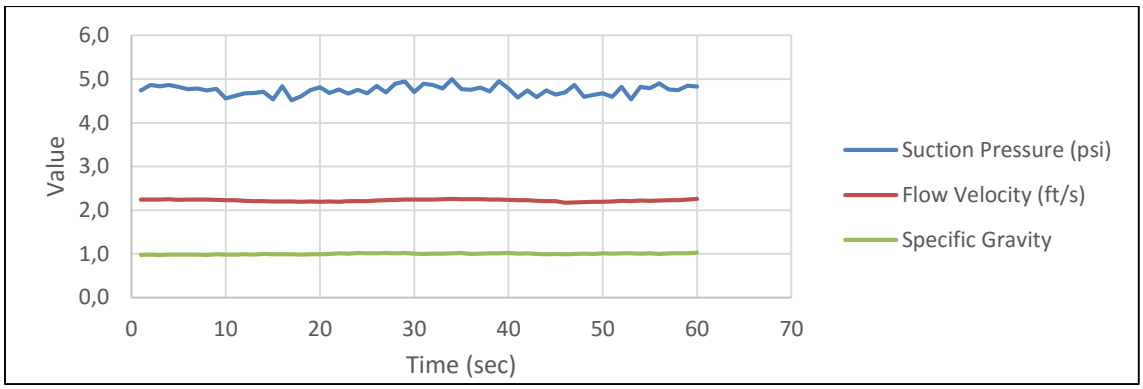

Figure A 59: Test 59.

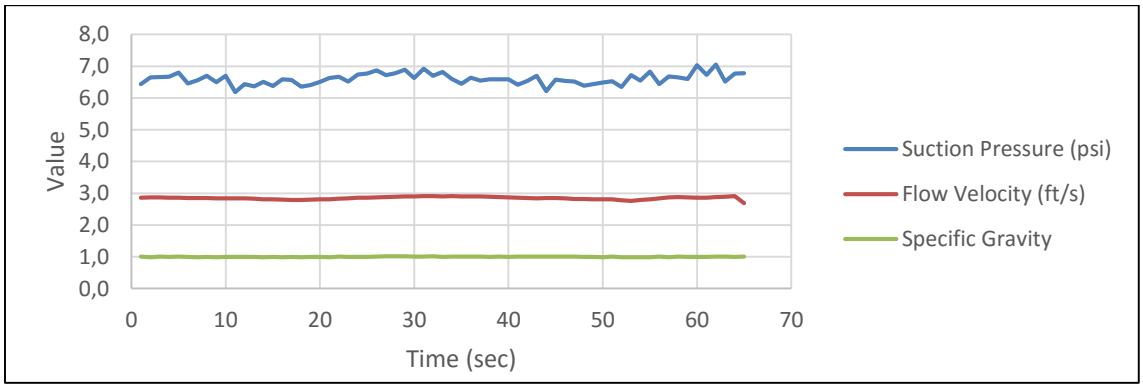

Figure A 60: Test 60.

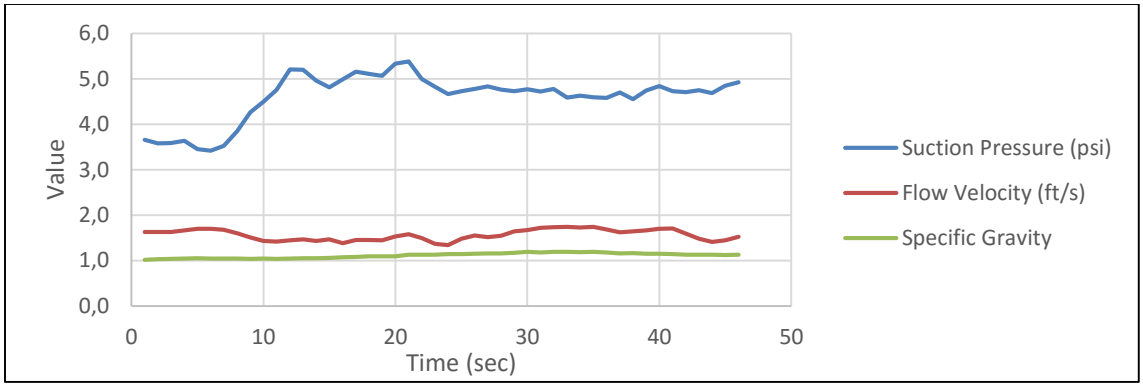

Figure A 61: Test 61.

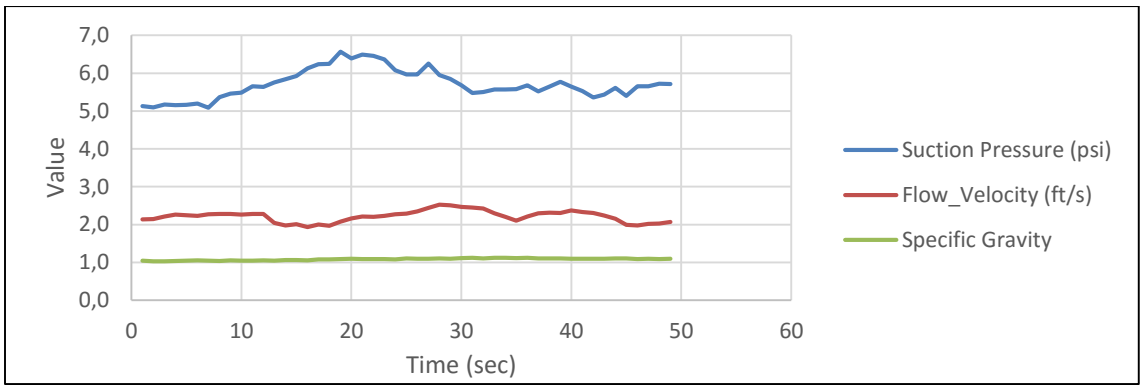

Figure A 62: Test 62.

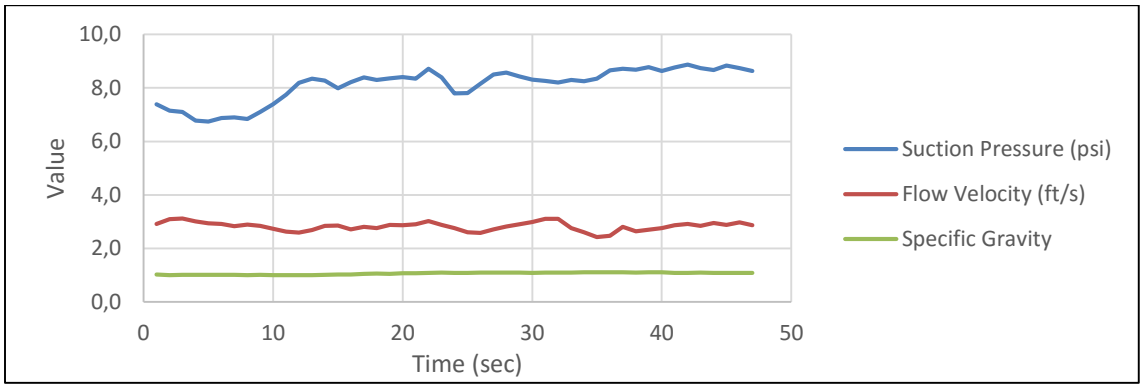

Figure A 63: Test 63.

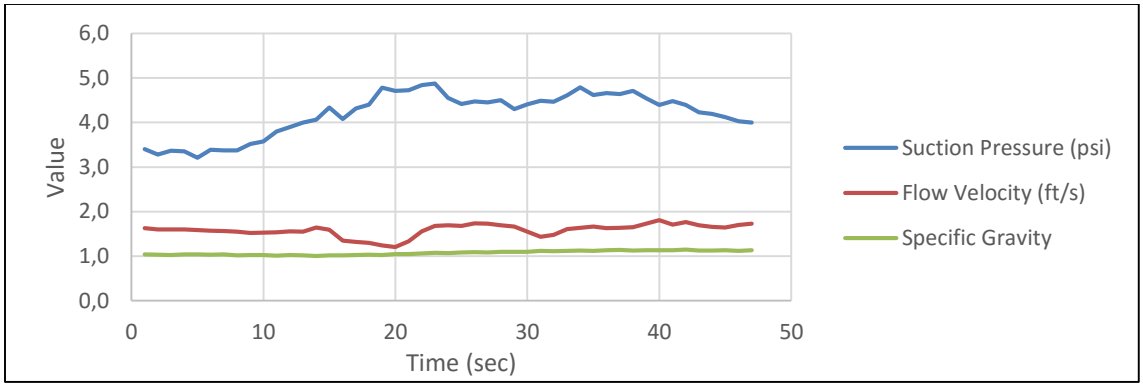

Figure A 64: Test 64.

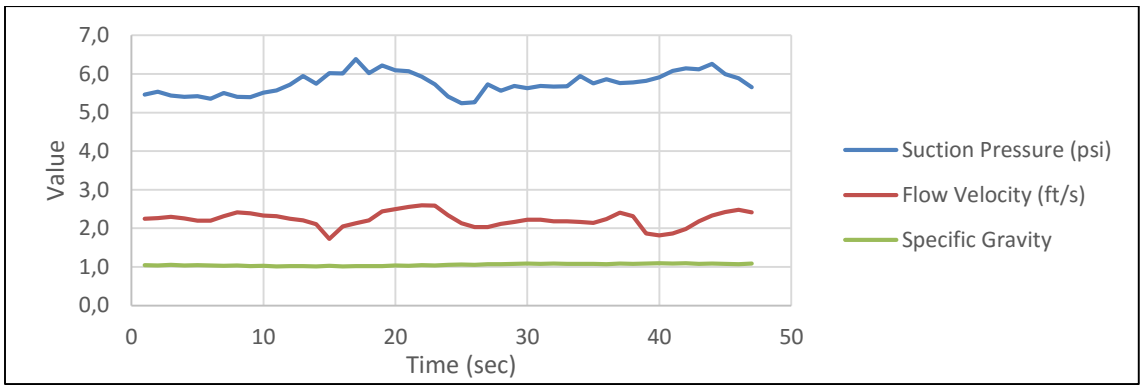

Figure A 65: Test 65.

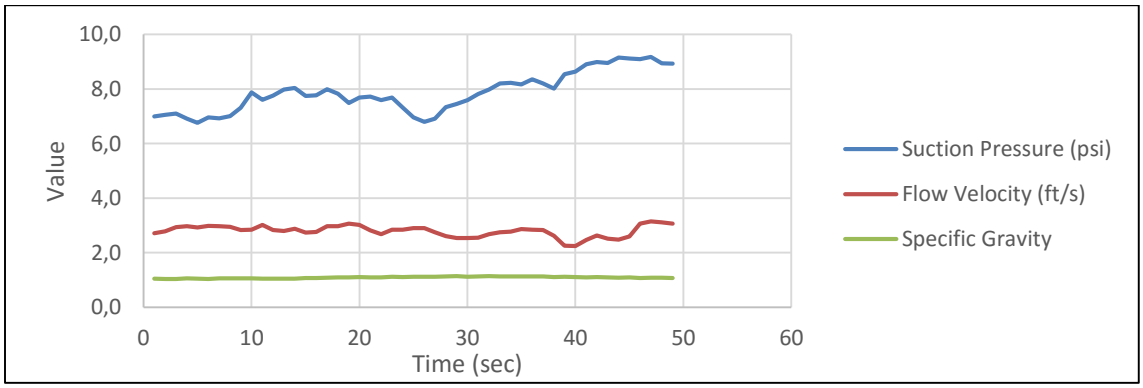

Figure A 66: Test 66.

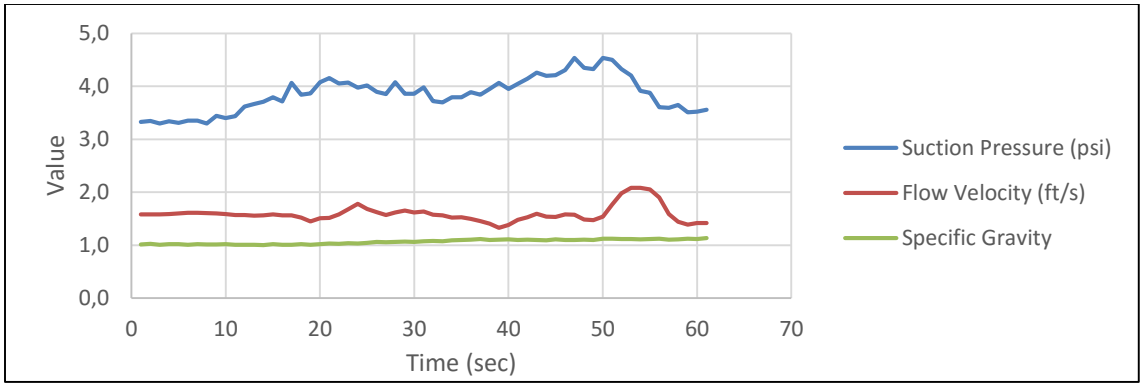

Figure A 67: Test 67.

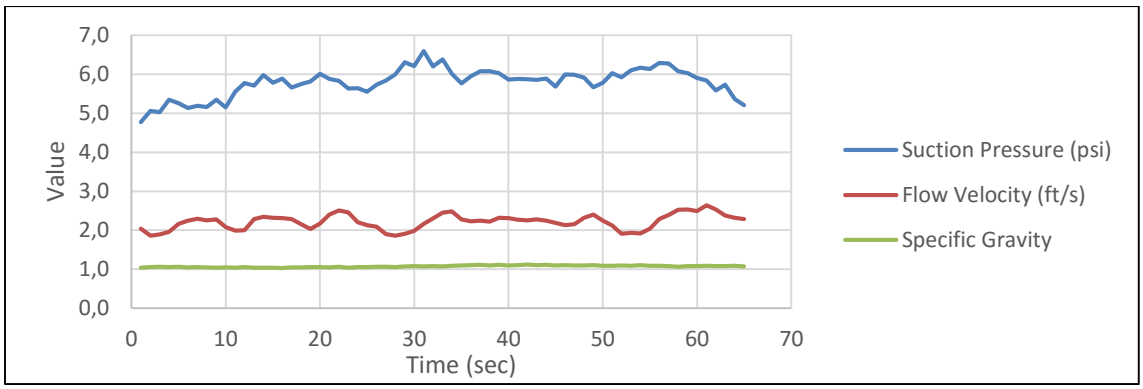

Figure A 68: Test 68.

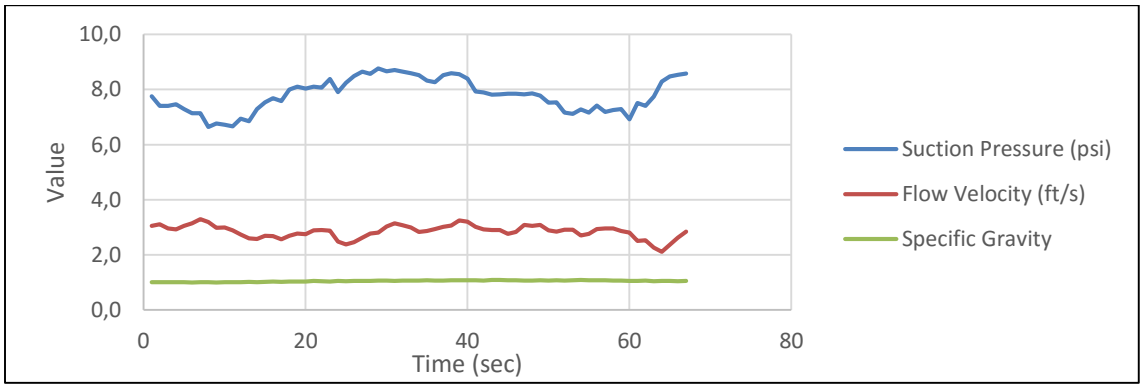

Figure A 69: Test 69.

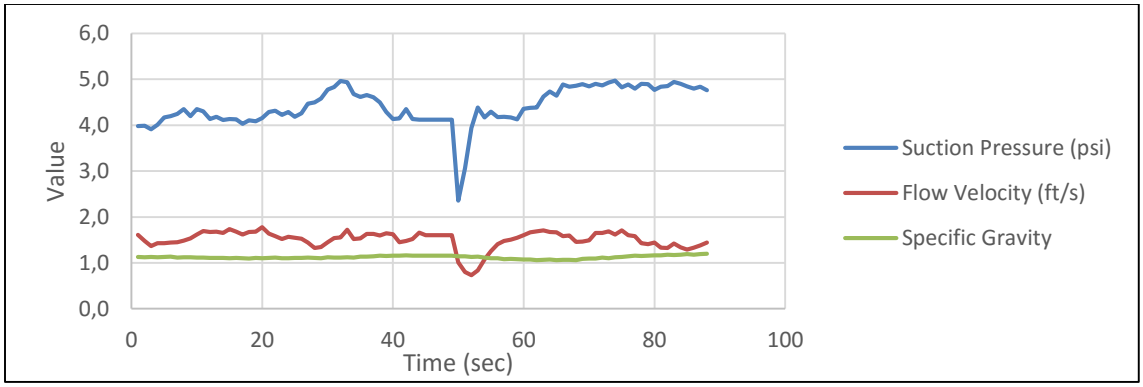

Figure A 70: Test 70.

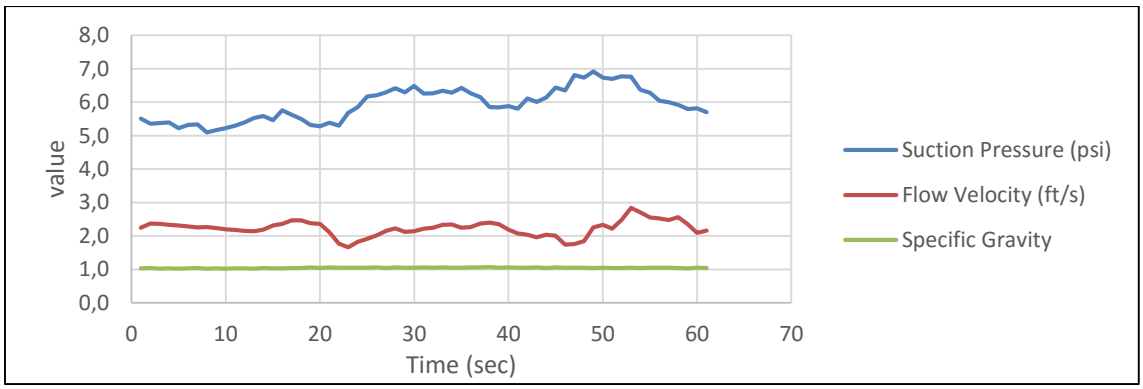

Figure A 71: Test 71.

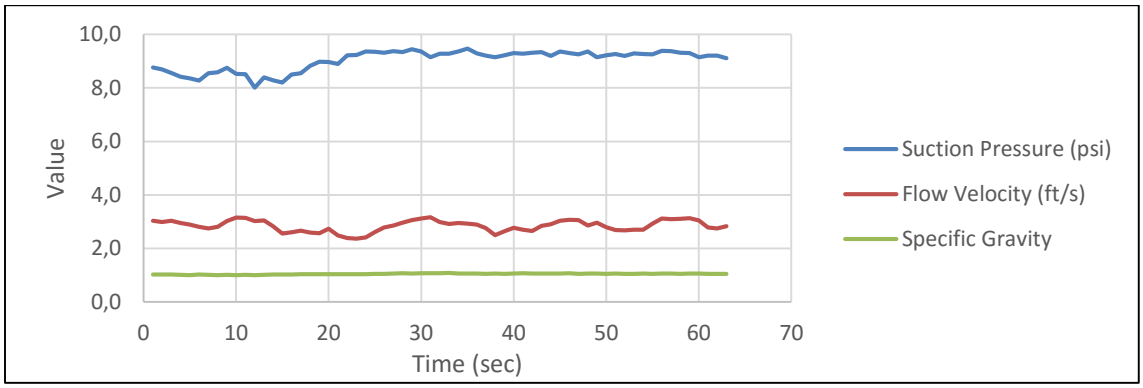

Figure A 72: Test 72.

APPENDIX B – TEST PLANS

Table B 1: Test Plan for the Screen 0.

Test Run	Day	Screen Number	Cutting Thickness (in)	Swing Speed (in/s)	Cutterhead Speed (rpm)	Flow Rate Set Point (GPM)	Ladder z (cm)	Carriage x1 (cm)	Carriage y1 (cm)
1	21. Oct	0	0	2	45	250	50	1950	240
2	21. Oct	0	0	2	45	350	50	1905	236
3	21. Oct	0	0	2	45	450	50	1890	229
4	21. Oct	0	0	2	55	250	50	1850	230
5	21. Oct	0	0	2	55	350	50	1805	229
6	21. Oct	0	0	2	55	450	50	1777	228
7	22. Oct	0	0	3	45	250	50	1912	228
8	22. Oct	0	0	3	45	350	50	1883	232
9	22. Oct	0	0	3	45	450	50	1852	243
10	22. Oct	0	0	3	55	250	50	1812	232
11	22. Oct	0	0	3	55	350	50	1765	227
12	22. Oct	0	0	3	55	450	50	1720	229
13	22. Oct	0	10	2	45	250	105	1950	225
14	22. Oct	0	10	2	45	350	105	1900	227
15	22. Oct	0	10	2	45	450	105	1835	226
16	22. Oct	0	10	2	55	250	104	1800	225
17	22. Oct	0	10	2	55	350	105	1755	223
18	22. Oct	0	10	2	55	450	104	1705	230
19	22. Oct	0	10	3	45	250	105	1665	230
20	22. Oct	0	10	3	45	350	105	1620	238
21	22. Oct	0	10	3	45	450	105	1600	230
Run ADV									
Level Sand in Barge									
22	23. Oct	0	20	3	55	250	120	1915	233
23	23. Oct	0	20	3	55	350	121	1880	237
24	23. Oct	0	20	3	55	450	120	1850	235
Change Screens, Refurbish Pit, Reset the Carriage to X = 1960									

Table B 2: Test Plan for the Screen 1.

Test Run	Day	Screen Number	Cutting Thickness (in)	Swing Speed (in/s)	Cutterhead Speed (rpm)	Flow Rate Set Point (GPM)	Ladder z (cm)	Carriage x1 (cm)	Carriage y1 (cm)
25	26. Okt	1	0	3	45	250	61	1962	232
26	26. Okt	1	0	3	45	350	61	1940	235
27	26. Okt	1	0	3	45	450	61	1923	235
28	26. Okt	1	0	3	55	250	61	1911	238
29	26. Okt	1	0	3	55	350	61	1892	233
30	26. Okt	1	0	3	55	450	61	1875	228
31	26. Okt	1	0	2	45	250	61	1850	229
32	26. Okt	1	0	2	45	350	61	1830	222
33	26. Okt	1	0	2	45	450	61	1810	228
34	26. Okt	1	0	2	55	250	61	1802	225
35	26. Okt	1	0	2	55	350	61	1782	227
36	26. Okt	1	0	2	55	450	61	1760	227
37	26. Okt	1	10	2	55	250	104	1962	228
38	26. Okt	1	10	2	55	350	104	1920	228
39	26. Okt	1	10	2	55	450	104	1880	227
40	26. Okt	1	10	2	45	250	104	1842	229
41	26. Okt	1	10	2	45	350	104	1802	235
42	26. Okt	1	10	2	45	450	104	1710	227
43	26. Okt	1	10	3	45	250	104	1675	226
44	26. Okt	1	10	3	45	350	104	1640	235
45	26. Okt	1	10	3	45	450	104	1605	235
46	26. Okt	1	20	3	55	250	115	1962	238
47	26. Okt	1	20	3	55	350	121	1917	231
48	26. Okt	1	20	3	55	450	121	1862	233
Run ADV									
Change Screens, Refurbish Pit, Reset the Carriage to X = 1960									

Table B 3: Test Plan for the Screen 2.

Test Run	Day	Screen Number	Cutting Thickness (in)	Swing Speed (in/s)	Cutterhead Speed (rpm)	Flow Rate Set Point (GPM)	Ladder z (cm)	Carriage x1 (cm)	Carriage y1 (cm)
49	27. Oct	2	0	3	45	250	61	1954	236
50	27. Oct	2	0	3	45	350	61	1938	236
51	27. Oct	2	0	3	45	450	61	1913	232
52	27. Oct	2	0	3	55	250	61	1899	229
53	27. Oct	2	0	3	55	350	61	1885	229
54	27. Oct	2	0	3	55	450	61	1865	231
55	27. Oct	2	0	2	45	250	61	1961	235
56	27. Oct	2	0	2	45	350	61	1950	221
57	27. Oct	2	0	2	45	450	61	1930	229
58	27. Oct	2	0	2	55	250	61	1911	229
59	27. Oct	2	0	2	55	350	61	1888	232
60	27. Oct	2	0	2	55	450	61	1872	227
61	27. Oct	2	10	3	55	250	101	1919	230
62	27. Oct	2	10	3	55	350	101	1880	226
63	27. Oct	2	10	3	55	450	101	1845	228
64	27. Oct	2	10	3	45	250	101	1802	230
65	27. Oct	2	10	3	45	350	101	1764	232
66	27. Oct	2	10	3	45	450	101	1722	231
67	27. Oct	2	10	2	45	250	101	1680	230
68	27. Oct	2	10	2	45	350	101	1640	226
69	27. Oct	2	10	2	45	450	101	1600	227
70	27. Oct	2	20	2	55	250	116	1960	229
71	27. Oct	2	20	2	55	350	116	1920	229
72	27. Oct	2	20	2	55	450	116	1880	223
Run ADV									
Change Screens, Refurbish Pit, Reset the Carriage to X = 1960									